UNIVERSIDADE FEDERAL DO RIO GRANDE DO SUL
INSTITUTO DE FÍSICA
DEPARTAMENTO DE ASTRONOMIA

# COMPACT STARBURST GALAXIES IN GROUPS OF DWARF GALAXIES

**Vitor Eduardo Buss Bootz**

**Porto Alegre, Rio Grande do Sul**
**2022**

**Vitor Eduardo Buss Bootz**

# COMPACT STARBURST GALAXIES IN GROUPS OF DWARF GALAXIES

Msc. dissertation taken under the supervision of Dr. Marina Trevisan submitted to the Graduate Program of Instituto de Física - Universidade Federal do Rio Grande do Sul (UFRGS) as part of the fulfilment to obtain the master's degree in physics with emphasis in astrophysics.

Advisor: Marina Trevisan

Porto Alegre, Rio Grande do Sul

2022

*I dedicate this work to all those who still*
*find themselves admiring the sky of a starry night*

# Acknowledgements

I cannot see this document as a mere result of my work, but rather as the fruit of an entire stage of my life, a reflection of the transformation between who I was at the beginning of this journey and who I have become. It is in the acknowledgments that we have the opportunity to expose our soul, hidden behind every word, equation or figure in this dissertation. Therefore, I would like to express it in its purest form: in Portuguese.

Meu mais profundo agradecimento:

Aos meus pais, Marlene Buss e Stanley Henrique Bootz, que plantaram a semente da curiosidade na minha cabeça ainda na infância e que regaram essa planta com muito amor e carinho por duas décadas. A planta cresceu um pouco mais do que o esperado, mas conseguiu escrever essa dissertação! Um agradecimento especial também ao meu padrinho Everton Ricardo Bootz e sua filha Luiza Bootz pelo acolhimento em seu lar durante a pandemia e, é claro, pelo apoio acadêmico, financeiro e emocional oferecidos nos últimos anos. Obrigado também a todos e todas das famílias Buss e Bootz, sou muito grato pela oportunidade de eternizar o amor que sinto por todos vocês neste documento.

À Dra. Marina Trevisan que primeiro conheci como professora, tornou-se então orientadora e, ao longo do percurso, minha amiga. Marina, você é a peça central de uma etapa muito importante da minha vida. Te agradeço não somente pelas infinitas contribuições acadêmicas, mas também por ter sido um porto seguro durante toda essa jornada. Obrigado também aos meus amigos e colaboradores Rodrigo Freitas e Maitê Mückler, excelentes companhias tanto no laboratório quanto no bar.

Aos profissionais do Instituto de Física e Departamento de Astronomia da UFRGS: educadores, pesquisadores e extensionistas de excelência! Em especial, aos professores que contribuíram na minha formação acadêmica para além do que os planos de ensino exigem: Dr. Alan Alves Brito, Dr. Rogério Riffel, Dr. Allan S. Müller e Dra. Alejandra Romero, além dos professores que constituem a banca examinadora deste trabalho: Dra. Cristina Furlanetto, Dr. Basílio X. Santiago e Dra. Karin Menendez-Delmestre.

Aos amigos de todas as esferas da minha vida: vocês foram essenciais para a construção desse trabalho. Em especial, *aos amigos rondonenses*: Mathias K., Gabrieli D., Luisa K., Giordano B., Elemar B., Guilherme K., Samira M., Família Herrmann, Prof. Deisi T. A., Regente Gerson D. G.; *às minhas irmãs*: Alessandra B. G. e Thais B.; *aos amigos da UFRGS*: Pedro C., João B., Eduardo H., Mark, A., Isadora E., Carlos R.; *aos amigos porto-alegrenses*: Bibiana M., Elisa J., Soila G., Pedro P., Lucas M., Daniel N. O., Famílias Brito, Santos e Cocco; *aos irmãos escoteiros*: João V., Louise M., Izabella F., Alvantino C., Evelise R., Márcio S., Christian H.; ... (vocês são MUITOS, obrigado!). Um agradecimento especial a todes dos Grupos Escoteiros 25 de Julho (11/PR), Charruas (03/RS) e Arno Friedrich (43/RS): bem cedo junto ao fogo, tornaremos a nos ver.

À Universidade Federal do Rio Grande do Sul, às agências de fomento à pesquisa CAPES, FAPERGS e CNPq e ao Governo Federal.

*All that you touch*
*And all that you see*
*All that you taste*
*All you feel*
*And all that you love*
*And all that you hate*
*All you distrust*
*All you save*
*And all that you give*
*And all that you deal*
*And all that you buy*
*Beg, borrow or steal*
*And all you create*
*And all you destroy*
*And all that you do*
*And all that you say*
*And all that you eat*
*And everyone you meet*
*And all that you slight*
*And everyone you fight*
*And all that is now*
*And all that is gone*
*And all that's to come*
*And everything under the sun is in tune*
*But the sun is eclipsed by the moon*

*(Eclipse – Pink Floyd, 1973)*

# Abstract

The mechanisms behind the peculiar characteristics of Compact Starburst Galaxies (CSBGs), such as extremely high star formation rates (SFRs) and low gas metallicities, are still poorly understood. They have formed a large fraction of their stellar mass over the last billion years and are true cosmic laboratories for studying the processes that trigger intense star formation activity in galaxies. Based on previous studies about the role of different environments on the extreme properties of CSBGs, we found some of these galaxies in groups of star-forming dwarf galaxies. In the hierarchical framework of galaxy formation and evolution, these groups represent a unique opportunity to investigate the role of interactions and mergers in the stellar mass buildup in low-mass systems. In this monography, we aim to investigate the role of the group environment and gas-rich interactions in the formation and evolution of these CSBGs. We defined a sample of 67 group candidates containing one spectroscopically confirmed CSBG and at least two other star-forming galaxies (SFGs) using data from the Sloan Digital Sky Survey. We then carried out observations at the Gemini South and North Observatories, resulting in 12 spectroscopically confirmed groups, which form the sample studied in this work, together with a control sample of 42 isolated CSBGs. We found that the SFRs, oxygen abundances, ionization properties and concentration parameters of isolated and non-isolated CSBGs are similar, indicating that the extreme properties of CSBGs are more related to processes internal to the galaxy than to environmental effects. Despite identifying morphological perturbations in SFG within groups, few signs of these disturbances were identified in CSBGs. Most CSBGs have normal gas metallicities compared to similar galaxies in different environments, but there is a tendency for the CSBG to be the most metal-poor among galaxies in the same group. Finally, by analyzing the star formation history among members of each group, we identified clear signs of synchronous bursts of star formation in some of these groups. Besides, we found that all CSBGs have an old stellar population and had several bursts of star formation since their formation.

*Keywords:* galaxies: starburst, galaxies: dwarfs, galaxies: groups: general

# Resumo

As características peculiares das Galáxias Starburst Compactas (CSBGs), como altas taxas de formação estelar (sSFRs) e baixa metalicidade, ainda são pouco compreendidas. Estas galáxias formaram grande parte de sua massa estelar nos últimos bilhões de anos e são verdadeiros laboratórios cósmicos para estudar os processos que desencadeiam intensa atividade de formação estelar. Baseando-se em estudos anteriores sobre o papel de diferentes ambientes nas propriedades extremas das CSBGs, encontramos algumas dessas galáxias em grupos de galáxias anãs. No contexto da formação e evolução hierárquica das galáxias, esses grupos de galáxias anãs representam uma oportunidade única para estudar como as interações e fusões contribuem para o crescimento da massa estelar em sistemas de baixa massa. Nesta monografia, investigaremos o papel do ambiente e das interações ricas em gás na formação e evolução das CSBGs. Para isso, definimos uma amostra de 67 candidatos a grupos contendo uma CSBG espectroscopicamente confirmada e pelo menos duas outras galáxias *star-forming* usando dados do Sloan Digital Sky Survey. Descobrimos que as sSFRs, abundâncias de oxigênio, campos de radiação ionizante e os parâmetros de concentração entre CSBGs isoladas e não isoladas são semelhantes, indicando que as propriedades extremas das CSBGs estão mais relacionadas a processos internos à galáxia do que à efeitos ambientais. Apesar de identificarmos diversas perturbações morfológicas nas galáxias vizinhas às CSBGs, poucos sinais desses distúrbios foram encontrados nas CSBGs em si. Também identificamos uma tendência que aponta que as CSBGs possuem a menor abundância de oxigênio comparado com as outras galáxias de um mesmo grupo. Analisando o histórico de formação estelar entre os membros de cada grupo, identificamos sinais claros de surtos síncronos de formação estelar em alguns desses grupos. Além disso, descobrimos que todas as CSBGs têm uma população estelar velha e tiveram vários surtos de formação estelar desde sua formação.

*Keywords:* galáxias: starburst, galáxias: anãs, galáxias: grupos

# Summary

# 1 INTRODUCTION

## 1.1 Compact star-forming galaxies

Compact star-forming galaxies (CSFGs) are true cosmic laboratories for studying the mechanisms that trigger intense star formation activity in galaxies. These objects have formed a large part of their stellar mass over the last billion years (e.g. Tweed et al., 2017; Mamon et al., 2020; Trevisan et al., 2021a) and are characterized by extremely low oxygen abundances (12+log(O/H) $\lesssim$ 8.0, e.g. Skillman & Kennicutt, 1993; Izotov & Thuan, 1998; Kunth & Östlin, 2000; Guseva et al., 2017), extending down to the metal-poorest known system, J0811+4730, with $12 + \log(\mathrm{O/H}) = 6.98$ (Izotov et al., 2018a).

The characterization of some important subclasses of CSFGs based on different photometric and spectroscopic criteria is the main topic of several studies. One of the well-known subsets of CSFGs found in the literature is a result of the success of the Galaxy Zoo project (Lintott et al., 2008). After more than ten years, the Galaxy Zoo project has classified the morphological type of nearly 5 million galaxies through the visual inspection of hundreds of thousands of volunteer members. One type of object caught the attention of the volunteers, who named it "Green Pea" galaxies (GP), as they appeared to be unresolved round point sources that looked green in the Sloan Digital Sky Survey (SDSS) *gri* composite. Shortly after the volunteers identified these objects, Cardamone et al. (2009) carried out a detailed study of their main characteristics, identifying that the green colouration is the result of a very powerful [O III]$\lambda$5007 Å emission line that substantially increased the $r$-band luminosity relative to the adjacent $g$ and $i$ SDSS bands of galaxies at redshifts between $0.112 \lesssim z \lesssim 0.360$. From this study, the authors concluded that GPs are low-mass galaxies ($\sim 10^{9.5}\mathrm{M}_{\odot}$), with high specific star formation rates (sSFRs $\sim 10$ $\mathrm{Gyr}^{-1}$) and large UV luminosities ($\sim 3 \times 10^{10}\mathrm{L}_{\odot}$). Similarly, Yang et al. (2017) explored a subset of local ($z \lesssim 0.05$) dwarf starburst galaxies with very small sizes ($< 1\,\mathrm{kpc}$), low stellar masses ($M_{\star} \sim 10^{6} - 10^{7}\mathrm{M}_{\odot}$) and high [O III]$\lambda$5007 / [O II]$\lambda$3727 ($\mathrm{O}_{32}$) ratio ($\gtrsim 10 - 60$), named "Blueberry" galaxies.

However, these colour-based photometric criteria exclude galaxies with global proper-

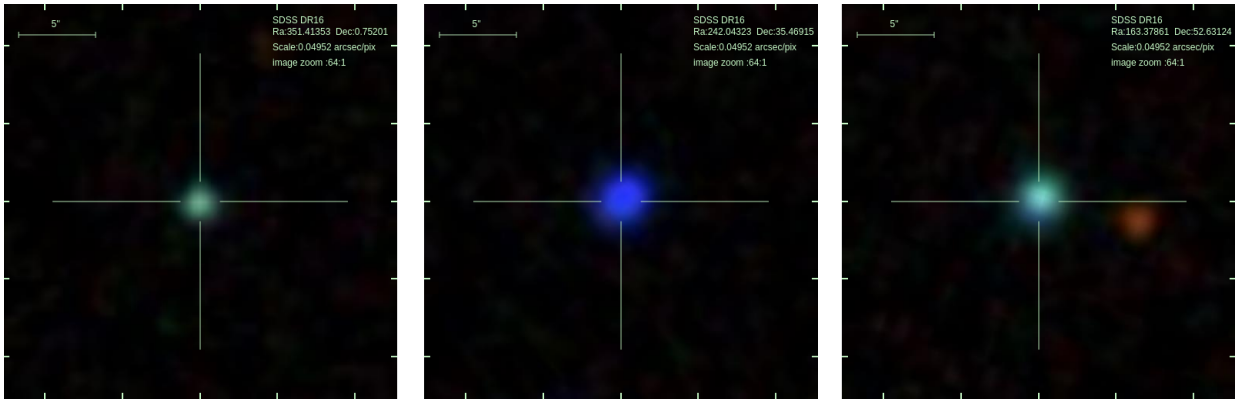


**Figure 1.1:** Examples of Green Pea, Blueberry and Luminous Compact Galaxy. Despite their photometric differences, they are galaxies with common spectroscopic characteristics. All three images are at the same scale and were taken from SDSS Data Release 16.

ties similar to GPs and Blueberries that do not fall into the appropriate redshift range for that specific colour. To work around this problem, Izotov et al. (2011) selected the so-called Luminous Compact Galaxies (LCGs) from the SDSS-DR7 based on both photometric and spectroscopic criteria in a wider redshift range ($z = 0.02 - 0.63$). With typical stellar masses of $\sim 10^9\,M_\odot$ and oxygen abundances ranging from $12+\log(O/H) \sim 7.8-8.3$, they are characterized by extremely high sSFRs ($\sim 10^{-9} - 10^{-7}$ yr$^{-1}$), comparable to those derived in high-redshift galaxies. In figure 1.1, we present an example of Green Pea, Blueberry and Luminous Compact Galaxy, respectively. In later works (e.g. Izotov et al., 2016a, 2016b, 2016c Izotov et al., 2018b, 2018c), the authors also studied more comprehensive samples of CSFGs with high sSFRs (up to 1000 Gyr$^{-1}$) at low redshifts ($z \lesssim 1$), even finding cases of Lyman Continuum (LyC) leaking galaxies. Therefore, extremely high star formation rates, unusual ionization levels and the escape of ionizing radiation in compact low-$z$ galaxies were pointed out as strong indicators that these galaxies may be excellent local analogues of high-$z$ SFGs ($z \gtrsim 1.5$, Izotov et al., 2021b).

## 1.2 Local CSFGs as analogues for high-$z$ SFGs

Identifying the sources responsible for the Universe's reionization remains one of the most significant challenges in modern cosmology. While the numbers of AGNs and massive star-forming galaxies (SFGs) at $z \approx 6$ are insufficient to produce all the LyC radiation required to reionize the Universe completely, the low-mass SFGs are much more abundant and are generally thought to be the main source of the ionizing radiation. However, direct

observations of distant dwarf galaxies are challenging, and in recent years there have been many efforts in identifying local analogues of this galaxy population (e.g. Jaskot & Oey, 2013; Izotov et al., 2021b).

On the one hand, the presence of H$\alpha$, H$\beta$, [O II]$\lambda$3727, [O III]$\lambda$4959, [N II]$\lambda$6584 as well as extreme values of [O III]$\lambda$5007 associated with high $O_{32}$ ratios[1] are typical characteristics of the early lifetime phase of high-$z$ star-forming galaxies (Holden et al., 2016; Cohn et al., 2018; Tang et al., 2019). On the other hand, $z \sim 0$ main-sequence SFGs exhibit, on average, a much lower level of star formation activity at a fixed stellar mass. Besides, in the last decade, some studies on the spectra of high-$z$ SFGs (e.g. Steidel et al., 2014; Shapley et al., 2015) point out that these galaxies have an offset to higher [O III]$\lambda$5007/H$\beta$ at a fixed [N II]$\lambda$6584/H$\alpha$ ratio when compared to local main-sequence analogues (e.g. Kewley et al., 2013) in the Baldwin-Phillips-Terlevich (BPT) diagram (Baldwin et al., 1981).

Some subclasses of CSFGs, however, shed some light on the search for local analogues of high-$z$ SFGs. Compact Starburst Galaxies (CSBGs) such as the "SDSS J084527.60 +530852.8" (whose spectrum is shown in figure 1.2), have intense emission lines (especially [O III]$\lambda$5007 and H$\alpha$) and high $O_{32}$ ratio, in addition to several other emission lines whose detection indicates, among other things, highly ionized gas and intense star formation. These spectroscopic similarities between local CSFGs and high-$z$ SFGs indicate that the former are good local analogues of the latter. Moreover, after studying the global characteristics (absolute optical magnitudes, SFRs, stellar mass and oxygen abundances) of a sample of $\sim$ 5200 local CSFGs, Izotov et al. (2015) also found good agreements between low-$z$ and high-$z$ SFGs. Their results indicate very weak redshift evolution of global parameters and weak dependence of metallicity on SFR, strengthening the idea of a universality of the global relations for CSFGs with high-excitation H II regions over redshifts $0 < z < 3$. Besides, the extreme ionization properties of these galaxies appear to be an important factor favouring the escape of ionizing photons, as confirmed in recent studies based on HST-COS observations: in a sample of 11 local CSFGs selected by their high O32 ratios, all show direct indication of LyC leakage (Izotov et al., 2016c,a, 2018b,c). However, Izotov et al. (2018c) find a weak correlation between O32 ratios and $f_{\rm esc}$, suggesting that a high ionization parameter is a necessary condition, but it is not

[1] Defined by $I([\mathrm{O\,III}]\lambda5007\,) \,/\, (I([\mathrm{O\,II}]\lambda3727\,) + I([\mathrm{O\,II}]\lambda3729\,))$

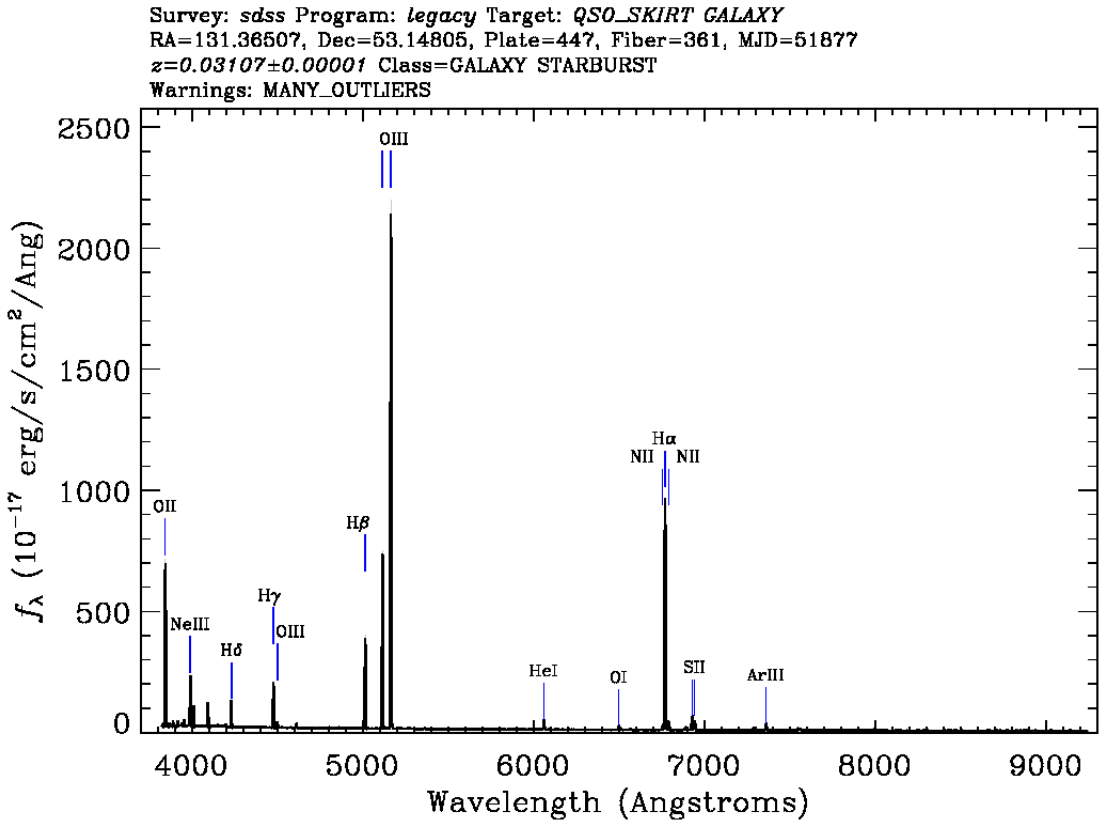


**Figure 1.2:** Spectrum of a Compact Starburst Galaxy (SDSS J084527.60+530852.8), characterized by intense emission lines and highly ionized gas. From left to right, the lines are identified as: [O II]$\lambda$3725, 3727, [Ne III]$\lambda$3868, H$\delta$, H$\gamma$, [O III]$\lambda$4363, H$\beta$, [O III]$\lambda$4959, [O III]$\lambda$5007, [He I]$\lambda$5876, [O I]$\lambda$6300, [N II]$\lambda$6548, H$\alpha$, [N II]$\lambda$6583, [S II]$\lambda$6716, 6730, [Ar III]$\lambda$7135.

sufficient for large $f_{\rm esc}$. In particular, $f_{\rm esc}$ of the galaxy with the highest $O_{32}$ is low. Therefore, large $f_{\rm esc}$ values might be a consequence of a combination of factors, such as the age and compactness of the starburst, the interstellar-medium (ISM) geometry and the gas kinematics. Besides, one key point is missing in the current samples of local CSFGs: the high-density and gas-rich environments that are increasingly common at higher $z$.

## 1.3 Environmental effects on the evolution of galaxies in the low-mass regime

Little is known about the processes that trigger the intense star formation activity in CSFGs. Simulations (L'Huillier et al., 2012) and semi-analytical models (Cattaneo, A. et al., 2011) of the formation and evolution of galaxies indicate that interactions and mergers between these objects play an essential role in the process of building massive systems, in which they acquire their mass mainly through mergers. Moreover, interactions

and mergers can also contribute to the morphological changes of these galaxies, transforming them from blue spirals to red ellipticals. These processes have been extensively studied in the high-mass regime (e.g. Krabbe et al., 2014; Rosa et al., 2014), especially in the local Universe. In this scenario, interactions and mergers of massive galaxies are known to enhance star formation activity, make them bluer and increase the Active Galactic Nucleus (AGN) fraction compared to their isolated analogues (e.g. Ellison et al., 2011, 2013; Scudder et al., 2012).

On the other hand, pairs and groups of interacting dwarf galaxies provide an unique window to address the hierarchical, gas-dominated assembly and the buildup of stellar mass in low-mass galaxies. However, most of the stellar mass of smaller galaxies ($M_\star \lesssim 10^{11}\mathrm{M}_\odot$) is formed via gas accretion (Cattaneo, A. et al., 2011), making interactions and mergers events between these systems rare. In isolated systems of dwarf galaxies (such as isolated dwarfs, as well as pairs and groups) and which fall within the stellar mass and redshift range where they and all of their close companions would be detectable by SDSS, Stierwalt et al. (2017) verified that fewer than 5% of dwarf galaxies are observed to have close companions. Besides, most galaxy surveys are not deep enough to detect the companions even when they are present. Nevertheless, the few that occur are mostly minor and gas-rich, i.e., drastically different from mergers between massive galaxies.

Aiming to study these rare isolated and interacting low-mass systems in the local Universe, Stierwalt et al. (2017) investigated 7 isolated groups of dwarf galaxies, 4 of which are shown in figure 1.3. In the figure, it is possible to see clear signs of interaction (e.g., morphological perturbations) that may be linked to the intense bursts of star formation identified in these galaxies (in red). Stierwalt et al. (2017) suggest that, given time, hierarchical merging will lead to the formation of intermediate-mass galaxies, which are more commonly seen in the local Universe. The finding of these dwarf-only groups provides an excellent opportunity to study the environment of compact starburst galaxies at high-$z$, since groups of star-forming dwarf galaxies are increasingly common at higher redshift. Moreover, the fraction of gas in galaxies increases with redshift. Since, in the local Universe, the lower the stellar mass, the higher the fraction of atomic gas in galaxies (e.g. Trevisan et al., 2021a), interactions within groups of dwarf galaxies are expected to be gas-rich and more similar to the gas-rich environments at high redshifts.

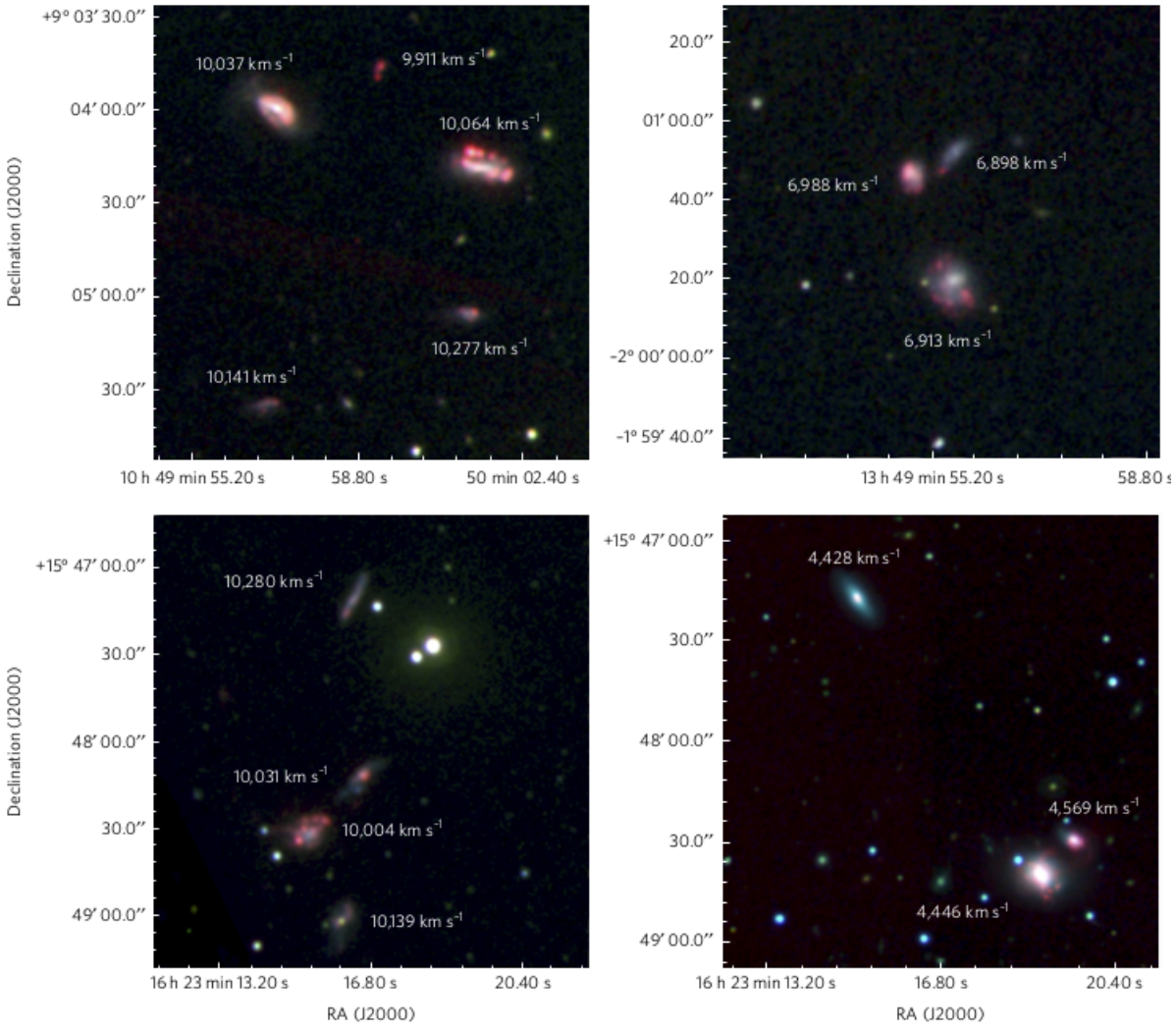


**Figure 1.3:** Four isolated groups of interacting dwarf galaxies. The red colour highlights the H $\alpha$ emission-line regions in each galaxy. Next to each galaxy member, the velocities derived from optical spectroscopy are displayed. Figure from Stierwalt et al. (2017).

In this context, some authors tried to understand how the environment influences the evolution of galaxies in the low-mass regime. For example, Privon et al. (2017a), while analyzing a pair of dwarf galaxies, found significant hydrodynamic differences when compared to massive systems interactions, such as more diffuse star formation and the absence of large-scale shocks. However, the study suffers from poor statistics, as they observe a single pair of dwarf galaxies. In a more comprehensive study of the demography of star-forming dwarf galaxies in different environments, Geha et al. (2012) found that for the same stellar mass and below the threshold of $M_\star < 1 \times 10^9\,\mathrm{M}_\odot$, quenched galaxies account for 23% of the dwarf population in denser environments, but only 0.06% for dwarf galaxies in the field (> 1.5 Mpc of a massive host galaxy). In particular, Stierwalt et al. (2015a) found that dwarf galaxy pairs closer than < 200 kpc from a massive galaxy

($M_\star > 10^{10}\,M_\odot$) have lower gas fractions when compared to their completely isolated counterparts. According to Luber et al. (2022), large-scale environmental effects (ram pressure or tidal stripping) appear to be ultimately what removes gas from dwarf galaxies.

Much more common than the suppression of star formation is the occurrence of starbursts in isolated systems of low-mass galaxies, even though the origins of these starbursts are still not clear (e.g. Johnson et al., 2004; McQuinn et al., 2010). Luo et al. (2014) found that $\sim 50\%$ of all galaxies identified as starbursts in their low-z ($0.01 \lesssim z \lesssim 0.20$) sample (covering a wide stellar mass range of $\log[M_\star/M_\odot] = 7 \sim 12$) show prominent interaction/merger features such as tidal tails, bridges between galaxies and close companions. For normal star-forming galaxies, in contrast, the fraction of galaxies with these features is significantly lower ($\sim 19\%$). In addition to these starbursts events, interactions may also be related to the compact surface brightness profiles observed in nearby blue compact dwarf galaxies (e.g., Lelli et al., 2014; Janowiecki & Salzer, 2014). In the TiNy Titans sample of interacting star-forming dwarf galaxies, (Stierwalt et al., 2015a) starbursts occur in 20% of both isolated and non-isolated pair systems, but only 6% (8%) of the matched isolated (non-isolated) single dwarfs.

Investigating the role of different environments on the extreme properties of Compact Starburst Galaxies, Trevisan et al. (in prep.) identified that some CSBGs are in groups of star-forming dwarf galaxies. These systems represent a unique opportunity to investigate the properties of CSBGs, which can be analogues high-$z$ star-forming galaxies, in gas-rich environments that were more common at high redshifts but are rare today. Therefore, in this Master Thesis, we aim to study a sample of CSBGs within groups of star-forming dwarf galaxies to address the following question: *Do the group environment and gas-rich interactions affect the formation and evolution of the Compact Starburst Galaxies?* Moreover, given that isolated groups of star-forming dwarf galaxies are such rare systems, in this monograph, we also present a detailed study of their properties and nature.

This work is organised as follows: In chapter 2, we present the criteria used to select the CSBGs and the groups to which they belong. Next, in chapter 3, we address the two observation programs carried out at the Gemini observatory, including a detailed data reduction description. In chapter 4, we present the methods adopted and results obtained from the analysis of CSBGs in groups of star-forming dwarf galaxies. Then, we discuss

these results in chapter 5. Finally, in chapter 6, we describe our conclusions and discuss future work prospects. Throughout the work, we adopt cosmological parameters of a flat Lambda Cold Dark Matter Universe with: $H_0 = 70\,\mathrm{km\,s^{-1}\,Mpc^{-1}}$, $\Omega_\mathrm{M} = 0.3$ and $\Omega_\Lambda = 0.7$.

# 2 DATA

## 2.1 Sample selection

The samples of Compact Star-Forming and Starburst Galaxy analysed in previous studies by Izotov et al.(2011; 2014; 2021a) were not selected to be complete and can present selection biases that are difficult to quantify. Hence, we used a new sample of CSBGs defined by Trevisan et al. (in prep.). The sample is based on the Sloan Digital Sky Survey Data-Release 17 (Abdurro'uf et al., 2022) and satisfies the following criteria:

**Completeness criteria:**

- $m_r \leq 18$, where $m_r$ is the extinction-corrected Petrosian magnitude in the $r$-band.
- Redshift range of $0.022 \leq z \leq 0.2$, in which the lower limit was adopted to ensure that the [O II]$\lambda$3727 emission line falls within the wavelength range of SDSS spectra.

**Compactness criteria:**

- $\theta_{50} < 3''$, where $\theta_{50}$ is the radius containing 50% of the Petrosian flux in the $r$-band.
- $\mu_r < 21.5$, where $\mu_r$ is the galaxy surface brightness in the $r$-band (in units of $\mathrm{mag\,arcsec^{-2}}$).
- $\theta_{90} < 4\,\theta_{50}$; where $\theta_{90}$ is the radius containing 90% of the Petrosian flux in the $r$-band.
- $f_{\mathrm{fiber}} > 30\%$, where $f_{\mathrm{fiber}} = 10^{-0.4(m_{\mathrm{fiber},r} - m_{\mathrm{petro},r})}$ is the fraction of the $r$-band Petrosian flux within the SDSS fiber.

**Starburst galaxy criteria:**

- EW([O III]$\lambda$5007 + H$\beta$) > 20 Å
- log([NII]$\lambda$6584/H$\alpha$) < −0.6

- $(g - i) < 0.7$, where $g$ and $i$ are the extinction-corrected, k-corrected magnitudes in the $g$ and $i$ bands, respectively.

Furthermore, spiral galaxies, mergers and H II regions that are part of a larger galaxy were excluded from the sample. Galaxies close to bright stars or to the borders of the SDSS survey were also excluded from the sample by requesting that at least 95 per cent of the region within 200 kpc from each galaxy lies within the SDSS coverage area. For this purpose, they used the SDSS-DR7 spectroscopic angular selection function mask[1] provided by the NYU Value-Added Galaxy Catalog team (Hamilton & Tegmark, 2004; Blanton et al., 2005; Swanson et al., 2008).

All selection criteria above lead to a final sample of **3611 CSBGs**.

To identify CSBGs residing in groups of dwarf galaxies, we selected all galaxies within $R < 200$ kpc from each CSBG in the sample. The SDSS photometric catalogue was used to identify potential lower-mass neighbours with magnitudes higher than $m_r = 17.77$, since this is the limit for which the SDSS spectroscopic catalogue is 95% complete. By doing this, we identified candidates (since there is no spectroscopic confirmation) of groups of star-forming dwarf galaxies containing at least one CSBG using the following criteria:

1. Each group must have at least 3 star-forming galaxies (including the CSBG) that are brighter than $m_r \leq m_{\mathrm{CSBG},r} + 1 \leq 19$, in which $m_{\mathrm{CSBG},r}$ is the apparent magnitude of the CSBG in the $r$-band, corrected by Galactic extinction.

2. The radius of the group, which corresponds to the radius of the smallest circle containing all member galaxies, must be $R_{\mathrm{group}} \leq 100\,\mathrm{kpc}$.

3. There should be no galaxies in the red sequence within $R < R_{\mathrm{group}} + 50\,\mathrm{kpc}$.

We determined the group's centre and radius iteratively: first, we defined the centre at the CSBG position and $R_{\mathrm{group}} = 100$ kpc. Then, we redefined the radius and centre position until we found the smallest radius for which there was no further change in the number of galaxies in the group. Besides, we used a method similar to that described

[1] File `sdss_dr72safe0_res6d.pol` from `https://space.mit.edu/~molly/mangle/download/data.html`

in Trevisan et al. (2021b) to identify red sequence galaxies in different redshifts: first, we selected galaxies whose spectroscopic redshift are in the range between $z_{\rm CSBG} - \Delta z$ e $z_{\rm CSBG} + \Delta z$ (in which $z_{\rm CSBG}$ is the redshift of the CSBG of the group). Then, to identify red sequence galaxies, we used the R (R Core Team, 2015) package `mclust` (Fraley et al., 2012; Fraley & Raftery, 2002) to cluster the data. We ran `mclust` on 100 bootstrap re-samplings for each redshift bin, selecting 5000 galaxies in each run, performing a linear regression of the form $(g-i)_{\rm rs} = a_{\rm rs} + b_{\rm rs}\, r$ and determining the scatter $\sigma_{\rm rs}$ of the relation. From this linear regression, we defined that the galaxies are: i) **blue** if $g-i < (g-i)_{\rm rs} - 4\sigma_{\rm rs}$; ii) **red** if $g-i$ has a value between $(g-i)_{\rm rs} \pm 4\sigma_{\rm rs}$; and iii) **background** if $g-i > (g-i)_{\rm rs} + 4\sigma_{\rm rs}$, in which $(g-i)_{\rm rs}$ and $\sigma_{\rm rs}$ are, respectively, the colour and the standard deviation of the red sequence in the plane $g-i$ vs $r$.

These criteria lead to a sample of 67 candidates for groups of star-forming galaxies between $0.024 \leqslant z \leqslant 0.181$ and containing at least one CSBG. Of these, 43 are completely isolated, that is, there are no massive galaxies ($\log[M_\star/{\rm M}_\odot] > 10$) within $R < 10\, R_{\rm group}$ with velocities between $\pm 3000\,{\rm km\,s^{-1}}$, relating to the CSBG of the group. Since most of the properties we are interested in studying come from the spectra of these galaxies (e.g., stellar mass, sSFR, flux ratios, chemical abundance), we are only interested in groups in which all member galaxies have available spectra. Besides, this prevents galaxies without spectrum and that do not fulfill the previously described criteria from contaminating the groups. However, among the 67 candidates, only 8 have SDSS spectra available for all member galaxies. For this reason, we performed two observations at the Gemini South and North observatories (see section 3 for a full description). From these observations, we increased our sample by 4, totalling **12 groups of star-forming dwarf galaxy containing at least one CSBG**. Besides, there are 14 CSBGs, since in two of these confirmed groups, there are two CSBGs. In figure 2.1, we present the images of our 12 groups. These images were retrieved from the LEGACY-DR9 survey database (Dey et al., 2019), and, in each image, we indicate the smallest circle that contains all member galaxies. We also include in the figure some important information about each group, such as the coordinates of the centre of the group, the value in kpc of the radius $R_{\rm group}$, the redshift of the group's CSBG and the logarithm of the sum of the stellar masses of the member galaxies. In figure 2.2, we show the colour-magnitude diagram of the member galaxies.

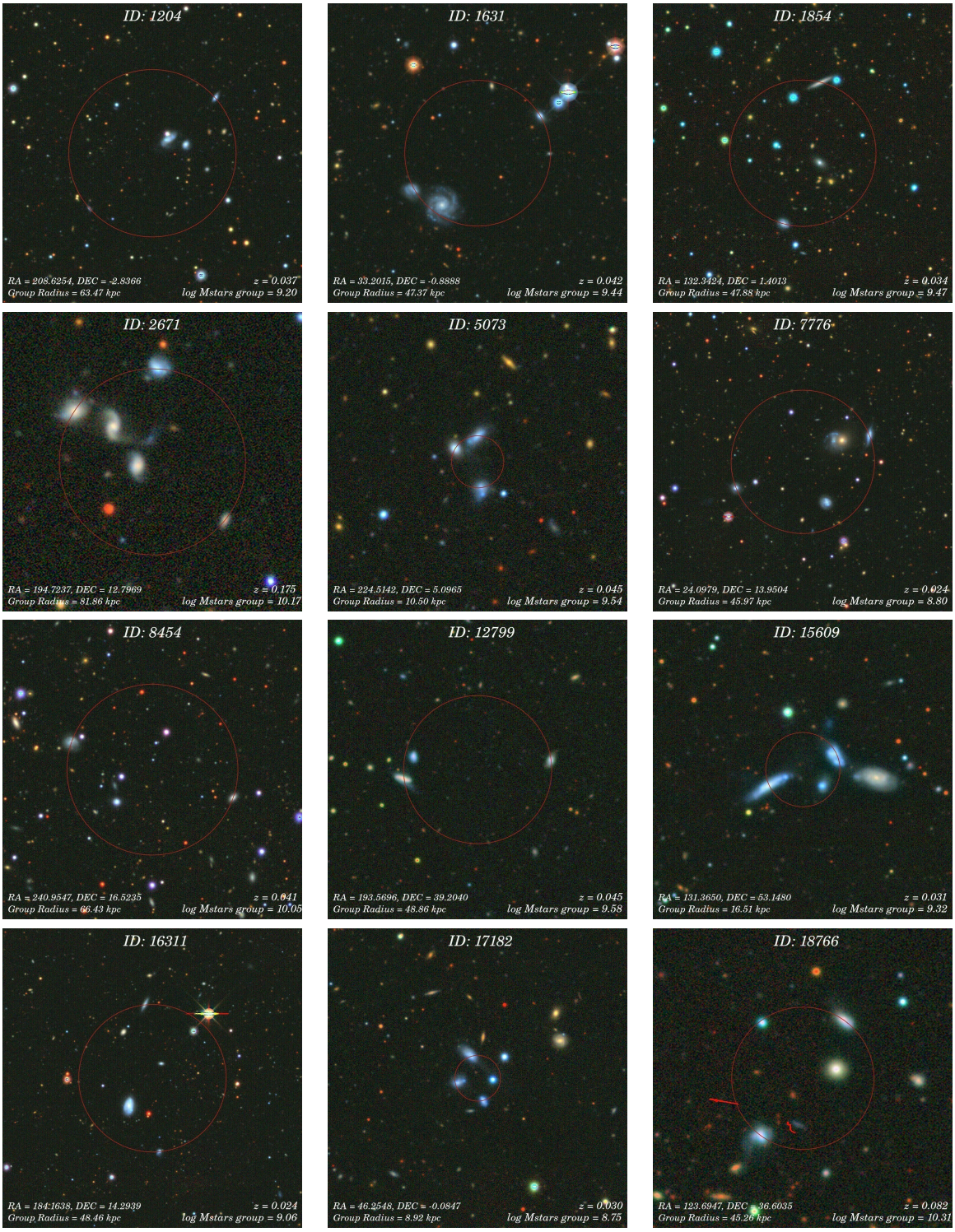


**Figure 2.1:** Images of the 12 confirmed groups of star-forming dwarf galaxies. The image size is $(2R_{\text{group}} + 100)$ kpc, where $R_{\text{group}}$ is the radius of each group. The red circle represents the smallest circle that contains all the member galaxies of the group. In the lower region of the figure, there are the coordinates of the centre of the group; the radius $R_{\text{group}}$ of the group in kpc; the redshift $z$ of the group's CSBG and the logarithm of the sum of the stellar masses of the member galaxies (details in Sec. 4.2.1). The images were obtained from the LEGACY-DR9 Survey.

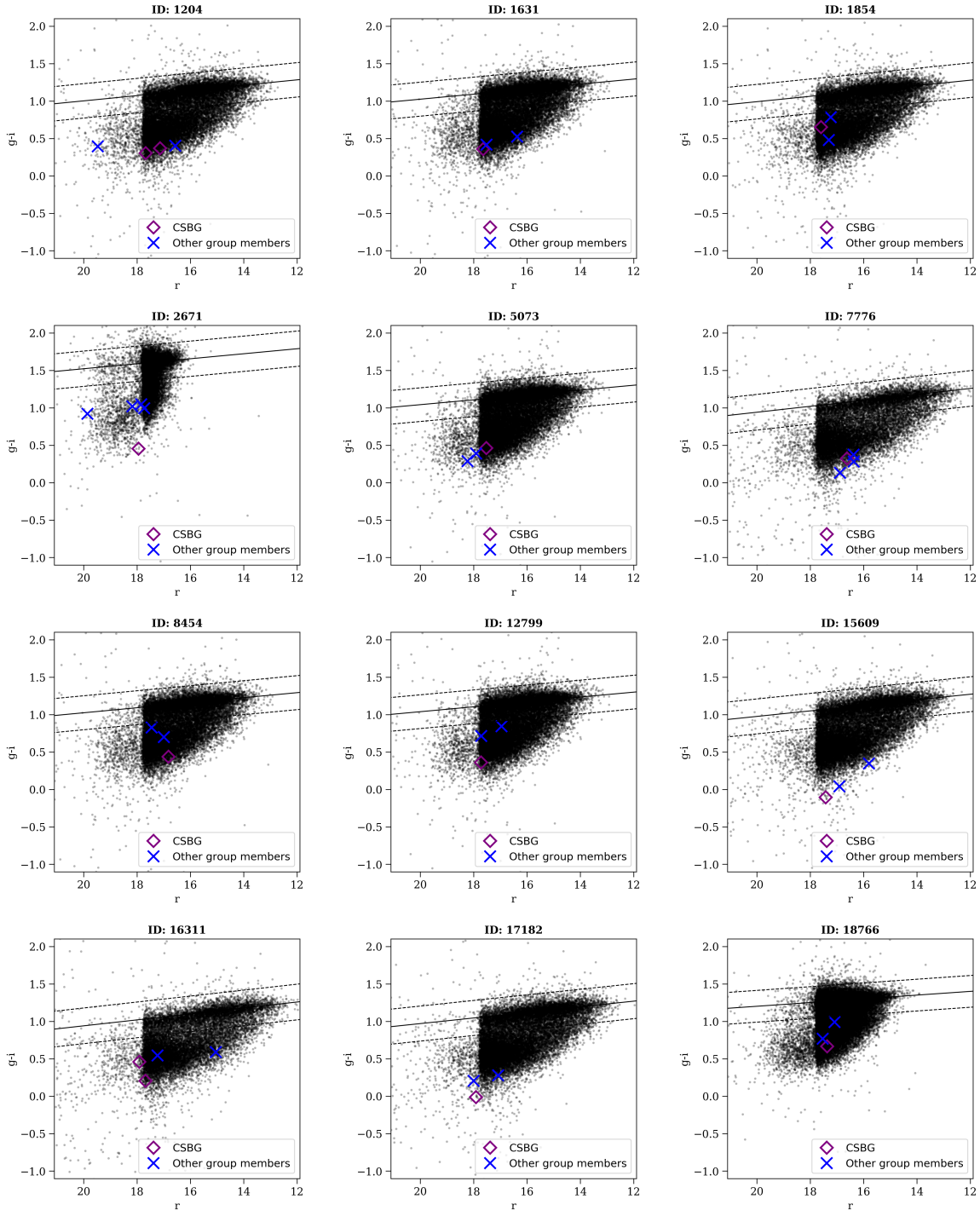


**Figure 2.2:** Colour-magnitude diagrams of the 12 confirmed groups of star-forming galaxies. The black dots in the background show SDSS galaxies that are within the range $z = z_{\mathrm{CSBG}} \pm \Delta z$ with $c\Delta z = 1000\ \mathrm{km\,s^{-1}}$. The solid and dashed black lines represent the best fit over the galaxies in the red sequence and $\pm 4\sigma_{\mathrm{rs}}$, respectively, where $\sigma_{rs}$ is the standard deviation of the fit.

## 2.2 Control sample

To verify the contribution of interactions on the properties of CSBGs within groups, we selected all CSBGs considered isolated in the SDSS photometric catalogue, i.e., that do not have any other galaxies within $R < 200$ kpc. Then, pairing by redshift, we defined a control sample consisting of 42 isolated CSBGs (i.e., 3 times the number of CSBGs within groups). By matching by redshift, we: *i*) ensure that the region in units of kpc within the SDSS fibre, which has a fixed aperture of 3 arcseconds, is similar for both samples; and *ii*) avoid a selection bias where only more luminous and massive CSBGs would be selected at higher redshifts: since we are dealing with dwarf galaxies, slight redshift variations can affect with the sample's completeness. Consequently, for high-z, brighter and more massive CSBGs will be preferentially selected, which creates a bias when compared with closer CSBGs. To perform that, we applied the Propensity Score Matching (PSM) technique (Rosenbaum & Rubin, 1983; de Souza et al., 2016) using the `MatchIt` package (Ho et al., 2011), written in R, and adopting the Mahalanobis distance approach (Mahalanobis, 1936; Bishop, 2006) and the nearest-neighbour method. Figure 2.3 shows the distribution of redshift between the isolated and non-isolated CSBG samples.

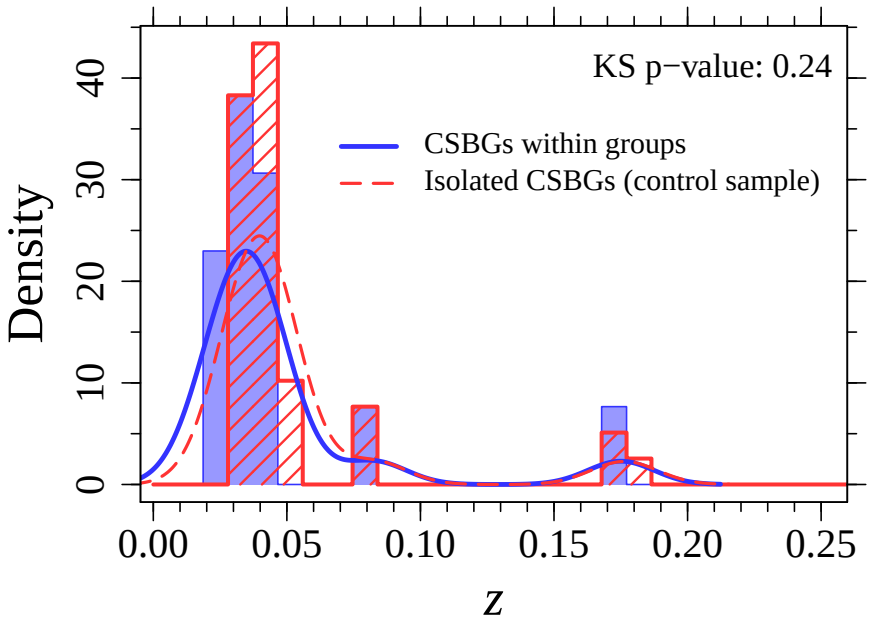


**Figure 2.3:** Redshift density distributions of isolated (red) and non-isolated (blue) CSBGs. The $p$-value of the Kolmogorov–Smirnov test between the two samples is displayed in the upper right corner of the frame. The ratio of isolated to non-isolated CSBGs is 3.

# 3 OBSERVATIONS AND DATA REDUCTION

## 3.1 Gemini observations

Among the 67 candidates of groups of star-forming galaxies containing at least one CSBG, only 8 have SDSS spectra available to all group members (and therefore, only these 8 are confirmed as groups). To increase the number of confirmed groups, we performed two sets of astronomical observations on group candidates using the Gemini South & North Observatories. The observations were carried out in the first half of 2018 (program GS-2018A-Q-219, hereafter GS2018/01) and the second half of 2019 (program GN-2019B-Q-233, hereafter GN2019/02), respectively, using the Multi-Object Spectroscopy (MOS) technique with the Gemini Multi-Object Spectrograph (GMOS)[1].

We used the B600-G5307 diffraction grating in both observations with a resolution $R \sim 1700$, covering the wavelength range between 4300Å−7300Å. We also used the GG455_G0305 long-pass filter to block 2nd-order contamination of the spectra. In the observed spectral range (and considering the redshift range of the sample), the detectable emission lines are: H$\gamma$, H$\beta$, [O III]$\lambda$4363, $\lambda$4959, $\lambda$5007 Å, H$\alpha$, [N II]$\lambda$6548, $\lambda$6584 Å and [S II]$\lambda$6717, $\lambda$6732 Å, in addition to the Mgb absorption region. We built the mask's design using the `GMMPS` (*Gemini's mask making software*[2]) and the width of the mask slits is 0.5 arcsec. Figure 3.1 exemplifies one of these masks (Group 1204 from table 1). In GS2018/01 and GN2019/02 programs, we observed four and two candidates, respectively. In both cases, each candidate was submitted to 3 exposures of 1200 seconds, totalling 60 minutes per group.

[1] We have further submitted two observation proposals to the Gemini North Observatory (programs GN-2020A-Q-305 and GN-2021A-Q-309) for the study of 8 group candidates. Both proposals were approved, however observations were not carried out due to the COVID-19 pandemic.

[2] `https://gmmps-documentation.readthedocs.io/en/latest/`

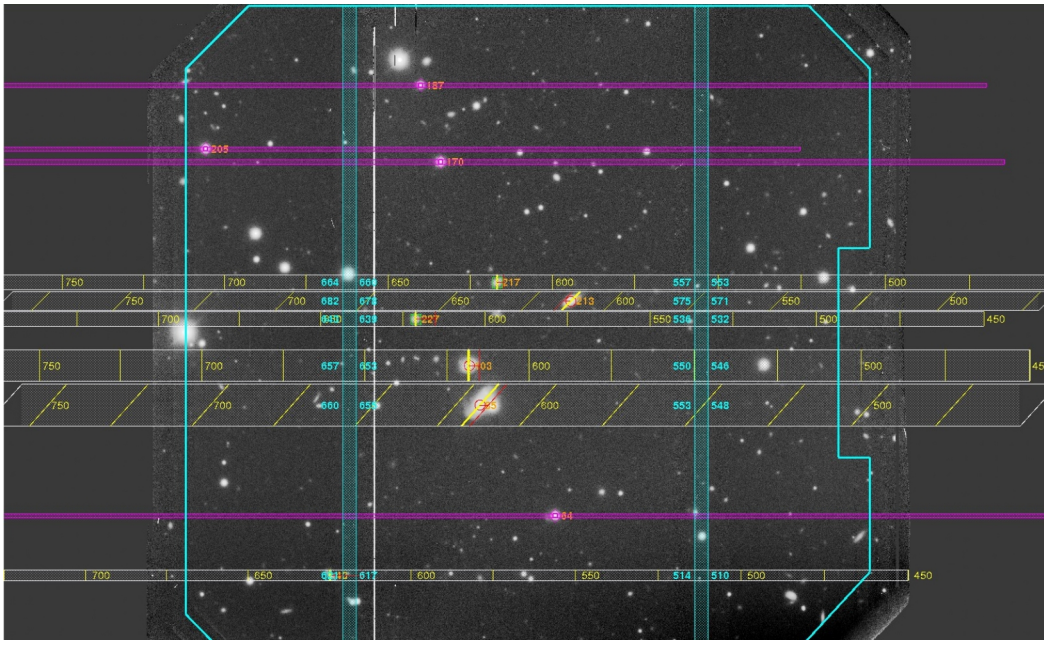

**Figure 3.1:** Mask design used in the observation of Group 1204. The thicker yellow lines over the galaxies represent the slits, while the diffraction results are illustrated by the wide bands that cross the image horizontally. The blue vertical bands represent the gaps between the CCDs (whose information is lost).

## 3.2 Data reduction

Data reduction from both (GS2018/01 and GN2019/02) observations were performed using IRAF (Image Reduction and Analysis Facility, Tody, 1986). Below, we describe the data reduction process accomplished.

First, it is important to know that the raw files resulting from the observations, i.e. *science*, *flats*, *bias* and *arcs* files, are in the FITS (*Flexible Image Transport System*) format. Except for the mask, all files have 13 extensions: 1 header and 12 extensions referring to the 12 amplifiers (4 amplifiers in each of the 3 CCDs) that constitute the telescope detection system. Furthermore, as described in 3.1, each group has 3 exposures of 1200s, but each exposure has a different central wavelength (with a variation of 10Å from each other). Then, for each group, we perform the following steps:

- First, we combine all *bias* files using the `gbias` task. These files come from zero-time observations (provided by the observatory) and are intended to correct the unwanted signal coming from the electronics.
- Using the `gprepare` task, we add the group's mask as a new extension in all *flat,*

*arc* and *science* files, so now these files have the information about the position and dimensions of the slits. We also used this task to perform the *bias* correction over these files.

- The `gmosaic` task then merges the 12 extensions containing the amplifier detections into a single image. Then, the task `gscut` cuts this image into '$n$' extensions, where $n$ is the number of spectra in the image, indicated by the mask. We perform this operation on all files *flat, arc* and *science*.

- The `gsflat` task then creates the normalized *flat* files, which are later used to correct pixel-by-pixel variations of the *arc* and *science* files.

- Next, we compute the wavelength calibration function using the *arc* files and the `gswavelength` task. For this, we used a 5th order Chebyshev polynomial (Mason & Handscomb, 2002), whose function quality can be quantified through its Root Mean Square (RMS). For our data set, we consider values of RMS $\lesssim 0.25$ to be acceptable.

- With the wavelength calibration function, it is then possible to correct the quantum efficiency (QE) of the different CCDs, which we perform using the `gqecorr` task. The QE is the measure of the effectiveness of a CCD to convert incident photons into electrons.

- After applying the *flat* and QE corrections to the *science* files, the `gemcrspec` (Cosmic-Ray Rejection by Laplacian Edge Detection, van Dokkum, 2001) task removes all spectra cosmic ray trails.

- Then, the `gstransform` task calibrates the *science* file by wavelength using the function previously calculated by `gswavelength`.

- Finally, the `apall` task subtracts the sky contribution and performs the spectrum extraction.

Then, we repeat all these steps on the standard star files chosen by the observatory. The standard stars of the GS2018/01 and GS2019/02 observations were *CD-32-9927* and *wolf1346*, respectively. Since the flux of these stars is known, we can calculate a sensitivity function as a function of wavelength. Then, using the `calibrate` task, we calibrate the reduced galaxy spectra by flux.

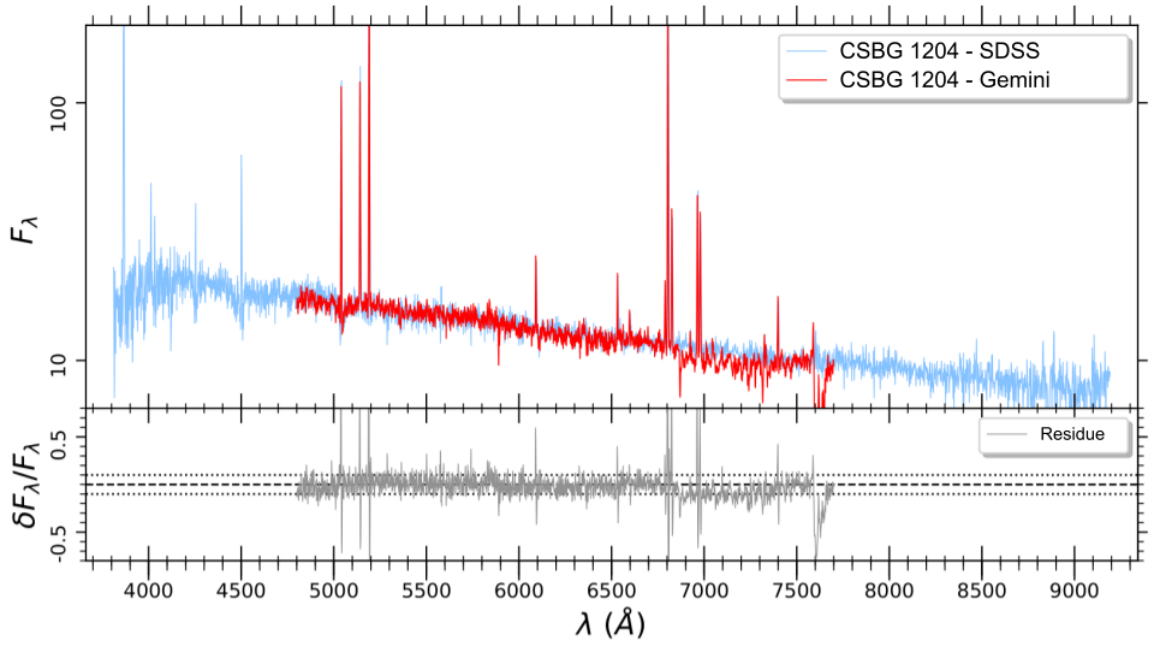


**Figure 3.2:** Comparison between the spectrum collected from SDSS (in blue) and the GS2018/01 observation product (in red) for the CSBG 1204 (Table 2). In the lower frame, the residue of the combination of both spectra.

Lastly, using the `scombine` task, we combine the three flux-calibrated spectra through the median of their fluxes. This step is crucial, as it recovers the information lost in the gaps between the CCDs (since the three spectra have different central wavelengths) and eliminates any imperfections derived from the observation or the reduction process. Then, we calculate the errors of each spectrum as a function of the wavelength, which are then combined using the following equation:

$$\sigma = \frac{\sqrt{\sigma_1^2 + \sigma_2^2 + \sigma_3^2}}{3}. \tag{3.1}$$

Since all CSBGs have spectra available in the SDSS, we could compare the quality of the data reduction using the reduced spectra of these galaxies. Figure 3.2 exemplifies this comparison for the case of CSBG 1204 (Tab. 1). The residue of this combination (bottom panel) indicates a flux variation for the continuum of ±10%. For the emission lines, the variation is stronger (> 50% in modulus), which can be explained by the different spectra resolutions.

To determine the redshift of each galaxy within the group candidate, we used the task `emsao` of the IRAF package RVSAO (Radial Velocity Package developed at the Smithsonian

Astrophysical Observatory[3], Kurtz & Mink, 1998), which returns the radial velocity and the respective error of each emission line identified in the spectrum. Then, we calculate the radial velocity of the galaxy using the average of these velocity values ($v_i$) weighted by their respective errors ($\sigma_i$), following the equation:

$$v_r = \frac{\sum_i \left(v_i/\sigma_i^2\right)}{\sum_i \left(1/\sigma_i^2\right)} \,. \tag{3.2}$$

By doing this, we confirmed that 4 out of 6 observed candidates were, in fact, groups, thus totalling 12 confirmed groups containing at least 3 galaxies. In table 1, we present the main properties of these groups (see section 4 for a full description of each property). Future observations will be carried out for the analysis of the remaining candidates.

[3] `http://tdc-www.harvard.edu/iraf/rvsao/`

# 4 METHODS AND RESULTS

## 4.1 Group properties

This section presents the methods used to measure the global properties of our groups. All results are shown in table 1.

### 4.1.1 General properties

The **radius of each group** were determined using two approaches: *i*) estimating the smallest circle that contains all member galaxies of the group using the Python module `miniball`[1] (indicated as "$R_{\rm group}$ [kpc]" in Table 1); and *ii*) calculating the inertial radius of each group following the method described in Tully et al. (2006); Yaryura et al. (2020) ("$R_{\rm inertial}$ [kpc]" in Table 1):

$$R_{\rm inertial} = \left( \sum_{i}^{N} r_i^2 / N \right)^{1/2} , \tag{4.1}$$

where $r_i$ is the projected distance of a galaxy from the system centroid.

The **velocity dispersion of each group** was also determined using two different methods. First, considering an ordered vector of radial velocity observations $x_1 < x_2 < ... < x_n$ (in which $x_i$ is defined as the difference between the measured radial velocity of each galaxy and the mean radial velocity of the group), whose gaps between these observations are defined by:

$$g_i = x_{i+1} - x_i, \quad i = 1, ..., n-1 \, . \tag{4.2}$$

Wainer & Thissen (1976) proposed that for a set of approximately Gaussian weights

$$w_i = i(n-i), \quad i = 1, ..., n-1 \tag{4.3}$$

a robust measure of scale, in this case represented by the group velocity dispersion along the line of sight, can be obtained through the relation:

$$\sigma_{W\&T} = \frac{1}{(\overline{z}+1)} \frac{\sqrt{\pi}}{n(n-1)} \sum_{i=1}^{n-1} w_i g_i \, , \tag{4.4}$$

[1] https://pypi.org/project/miniball/

in which $\overline{z}$ is the mean redshift of the galaxies in the group.

The second approach for determining the velocity dispersion of the groups was carried out following the method employed by Yaryura et al. (2020):

$$\sigma_Y = \frac{1}{(\overline{z}+1)}\left[\sum_i^N v_i^2/(N-1)\right]^{1/2} . \tag{4.5}$$

Both measurement results are displayed in Table 1.

We retrieved the neutral hydrogen gas mass from the ALFALFA Survey (*Arecibo Legacy Fast ALFA*, Haynes et al., 2018) for those CSBGs included in the catalogue. In table 4 we show the neutral hydrogen gas mass ($M_{HI}$) for each isolated CSBG, while for the groups (Table 1) the values of $M_{HI}$ represent the group as a whole, since the resolution limit of the *Arecibo L-band Feed Array*[2] (ALFA) is of the order of the groups' size (Beam size: $3.8 \times 3.3$ arcminutes).

Also following Yaryura et al. (2020), we estimate the virial mass of the system (assuming a virial equilibrium) by using the expression:

$$M_{\rm vir} = 3[(N-1)/N]\sigma_Y^2 R_G/G\,, \tag{4.6}$$

where $R_{\rm G} = N^2/\sum_{\rm pairs}(1/r_{ij})$, and $r_{ij}$ is the projected separation between each pair in the system (counted only once).

Finally, we measured the group surface brightness $\mu_r$ using the Petrosian magnitude in the $r$-band measured by SDSS for each galaxy member through the equation (in units of mag arcsec$^{-2}$):

$$\mu_r = m_{\rm Petro}^{\rm total} + 2.5\log\left(4\pi R_{\rm group}^2\right) - 10\,\log(1+z_{\rm CSFG})\,, \tag{4.7}$$

in which the last term corrects the so-called cosmological surface brightness dimming, related to the contributions of time dilation and curvature of the universe in the dimming of light from galaxies with progressively higher redshifts (e.g., Phillipps et al., 1990; Calvi et al., 2014).

To calculate the total mass density of each group, we follow Muldrew et al. (2012):

$$\Sigma_{\rm total} = \frac{M_{\rm vir}}{\pi R_{\rm group}^2}\,. \tag{4.8}$$

[2] For more information about the *Arecibo L-band Feed Array*: `http://egg.astro.cornell.edu/alfalfa/ugrad/alfa.htm`

Substituting $M_{\rm vir}$ by $M_\star$, we get the stellar mass density:

$$\Sigma_\star = \frac{M_\star}{\pi R^2_{\rm group}}\,, \tag{4.9}$$

both with dimensions $[\mathrm{M}_\odot\,\mathrm{kpc}^{-2}]$.

### 4.1.2 Isolation criteria

After selecting the groups following the criteria described in section 2.1, we used three isolation criteria to further characterize their environment:

1. If there are no massive galaxies ($M_\star > 10^{10}\,\mathrm{M}_\odot$) within $R < 10\,R_{\rm group}$ (projected distance) and $\sigma = \pm 3000\,\mathrm{km\,s^{-1}}$.
2. If there are no massive galaxies closer than 500 kpc (three-dimensional distance).
3. If there are no massive galaxies closer than 1 000 kpc (three-dimensional distance).

Table 1 shows whether each of the 12 groups of star-forming galaxies containing at least one CSBG is isolated or not according to each criterion (columns $\mathrm{Iso_M}$, $\mathrm{Iso_{D<500}}$ and $\mathrm{Iso_{D<1\,000}}$, respectively).

### 4.1.3 Position relative to large-scale structures

To locate the isolated and non-isolated CSBGs relative to large-scale structures (knots, filaments, sheets or voids), we plotted the spatial distribution of all galaxies from the Sloan Digital Sky Survey between $0 < z < 0.06$. Figure 4.1 shows the position of all CSBGs within this distribution. Visually, we verified that the vast majority of CSBGs, either within groups or isolated, are found on filaments. In some cases, however, we find CSBGs of both samples located in knots (e.g., RA/DEC: $\sim [240, 15]$ deg) and some isolated CSBGs in voids (e.g., RA/DEC: [189.35, 23.09] deg; RA/DEC: [217.58, 64.50] deg).

## 4.2 Galaxy properties

Through a combined analysis of photometric and spectroscopic data, we show in this section the techniques employed and the results obtained in comparing the properties of

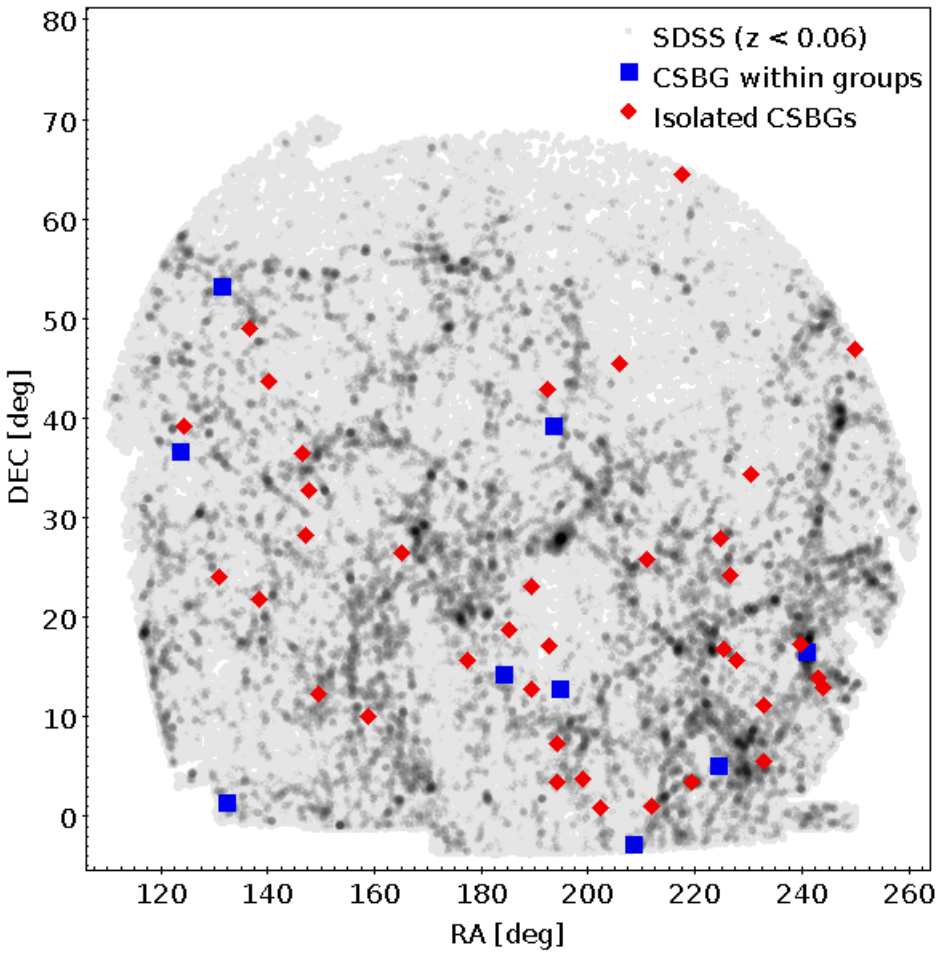


**Figure 4.1:** Spatial distribution of isolated CSBGs (red diamond) and within groups of star-forming galaxies (blue squares) relative to the large scale distribution of galaxies from the SDSS between $0 < z < 0.06$ (grey circles).

CSBGs within groups of star-forming galaxies with their isolated counterparts. All results are summarized in tables 2 (for CSBGs within groups) and 4 (for isolated CSBGs).

### 4.2.1 Stellar population

To characterize the galaxy stellar populations, we used the STARLIGHT fitting code (Cid Fernandes et al., 2005), which combines the spectra of multiple Single Stellar Populations (SSPs) with different ages and metallicities to reproduce the observed spectrum. We used 112 SSPs from a combination of Vazdekis et al. (2010) (based on stars from the MILES library, Sánchez-Blázquez et al., 2006), and Delgado et al. (2005) (based on the synthetic stellar spectra from GRANADA library, Martins et al., 2005) spectra, updated with MILES V11 models (Vazdekis et al., 2016). A complete description of this SSP base set is found in Fernandes et al. (2014); Riffel et al. (2021). The Salpeter

(1955) IMF was adopted together with "Padova 2000" (Girardi et al., 2000) evolutionary tracks, covering the age range from 0.001 Gyr to 14 Gyr (with 28 bins) and metallicities $Z = 0.004, 0.008, 0.019, 0.033$. We also chose $\lambda_B = 5635$ Å as the normalization wavelength of the base file spectra and 5590 Å $\leq \lambda_N \leq$ 5680 Å as the normalization range for the galaxy spectra. Besides, we measured the colour excess $E(B-V)$ by using the Schlegel et al. (1998) extinction maps and assuming a reddening law based on the Cardelli et al. (1989) extinction curves and using $R_V = 3.1$.

Considering that the observed spectrum flux is in units of $10^{-17}\,\mathrm{erg\,s^{-1}\,cm^{-2}\,\AA^{-1}}$, the stellar mass of a galaxy (in units of $\mathrm{M}_\odot$) is obtained through the equation (Cid Fernandes et al., 2005):

$$M_\star = \mathrm{M}_{\mathrm{cor\_tot}} \times 10^{-17} \times 4\pi D_L^2 \times L_\odot^{-1}\,, \tag{4.10}$$

in which $\mathrm{M}_{\mathrm{cor\_tot}}$ is an output parameter from the STARLIGHT modeling whose value represents the combined current stellar mass contributions of all SSPs. In fact, this value is first obtained in terms of the light fraction of each SSP, which is then converted to the current stellar mass fraction[3]. Besides, $D_L$ is the galaxy luminosity distance and $L_\odot$ is the solar luminosity. To take into account the light outside the Gemini slit (with a 0.5 arcsec width) and SDSS fibre (with a 3 arcsec diameter) apertures, we corrected the mass values by the factor:

$$M_{\star,\mathrm{corr.}} = \frac{M_\star}{10^{-0.4\,(m_{\mathrm{ab},r} - m_{\mathrm{Petro},r})}}\,, \tag{4.11}$$

where $m_{\mathrm{ab},r}$ corresponds to the magnitude measured in the SDSS fiber ($m_{\mathrm{ab},r} = m_{\mathrm{fiber},r}$) or in the Gemini slit ($m_{\mathrm{ab},r} = m_{\mathrm{slit},r}$), and $m_{\mathrm{Petro},r}$ is the Petrosian magnitude in the $r$-band.

Figure 4.2 shows a histogram of the stellar masses of non-isolated CSBGs and the control sample (redshift-paired isolated CSBGs). We found a statistically significant difference ($p$-value $= 3.19 \times 10^{-4}$) on the stellar mass distribution of these samples, with CSBGs within groups being less massive than their isolated counterparts. Besides, this difference is the reason why we did not use the stellar mass in the matching procedure to define the sample of isolated CSBGs (Sec. 2.2): for the same redshift, there are no isolated

[3] For more details, consult the STARLIGHT user guide, available at `http://www.starlight.ufsc.br/downloads/`

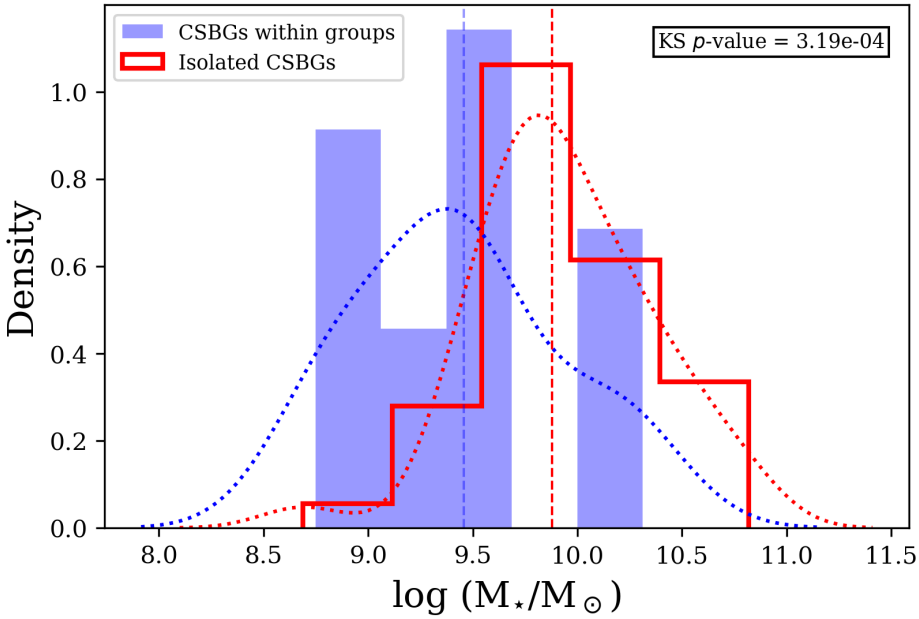


**Figure 4.2:** Stellar mass density distributions of isolated (red) and non-isolated (blue) CSBGs. The *p*-value of the Kolmogorov–Smirnov test between the two samples is displayed in the upper right corner of the frame.

CSBGs with stellar masses values sufficiently low to reproduce the mass distribution of CSBGs within groups.

### 4.2.2 Star-formation history

We measured, using the pPXF (*Penalized PiXel-Fitting*, Cappellari, 2012) method, the Star Formation History (SFH) of all galaxies that has SDSS spectra within the groups. Using a maximum penalized likelihood approach, the pPXF method can extract the stellar and gas kinematics and synthesize the stellar population of galaxies using their spectra's absorption-line features. In particular, pPXF considers the contribution of emission lines in calculating the SFH of galaxies, which is a useful feature in the context of the CSBGs spectra, characterized by intense emission lines and few absorption features. We determined the SFHs only for galaxies that have SDSS spectra because the wavelength range of our Gemini spectroscopic observations is narrower and do not include the 4 000 Å break, which is an important age indicator. The main goal of this analysis is to verify synchronicities in the star formation bursts between galaxies of the same group, which would be a strong indication that the interactions are affecting the star formation rates of these galaxies. Figure 4.3 and 4.4 shows the SFH of CSBGs and their neighbours for 10 groups (in which we exclude groups 2671 and 5073 since they have only one member

galaxy with SDSS spectrum available). In figure 4.3, we masked the emission lines to fit only the stellar continuum, while in figure 4.4, we fit the stellar continuum and the emission lines simultaneously, assuming Gaussian profiles for the emission lines. In both figures, the CSBG of the group is always represented by the solid blue region, while the other member galaxies are illustrated by different colours (red, black and purple outlines, according to the number of member galaxies). We computed the SFR for 20 age bins with an approximate difference of 0.2 dex between each bin. The width $\Delta x$ of each bin $i$ with central value $x_i$ follows the equation: $\Delta x = (x_{i+1} - x_{i-1})/2$.

To estimate the uncertainties in the SFHs, we created 100 Monte Carlo realizations of the spectrum of each galaxy by assuming that the observed flux in each pixel follows a Gaussian distribution with standard deviation equal to the flux error for that pixel. Then, we ran pPXF on these spectra, and the results were used to estimate the uncertainty on the SFR in each age bin, in which the 16% and 84% percentiles are represented by the lower and upper error bars in each age bin, respectively. When the 16% percentile is consistent with zero, the 84% percentile represents the upper limit in SFR for that bin (symbolized by downward pointing arrows).

### 4.2.3 Structural parameters

We measured the concentration of all galaxies based on the method developed by Conselice (2003), in which we used:

$$C = \log_{10}\left[\frac{R_{90}}{R_{50}}\right], \tag{4.12}$$

where $R_{90}$ = `petroR90_r` and $R_{50}$ = `petroR50_r` are the galaxy radius containing 90% and 50% of the Petrosian flux in the SDSS $r$-band, respectively. Figure 4.5 shows the distribution of concentrations between CSBGs within groups and isolated CSBGs. Even though the linear fit over both samples shows a trend of increasing concentration with increasing stellar mass, there is a large scatter. In any case, and taking into account the difference in concentrations due to differences in stellar mass, we did not find a statistically significant difference between the two samples.

We also calculated the surface brightness of each galaxy. We used the equation 4.7, and replaced $m^{\rm total}_{\rm Petro}$ by `petroMag_r` (the Petrosian magnitude in the SDSS $r$-band), $R_{\rm group}$ by

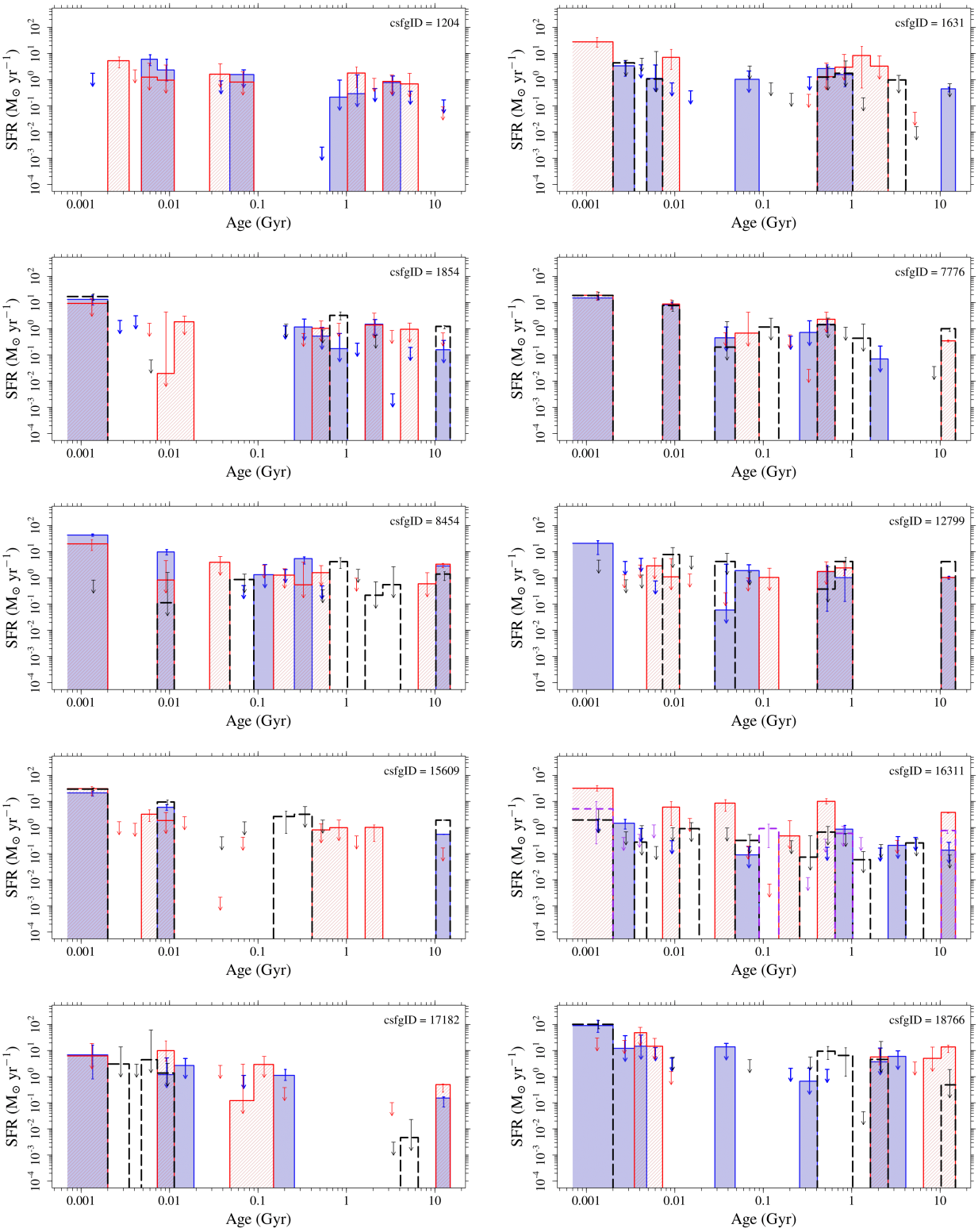


**Figure 4.3:** Star-formation history of all members that have SDSS spectra within each group of table 1. **This set of SFHs corresponds to the pPXF stellar continuum fit masking the emission lines**. The CSBG of the group is represented by the solid blue region, while the other member galaxies by red, black and purple outlines, according to the number of member galaxies. The x-axis is divided into 28 age bins between 0.001 – 14.1 Gyr, with a constant ratio of 0.2 dex between them. $1\sigma$ errors (details in the text) are represented by error bars at the top of each column, along with downward pointing arrows representing the SFR's upper limit for that age bin.

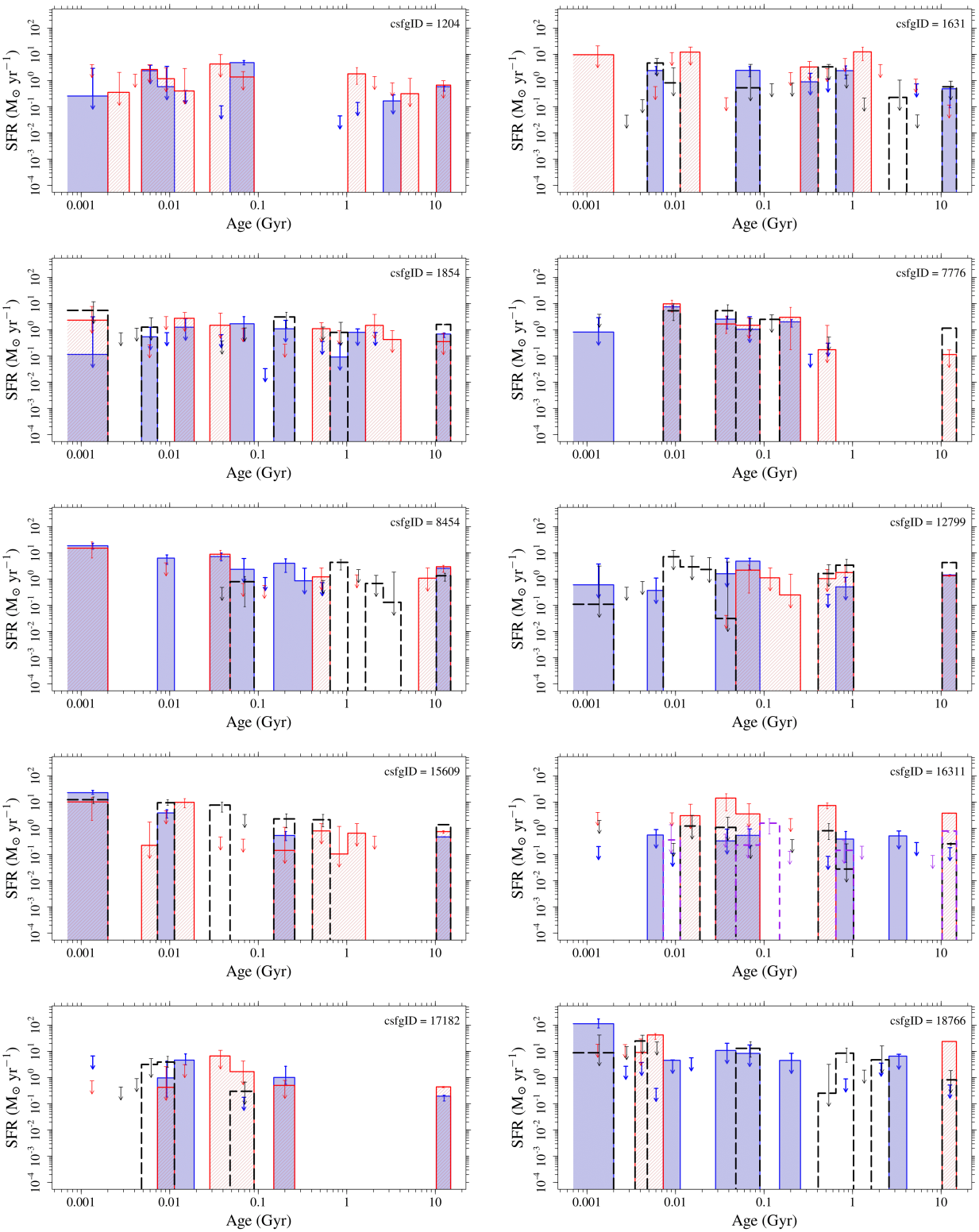


**Figure 4.4:** Star-formation history of all members that have SDSS spectra within each group of table 1. **This set of SFHs corresponds to the pPXF stellar continuum fit considering a single Gaussian component fit for the emission lines**. Colours and errors are the same as in figure 4.3.

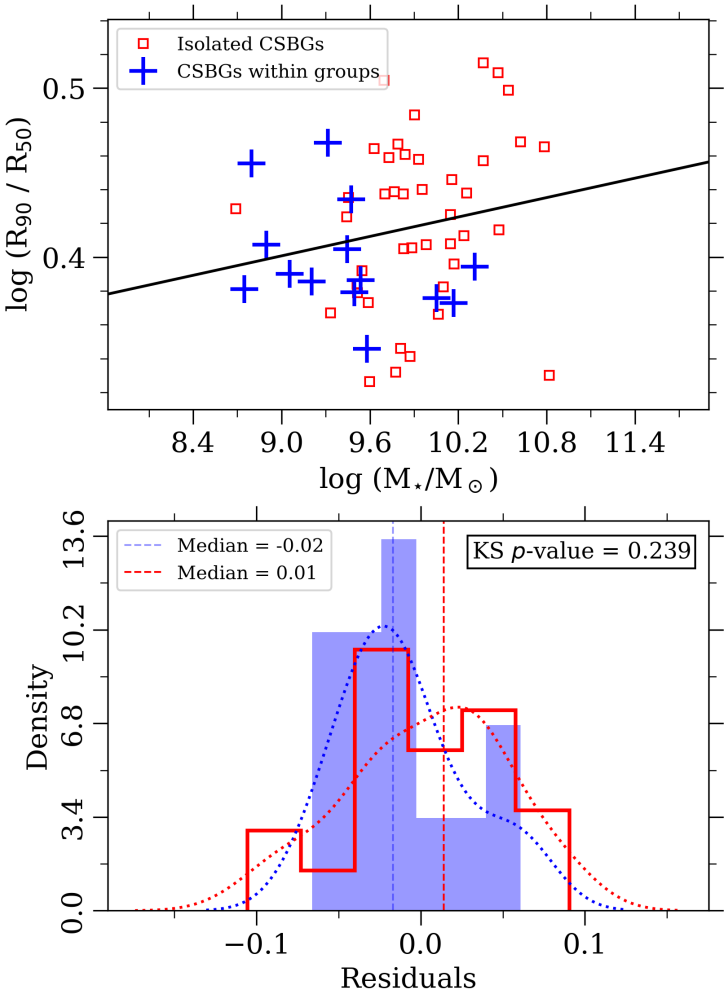


**Figure 4.5:** *Upper panel*: Concentration distribution as a function of stellar mass between CSBGs in groups of star-forming galaxies (blue targets) and isolated CSBGs (red squares). The black line represents the linear fit of the values of the two populations. *Bottom panel*: histogram of the residual of this fit, together with a Gaussian-type kernel density estimate (KDE) and the median values of the residuals of each population (dashed vertical lines). In addition, a KS test was performed on the distributions, whose $p$-value is indicated in the upper right corner of the lower panel.

`petroR90_r` and $z_{\mathrm{CSBGs}}$ by its respective redshift. Figure 4.6 shows no difference between the intensity of the surface brightness between isolated and interacting CSBGs.

### 4.2.4 Ionized gas

Using a non-linear least square method (Moré, 1978), we measured the spectra emission line fluxes by fitting a single Gaussian component on each of the continuum-subtracted lines. Within the wavelength range between $4600\,\text{Å} \lesssim \lambda \lesssim 7000\,\text{Å}$ of the spectra from observations at the Gemini Observatory, we detected the H$\beta$, [O III]$\lambda$4959 Å, $\lambda$5007 Å, H$\alpha$, [N II]$\lambda$6548 Å, $\lambda$6583 Å and [S II]$\lambda$6717 Å, $\lambda$6731 Å lines, while for the SDSS spectra

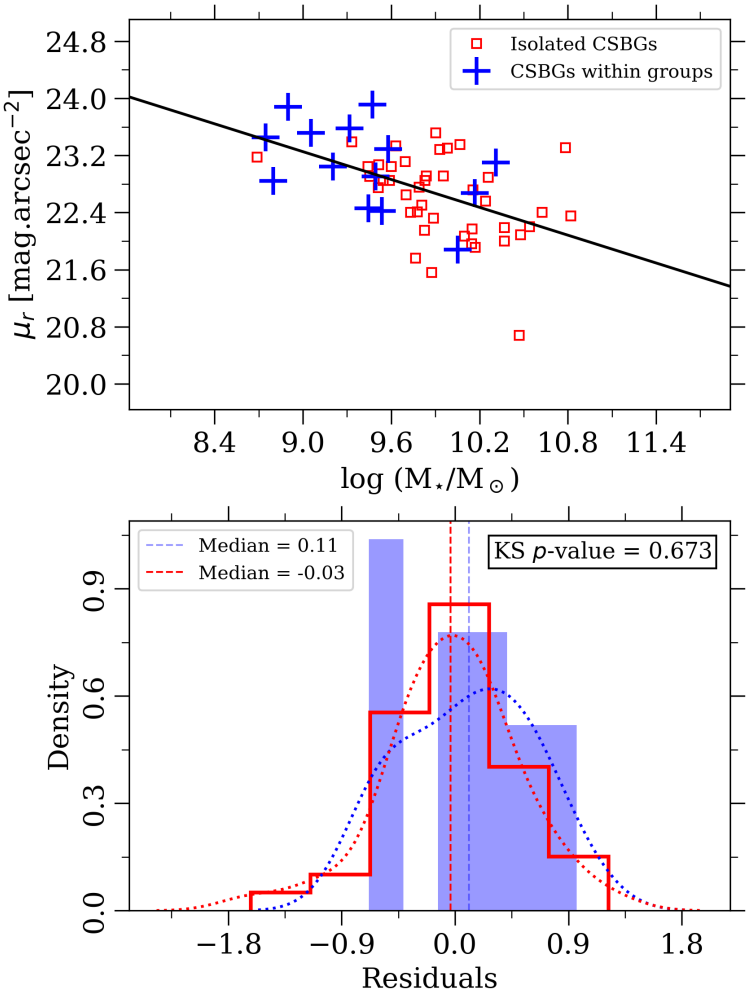


**Figure 4.6:** Distribution of the surface brightness as a function of stellar mass between CSBGs within groups (in blue) and isolated CSBGs (in red). Figure details similar to those described in figure 4.5.

(3700 Å $\lesssim \lambda \lesssim$ 6900 Å), we could also detect the [O II]$\lambda$3726, $\lambda$3729 Å doublet.

To recover the intrinsic flux of the emission lines, which underwent an extinction process by the interstellar medium, we assumed that the theoretical line ratio between H$\alpha$ and H$\beta$ – when there is no extinction and for $T_{\rm gas}$ = 10 000 K, $T_{\rm e^-}$ = 10 000 K and electron density of $N_{\rm e^-}$ = 100 cm$^{-3}$ (case B H I recombination) – would be $\rm F_{H\,\alpha}/F_{H\,\beta}$ = 2.87 (Savage & Mathis, 1979). By assuming the extinction curve of Calzetti et al. (1994), and using $R_V$ = 4.05, we calculate the reddening in the $V$-band through the relationship:

$$A_{\rm V} = 7.98\ \log_{10}\left[\frac{\rm F_{H\,\alpha}}{2.87\ \rm F_{H\,\beta}}\right] . \tag{4.13}$$

Then, the extinction at wavelength $\lambda$ is given by $A_\lambda = q(\lambda)\, A_{\rm V}$, which is used to recover the intrinsic flux $F^\lambda_{\rm int}$:

$$F^\lambda_{\rm int} = F^\lambda_{\rm obs}\ 10^{0.4 A_\lambda} . \tag{4.14}$$

To check the quality of the flux measurements and extinction corrections, we compared the intrinsic flux of the CSBG's emission lines with those measured by Tremonti et al. (2004) and Brinchmann et al. (2004). However, in both works the authors used data from the SDSS Data Release 2, but from the Data Release 6 onwards, the flux calibration is done using the PSF magnitudes of standard stars, instead of using the fiber magnitudes. Consequently, there is an offset between the fiber magnitude (i.e. the magnitude within a 3 arcseconds fiber) and the spectroscopic magnitude for extended objects. Therefore, we used the multiplicative scale factor "spectofiber"(from the SDSS table `GalSpecLine`) to convert the flux back to a photometric scale in this comparison. Figure 4.7 shows that all results agree with a minimum offset of 0.01 dex and a maximum of 0.04 dex, along with a minimum scatter of 0.02 dex and a maximum of 0.16 dex.

To determine the gas ionization source of the CSBGs and the other galaxies within the groups, we used the diagram proposed by Baldwin, Phillips & Terlevich (1981) (hereafter BPT diagram), comparing the [N II]$\lambda$6584/H$\alpha$ and [O III]$\lambda$5007/H$\beta$ line ratios. We also adopt the Kewley et al. (2001) and Kauffmann et al. (2003) separation curves between objects with ionized gas produced by photo-ionization from massive stars and non-stellar ionizing sources. Figure 4.8 shows that all non-isolated CSBGs, their neighbour SFGs (with one exception) and the control sample galaxies lie in the pure star-forming region of the BPT diagram. Moreover, the isolated and non-isolated CSBGs occupy the upper part of the pure star-forming region compared to their neighbouring SFGs, strengthening their starburst nature.

Knowing the gas ionization source of these galaxies, we measured their specific star formation rates (sSFR) calculating, first, the reddening corrected H$\alpha$ luminosity:

$$L_{\mathrm{H}\alpha} = F_{\mathrm{int}}^{\mathrm{H}\alpha}\, 4\pi D_L^2\,, \tag{4.15}$$

where $D_L$ is the galaxy luminosity distance. Then, by using the Kennicutt (1998) conversion factor, we calculate:

$$\mathrm{SFR} = L_{\mathrm{H}\alpha}\, 10^{-41.28}\,. \tag{4.16}$$

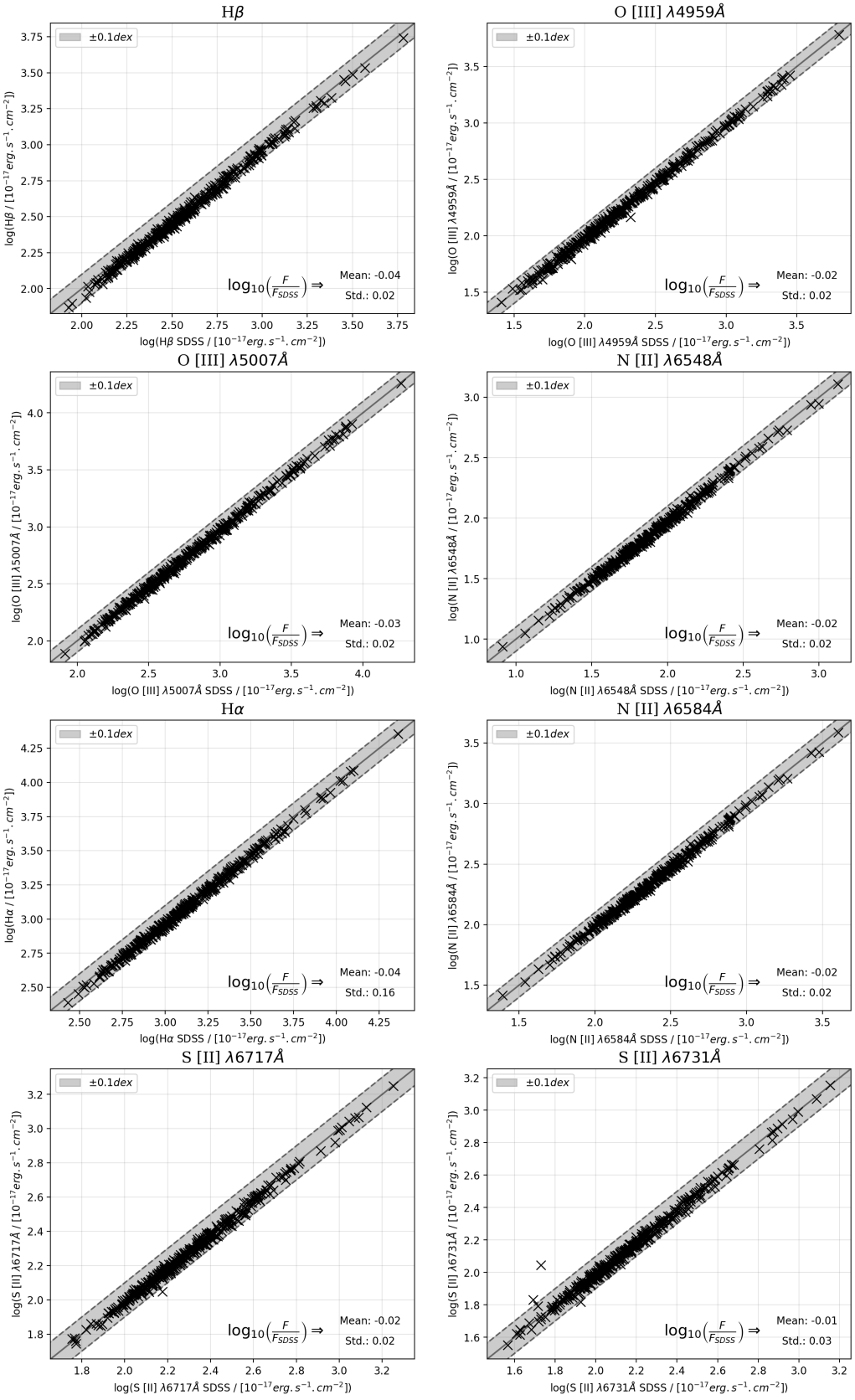


**Figure 4.7:** Comparison between the emission line fluxes measured by us (via the non-linear least square method) and by Tremonti et al. (2004) and Brinchmann et al. (2004) (`galSpecLine` table). The grey region represents a variation of ±0.1 dex to the $y = x$ line. In the lower right corner of each panel are the distribution's means and standard deviations.

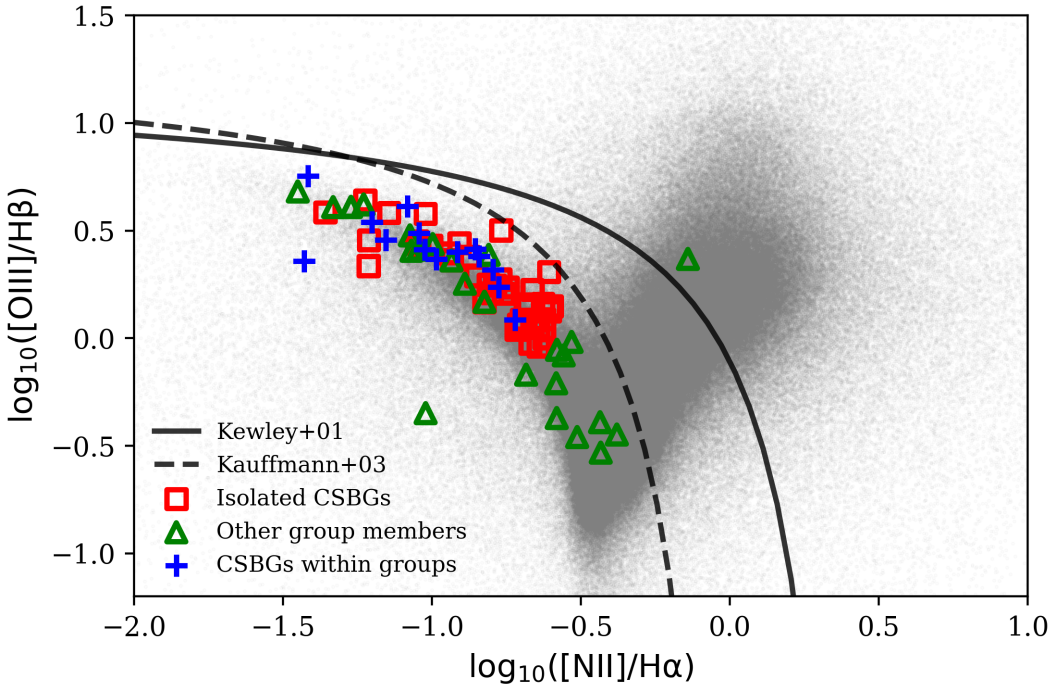


**Figure 4.8:** Distribution of non-isolated CSBGs (blue '+'), their neighbouring SFGs (green triangles) and control sample galaxies (red squares) in the BPT-N II diagram. The SDSS-DR7 galaxy sample is represented by grey dots and is available at `http://wwwmpa.mpa-garching.mpg.de/SDSS/DR7/Data/gal_line_dr7_v5_2.fit.gz`.

Figure 4.9 shows the distribution of sSFR (SFR/$M_\star$) as a function of stellar mass between CSBGs within groups and isolated CSBGs. We found no difference between the sSFR distributions of these two samples. Even with a significant difference in mass between the two samples, the almost identical shape of the residual histograms in the bottom frame of the figure confirms that the specific star-formation rates are very similar.

Since the [O III]$\lambda$4363Å auroral line, necessary for oxygen abundance determinations through the direct method, is too weak in SDSS nearby galaxy spectra (likewise for Gemini spectra, considering the exposure time of our observations), we used an indirect method described in Pilyugin & Grebel (2016) to determine the oxygen abundances of CSBGs and their neighbours. First, we choose the "S" calibration, proposed by Pilyugin & Mattsson (2011), to determine $(\mathrm{O/H})_\mathrm{S} = f(S_2, R_3, N_2)$, where the oxygen $R_3$, nitrogen $N_2$ and sulphur $S_2$ line intensities are defined as:

$$\begin{aligned} R_3 &= (\mathrm{F}_{[\mathrm{O\,III}]}\lambda4959 + \mathrm{F}_{[\mathrm{O\,III}]}\lambda5007)/\mathrm{F}_{\mathrm{H}\beta}\,, \\ N_2 &= (\mathrm{F}_{[\mathrm{N\,II}]}\lambda6548 + \mathrm{F}_{[\mathrm{N\,II}]}\lambda6583)/\mathrm{F}_{\mathrm{H}\beta}\,, \\ S_2 &= (\mathrm{F}_{[\mathrm{S\,II}]}\lambda6717 + \mathrm{F}_{[\mathrm{S\,II}]}\lambda6731)/\mathrm{F}_{\mathrm{H}\beta}\,. \end{aligned} \tag{4.17}$$

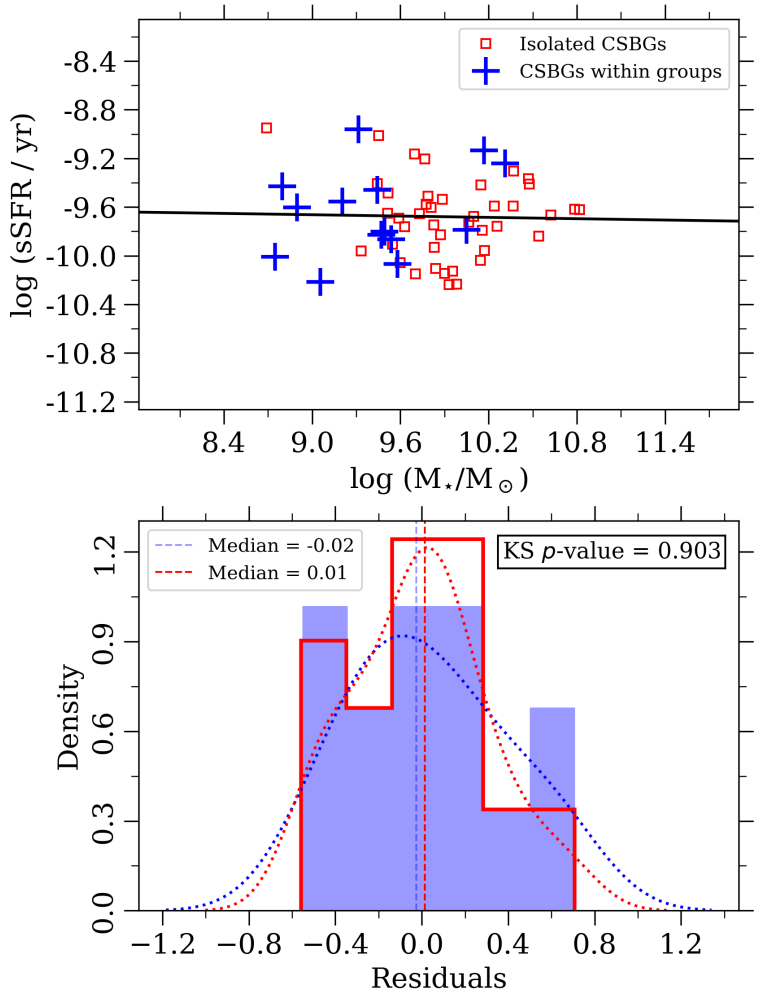


**Figure 4.9:** Distribution of the specific star formation rate (sSFR) as a function of stellar mass between CSBGs within groups (in blue) and isolated CSBGs (in red). Figure details similar to those described in figure 4.5.

Then, we use these relations to determine the oxygen abundance:

$$\begin{aligned} 12 + \log(\mathrm{O/H}) = 8.424 + 0.030\ \log(R_3/S_2) + 0.751\ \log N_2 \\ + [-0.349 + 0.182\ \log(R_3/S_2) + 0.508\ \log N_2] \\ \times \log S_2\,. \end{aligned} \tag{4.18}$$

Figure 4.10 shows the distribution of the oxygen abundance as a function of stellar mass between CSBGs within groups (blue '+') and isolated CSBGs (red squares). We did not find any statistically significant difference between the oxygen abundance of the two samples. It is clear, however, that the oxygen abundance increases with the stellar mass. To identify whether the mass-metallicity relation of the CSBGs follows the relation verified for typical star-forming galaxies, we added two samples of SF SDSS galaxies to the figure. These samples were paired by stellar mass and redshift in a 5:1 ratio to CSBGs

within groups (grey '+') and isolated CSBGs (grey squares), respectively. Both samples were first paired by stellar mass using the `lgm_tot_p50` parameter of the `galSpecLine` SDSS table. After selecting the star-forming galaxies whose stellar mass and redshift values were as similar as possible to the CSBGs, we re-calculated the stellar mass of all galaxies using STARLIGHT and following the methodology presented in section 4.2.1. We found that the mass-metallicity relation for typical SDSS star-forming galaxies (grey line) follows a similar trend to that calculated for CSBGs (black line) but with slightly higher values of oxygen abundance.

Even though the general spectroscopic characteristics between CSBGs and their neighbour SFGs are different, understanding the composition of the gas inside the groups can give clues about the role of interactions in the evolution of their member galaxies. In this context, figure 4.11 shows the variation of the oxygen abundance as a function of stellar mass between galaxies of the same group for each group. In 3/4 of the groups (Groups 1204, 1631, 1854, 2671, 12799, 17182, 15609, 16311, 18766), the galaxy with the lowest oxygen abundance is a CSBG. Even though the CSBG is the least massive galaxy in 5 of these 9 groups, the variation in stellar mass is not significant enough for the mass-metallicity relation to driving the oxygen abundance value (stellar mass ratios ranging between $\sim 1$ and $\sim 7$, except for group 16311 with a stellar mass ratio of $\sim 23$ between the most massive neighbour and the least massive CSBG). We also verified that all members of the '15609' and '17182' groups are far below the mass-metallicity relation fitted over the 3611 CSBGs of Trevisan et al. (in prep.). Interestingly, these two groups are among the three most compact groups in the sample (together with 5073). Besides, groups containing more massive galaxies ($\log(\boldsymbol{M_\star}/\mathrm{M}_\odot) \gtrsim 9.8$) have a large variation in oxygen abundance over a smaller mass range compared to groups containing less massive galaxies. We also emphasize that the oxygen abundance threshold verified at 12+log(O/H)$\sim$ 8.4 for the CSBG sample is a mere consequence of the sample definition due to the *Starburst galaxy criteria* (Sec. 2.1).

Using pPXF, we also extracted gas and stellar kinematics from the spectra of both interacting and isolated CSBGs. We first performed this extraction by masking the emission lines (resulting in stellar kinematics only) and then considering a Gaussian component over the emission lines for the fit (resulting in both stellar and gas kinematics). We present

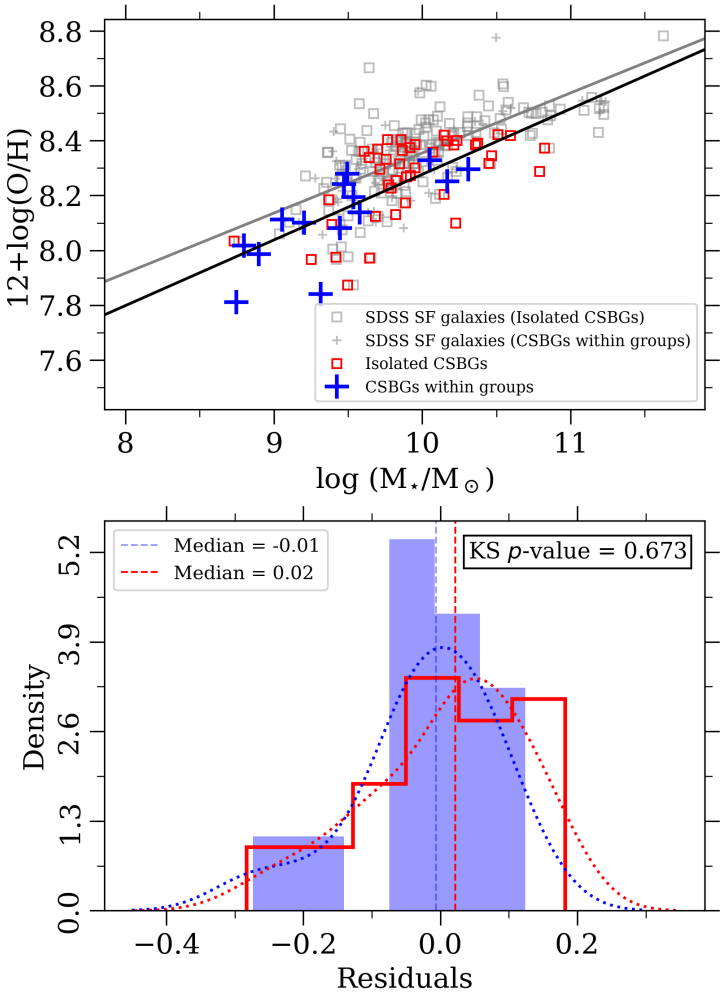


**Figure 4.10:** Distribution of the oxygen abundance as a function of stellar mass between CSBGs within groups (in blue) and isolated CSBGs (in red). The grey markings represent SDSS star-forming (SF) galaxies paired by stellar mass and redshift in a 5:1 ratio to CSBGs within groups (grey '+') and isolated CSBGs (grey squares), respectively. While the black line represents the linear fit of the values of the two CSBG populations, the grey line represents this same fit for the two populations of star-forming SDSS galaxies. Figure details similar to those described in figure 4.5.

the results in table 5.

Finally, we measured the $O_{32}$ ratio, defined by $I([\mathrm{O\,III}]\lambda5007\,)$ / $(I([\mathrm{O\,II}]\lambda3727\,) + I([\mathrm{O\,II}]\lambda3729\,))$ for all galaxies that have spectra available in SDSS (since the doublet $[\mathrm{O\,II}]\lambda3727$ and $[\mathrm{O\,II}]\lambda3729$ are not within the wavelength range of our Gemini observations). Figure 4.12 shows us this ratio as a function of the logarithm of the sum of the equivalent widths of the $[\mathrm{O\,III}]\lambda5007$ Å and H$\beta$ emission lines (whose relation between these two parameters indicates the ionization potential of the galaxy, e.g., Nakajima et al., 2020) for isolated and non-isolated CSBGs and the neighbouring SFGs. Knowing that the grey dots in the figure represent typical star-forming galaxies from the SDSS and that

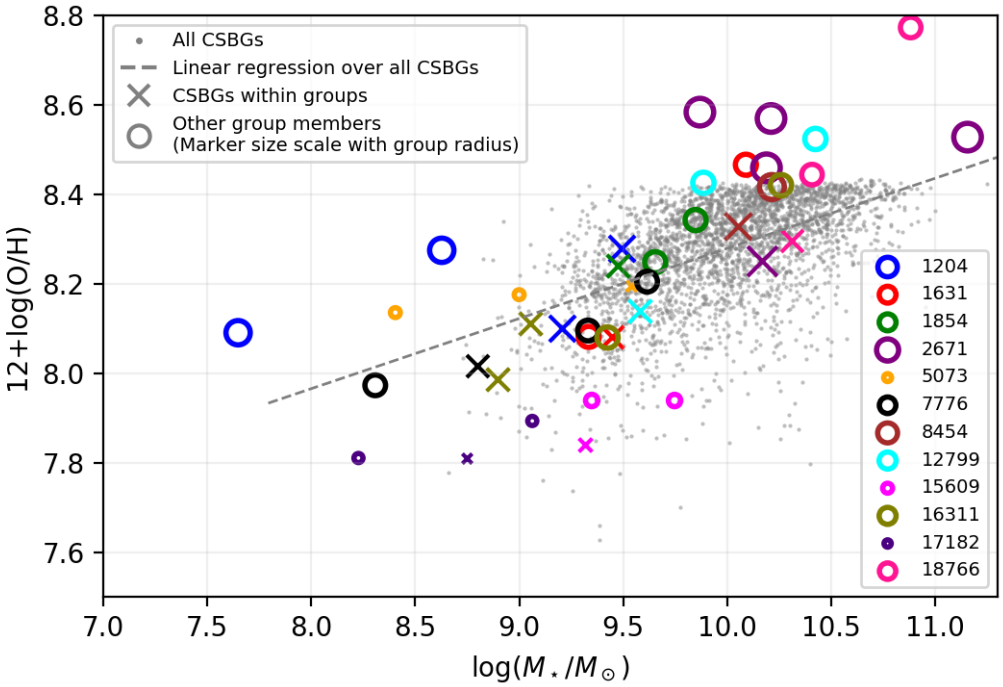


**Figure 4.11:** Oxygen abundance as a function of stellar mass between members of a same group for each group. We also fitted a linear regression over the 3611 CSBGs of our sample (dashed gray line). The "X" and "O" markers represent the CSBGs and neighbour SFGs of the group, respectively. The size of the colored markers is proportional to $R_{\mathrm{group}}$.

they were paired by redshift and by mass with each sub-sample in a 5:1 ratio, it is evident that CSBGs have a higher ionization potential compared to SFGs. Moreover, CSBGs within groups seem to occupy the same region as their isolated counterparts (except with CSBG 15609, with a more intense ionization potential). As for the other members of the groups, with few exceptions, they seem to occupy the same region as the SDSS SFGs.

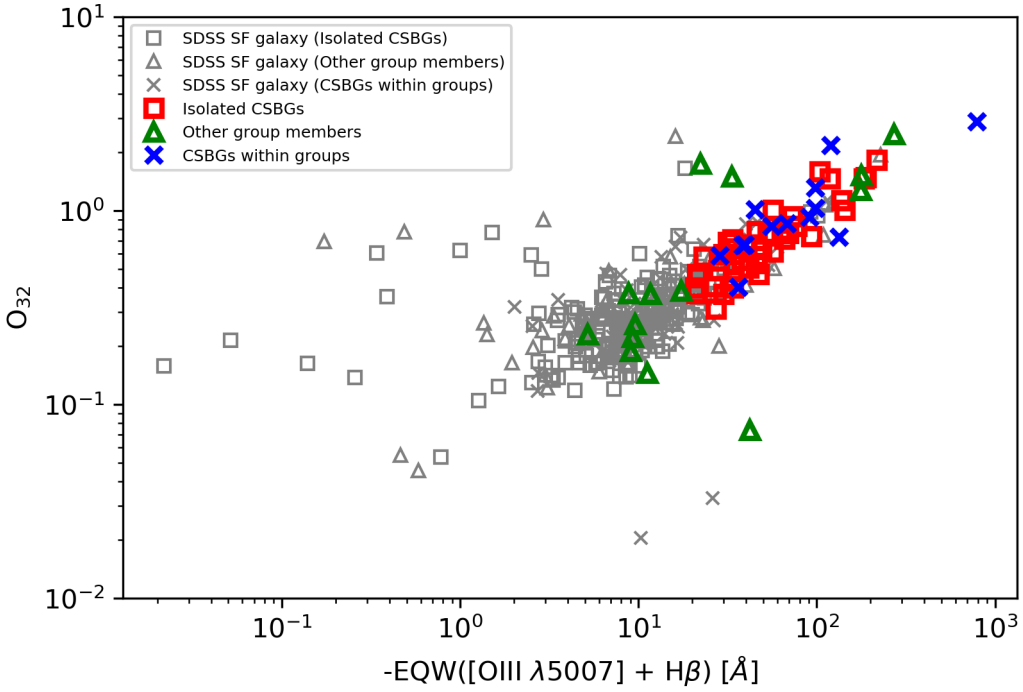


**Figure 4.12:** $O_{32}$ ratio as a function of the logarithm of the sum of the equivalent widths of [O III]$\lambda$5007 Å and H$\beta$ emission lines (using SDSS measurements in both cases) for: i) isolated CSBGs (red squares); ii) CSBGs within groups (blue 'x'); iii) the other group members (green triangles); and iv) star-forming SDSS-DR7 galaxies, paired by mass and redshift in a 5:1 ratio.

# 5 DISCUSSION

In this chapter, we discuss the results presented in chapter 4. First, we focus on addressing interesting aspects and properties of each group in our sample individually. We then discuss the role of the group environment and galaxy-galaxy interactions in the formation and evolution of CSBGs.

## 5.1 Groups of star-forming dwarf galaxies containing at least one CSBG

Below, we describe the main properties, interesting aspects and previous studies of each group in our sample. All of them are included in one or more catalogues of compact groups of galaxies (McConnachie et al., 2009), emission-line galaxies (Chang et al., 2015) and potential merging systems (Tempel et al., 2017).

**Group 1204:** It contains four spectroscopically-confirmed members, among them two CSBGs. The other two SFGs had their spectra taken via observations at the Gemini Observatory (GS2018/01). It meets two of the three isolation criteria at a distance of approximately 785 kpc from the nearest massive galaxy. It is also the farthest group to a filament, being at a distance of $9.635\,h^{-1}\,\mathrm{Mpc}$ from the axis of the nearest filament, with a luminosity ("L0.5 fil." in table 1) of $3.390 \times 10^{10}\,h^{-2}\,\mathrm{L}_{\odot}$. The two galaxies at the centre of the group (see figure 2.1) are at a projected distance of $d = 13.93\,\mathrm{kpc}$ and $\Delta v \approx 18\,\mathrm{km\,s^{-1}}$ from each other. One of them is a CSBG (RA/DEC: [208.6339, -2.8501]) and its neighbour (RA/DEC: [208.6391, -2.8488]), a galaxy with signs of morphological perturbation (presumably due to tidal effects), such as a clumpy surface brightness and asymmetric tails, one of which is stretched towards the CSBG. There are no apparent signs of morphological perturbations in the closer CSBG besides a not-so-regular brightness profile compared to the other CSBGs in the sample. Regarding the tidally disrupted neighbour, it has the youngest stellar population in the sample, with a weighted geometric mean age of only 3 Myr. Unfortunately, we did not measure its SFH, as its spectrum was obtained from Gemini observations, whose wavelength range is narrower (see more details

in Sec. 4.2.2). This group also contains the least massive galaxy measured in our sample (RA/DEC: [208.6618, -2.8686]), with $\log(M_\star/\mathrm{M}_\odot) = 7.65$. However, its spectrum has a low signal-to-noise ratio due to its low surface brightness. Thus, it is only possible to identify its emission lines (and therefore confirm that it is part of the group) but not the stellar continuum. Finally, the group has the lowest surface brightness (i.e., the highest $\mu_r$ value) in the $r$-band (Eq. 4.7) compared to other groups in the sample.

**Group 1631:** This group contains one CSBG out of three spectroscopically confirmed members, all with spectra available in the SDSS. It does not meet any isolation criteria, being at a distance of approximately 468 kpc from the nearest massive galaxy. The two galaxies in the lower left region of the group image in figure 2.1 are at a projected distance of $\sim 20\,\mathrm{kpc}$ and velocity separation along the line of sight of $\Delta v \approx 78\,\mathrm{km\,s^{-1}}$ from each other. The smallest one (RA/DEC: [33.2291, -0.9052]) appears to show faint signs of morphological perturbation (clumpy and asymmetric surface brightness), while the largest (RA/DEC: [33.2231, -0.9085]) is a spiral galaxy without any apparent signs of morphological perturbation.

**Group 1854:** It contains three spectroscopically confirmed members, including one CSBG, all with spectra available on the SDSS. It does not meet any isolation criteria, being at a distance of approximately 391 kpc from the nearest massive galaxy. It is included in the Haynes et al. (2018) neutral hydrogen gas mass catalogue, with $\log(\mathrm{MH_{tot}}/\mathrm{M}_\odot) = 9.89$, equivalent to a gas fraction of $f_{\mathrm{gas}} = \frac{\sum_i^{N_{\mathrm{gal}}} M_{\mathrm{HI,i}}}{\sum_i^{N_{\mathrm{gal}}} (M_{\mathrm{HI,i}} + M_{\star,\mathrm{i}})} = 0.35$.

**Group 2671:** It is the largest ($R_{\mathrm{group}} = 81.9\,\mathrm{kpc}$), most numerous (five galaxy members) and most distant ($z = 0.175$) group of the sample. Among its 5 members, there is a CSBG and 4 SFGs whose spectra were obtained in the GS2018/01 observation. Among the 4 neighbours, there is a massive galaxy ($\log(M_\star/\mathrm{M}_\odot) = 11.16$, an exception to the rule about the exclusivity of dwarf galaxies within the groups ($\log(M_\star/\mathrm{M}_\odot) < 10.5$ for galaxies whose stellar masses were measured using the Vazdekis et al. (2015) models, 0.5 dex more than the value described in Section 2.1 due to an overestimation of the stellar mass measured by STARLIGHT in relation to the mass `lgm_tot_p50` collected from the SDSS table `galSpecExtra`). It fulfils two of the three selection criteria, with the most distant massive galaxy being 742 kpc away. In figure 2.1, we first identified that all neighbours have a less bluish colour than other galaxies of different groups. However,

they still respect the colour criterion according to the colour-magnitude diagram of figure 2.2. The SFG of coordinates RA/DEC: [194.7307, 12.79342] has the highest sSFR of the entire sample, including the CSBGs. Furthermore, from figure 2.1, we also observe an evident tidal disruption in the morphology of the galaxy with coordinates RA/DEC: [194.7307, 12.79342] (central galaxy of the triplet on the left in the figure), in which its two spiral arms are stretched towards their nearest neighbouring galaxies. On the other hand, the galaxy near the centre of the image (RA/DEC [194.7254, 12.7889]) stands out for having the highest stellar metallicity and the fourth-highest oxygen abundance value of the entire sample. Finally, we point out that this group is included in the catalogue of Hickson-like groups of McConnachie et al. (2009).

**Group 5073:** Second most compact group in the sample ($R_{\rm group} = 10.53\,$kpc) containing one CSBG out of three spectroscopically confirmed members. It fulfils only one of the three isolation criteria, with the nearest massive galaxy at a distance of 366 kpc. It also has a neutral hydrogen gas mass of $\log(M_{\rm HI}/{\rm M}_\odot) = 9.83$ ($f_{\rm gas} = 0.59$). The small size of the group and the fact that the two galaxy members have an extremely young stellar population (weighted geometric mean age of 3 Myr and 5.14 Myr) characterizes the group for having the highest surface brightness (Eq. 4.7) of the entire sample. Furthermore, the group has the smallest velocity dispersions among all groups ($\sim 42.4\,{\rm km\,s^{-1}}$, according to equation 4.4) and second smallest ($\sim 36.6$ km s$^{-1}$, according to equation 4.5), in addition to the smallest virial mass ($\log(M_{\rm vir}/{\rm M_{group}}) = 10.45$, according to equation 4.6). Such low-velocity dispersion values indicate that these galaxies will likely merge. It is also the closest group to a filament, being only $0.317\,h^{-1}\,$Mpc from the axis of the nearest filament, with a luminosity ("L0.5 fil." in table 1) of $3.861\times10^{10}\,h^{-2}\,{\rm L}_\odot$. The neighbour bluish galaxies RA/DEC: [224.5114, 5.0981] and RA/DEC: [224.5109, 5.0916] are at a distance of $d = 10.25\,$kpc, $\Delta v \approx 51\,{\rm km\,s^{-1}}$ and $d = 19.02\,$kpc, $\Delta v \approx 24\,{\rm km\,s^{-1}}$ from the CSBG (RA/DEC: [224.5142, 5.0965]), respectively. In both cases, we see signs of morphological perturbations, with a clumpy surface brightness and interstellar material stretched towards the CSBG. However, the CSBG itself remains morphologically undisturbed.

**Group 7776:** One CSBG out of four spectroscopically confirmed members, one of them being confirmed with Gemini observations (GN2019/02). It fulfils all isolation criteria, with the nearest massive galaxy at a distance of 1.2 Mpc. The group has two me-

asures of H I in the ALFALFA catalogue: $\log(M_{HI}/M_\odot) = 10.26$ and $\log(M_{HI}/M_\odot) = 9.93$, centered on coordinates RA/DEC: [24.0771, 13.9508] and RA/DEC: [24.0525, 13.9617], respectively. Taking the sum of these two measurements, the total H I mass of the group is $\log(M_{HI}/M_\odot) = 10.43$ ($f_{gas} = 0.79$), the highest among all groups. The group's CSBG was classified as a "Dwarf Amorphous Nuclear Starburst" in a detailed photometric study of emission-line galaxies in low-density regions (object HS 0133+1341 from Vennik et al., 2000).

**Group 8454:** It contains three spectroscopically confirmed members, among them one CSBG. It does not meet any isolation criteria, being at a distance of approximately 216 kpc from the nearest massive galaxy. It is the group whose nearest filament is the brightest in the sample, being at a distance of $1.970\,h^{-1}$ Mpc from the axis of the nearest filament, with a luminosity ("L0.5 fil." in table 1) of $39.813\times10^{10}\,h^{-2}\,L_\odot$. One of its member galaxies (RA/DEC: [240.9227, 16.5246]) has the oldest stellar population in the entire sample, with a weighted geometric mean age of 2.01 Gyr. Indeed, in the colour-magnitude diagram of figure 2.2 this galaxy lies very close to the red sequence region, but it is still below the $4\sigma$ line, as required. The strength of the H$\delta$ absorption line (using the Lick H$\delta_A$ index from Worthey & Ottaviani, 1997 and collected from the `lick_hd_a` parameter within de SDSS Table `galSpecIndx`) indicates that this object as a post-starburst galaxy ($H\delta_A > 4$). Furthermore, the group has the highest velocity dispersion among all groups ($\sim 500\,km\,s^{-1}$ and $\sim 560\,km\ s^{-1}$, according to the equations 4.4 and 4.5, respectively). The high velocity dispersion suggests that this object may not be gravitationally bounded.

**Group 12799:** It has three spectroscopically confirmed members, including one CSBG. It fulfils all isolation criteria, with the nearest massive galaxy at a distance of 1.4 Mpc. The distance between the CSBG and its nearest neighbour (on the left in the image 2.1) is only $d = 16$ kpc and $\Delta v \approx 85\,km\,s^{-1}$. Analyzing figure 2.1, we highlight that this nearest neighbour (RA/DEC: [193.5722, 39.1993]) has an evident sign of morphological perturbation: a tail in the lower region of the galaxy, probably related to tidal effects. Once again, the CSBG remains without any sign of morphological perturbation. Furthermore, CSBG 12799 has the second lowest sSFR among all CSBGs.

**Group 15609:** Three spectroscopically confirmed members, including one CSBG. It fulfils two of the three isolation criteria, with the nearest massive galaxy at a distance of

646 kpc. It is the third most compact group in the sample ($R_{\rm group}$ = 16.54 kpc). Its CSBG has the highest sSFR (log(sSFR/yr) = -8.9591) and the highest $O_{32}$ ratio ($O_{32}$ = 2.54) among all CSBGs, in addition to being the most concentrated galaxy of the entire sample. It is only $d$ = 15.4 kpc, $\Delta v \approx 121\,{\rm km\,s^{-1}}$ and $d$ = 23.8 kpc, $\Delta v \approx 34\,{\rm km\,s^{-1}}$ away from its two neighbours, respectively, but does not show signs of morphological perturbation (Fig. 2.1). In particular, the neighbour galaxy of coordinates RA/DEC: [131.3605, 53.1545] is very clumpy and irregular, which could be related to tidal interactions. Looking at figure 2.1, we can see an intriguing bluish region between the three galaxies inside the circle representing the group's radius: most likely diffuse stars ripped from the outer regions of galaxies due to tidal interactions. Pearson et al. (2016), using observational data, identified H I gas bridges in 7 out of 10 pairs of dwarfs galaxies, with unbridged pairs being at larger separations (> 40 kpc). Finally, it is worth mentioning that the CSBG of this group is part of a sample of H-$\alpha$ emitters that are local analogues to $z > 4$ SFGs in Shim & Chary (2013) and is also part of a sample that photometrically analyzes the infrared properties of 781 Wolf-Rayet galaxies Chen et al. (2018).

**Group 16311:** Two CSBGs out of four spectroscopically confirmed members. It does not meet any isolation criteria, being at a distance of approximately 311 kpc from the nearest massive galaxy. Has a neutral hydrogen gas mass of $\log(\mathrm{MH_{tot}/M_\odot}) = 9.84$ ($f_{\rm gas}$ = 0.23). The CSBG with coordinates RA/DEC: [184.1644, 14.2603] is part of a study on the influence of environments of different densities on the chemical abundances of dwarf galaxies (Douglass et al., 2018). Furthermore, the neighbour galaxy at coordinates RA/DEC: [184.1765, 14.2778] is the least concentrated galaxy in the sample.

**Group 17182:** It is the most compact group in the sample ($R_{\rm group}$ = 8.93 kpc), the second brightest and contains one CSBG out of three spectroscopically confirmed members. It fulfils only one of the three isolation criteria, with the nearest massive galaxy at a distance of 203 kpc. The triplet occupies positions 1, 2 and 4 among the most metal-poor galaxies in the sample (12+log(O/H) = 7.81, 7.81 and 7.89, respectively), and the galaxy with coordinates RA/DEC: [46.2595, -0.0816] has the highest ionization potential of the whole sample ($O_{32}$ = 2.55). Interestingly, the sum of the stellar masses of the three galaxies is the smallest among all groups ($\log(M_{\star,\rm tot}/\mathrm{M_\odot}) = 9.27$). It is a group of low-mass galaxies characterized by very young stellar populations and supposedly

undergoing synchronous star formation. Indeed, when we analyze the figures 4.3 and 4.4, we verify a recent burst of star formation in all three galaxies and little presence of stellar populations of intermediate/old age.

**Group 18766:** It contains three spectroscopically confirmed members, among them one CSBG. It does not meet any isolation criteria, being at a distance of approximately 438 kpc from the nearest massive galaxy. According to the BPT diagram (Fig. 4.8), the neighbouring galaxy with coordinates RA/DEC: [123.6841, 36.6112] is an AGN, which also has the highest oxygen abundance of the entire sample (12+ log(O/H) = 8.77). The three members of the group are among the five most massive galaxies in the sample, including the most massive CSBG ($\log(M_\star/M_\odot)$ = 10.3). Furthermore, the group has the smallest and second smallest velocity dispersions according to equations 4.4 and 4.5, respectively.

## 5.2 The gas-rich group environment

As discussed in chapter 1, the intense bursts of star formation that characterize CSBGs must be directly linked with the amount of gas in these galaxies. Indeed, as can be seen in table 1, the neutral hydrogen gas fraction is high both in groups of star-forming dwarf galaxies and in isolated CSBGs. When we compare the specific star formation rates between isolated and non-isolated CSBGs (Fig. 4.9), we found no differences between these samples. Roychowdhury et al. (2022) when investigating pairs and groups of galaxies using both ALFALFA and DINGO (Deep Investigation of Neutral Gas Origins; Meyer, 2009; Duffy et al., 2012) H I 21 cm surveys, found large amounts of atomic hydrogen in the intergalactic space of low mass groups, i.e., not associated with any catalogued galaxy. They conclude, also based on Borthakur et al. (2010, 2015) work on large amounts of diffuse H I gas found in Hickson Compact groups, that the observed distribution of the gas was likely of tidal origin. Moreover, Marasco et al. (2016) using the cosmological hydrodynamical simulator EAGLE (*Evolution and Assembly of GaLaxies and their Environments*; Crain et al., 2015; Schaye et al., 2015) verified that satellite-satellite interactions are more effective at removing H I gas than ram pressure stripping or tidal stripping from a galaxy halo. The gas removal is perhaps not only caused by tidal interactions, as identified in some groups of figure 2.1, but also by stellar feedback. Even though Bradford et al. (2015)

found that stellar feedback is an insufficient mechanism to remove all gas from isolated low-mass galaxies, perhaps tidal effects contribute to the outflow of gas from galaxies in dense environments. This is the result found by Pearson et al. (2016) while investigating the role of the environment in removing gas from dwarf-dwarf systems: most dwarf galaxy pairs in their sample have more extended and dense gas envelopes compared to single dwarf galaxies. From this result, the authors conclude that dwarf-dwarf interactions move gas to the outskirts of these galaxies, "parking" them at larger distances.

In the same work of Pearson et al. (2016), the authors also conclude that the gas removed from the galaxies and found in the intragroup medium remains bound to these systems (if there are no massive galaxies nearby). Then, they suggest that this gas will be re-accreted by the member galaxies of the system, providing fuel for future star formation. This hypothesis is also a possible explanation for the difference in stellar mass observed between CSBGs within groups relative to their isolated counterparts: the gas shared between the group's members serves as fuel for star formation during more extended periods than the gas directly consumed and more efficiently re-accreted by isolated CSBG, i.e., the long-term star-formation efficiency between both samples is different. In this context, isolated CSBGs would already have formed more stars throughout their cosmic history, even if the current star formation rate between CSBGs in these different environments does not show any distinction. One interpretation for this possible difference in the gas depletion time is related to the different shapes of the potential wells of these systems: pairs and groups of galaxies have shallower potential wells compared to isolated CSBGs. Hence, the gas expelled from an isolated CSBG is more easily re-accreted by its own deeper potential well than the gas removed from CSBGs within groups.

Another possibility for the origin of neutral gas in galaxies is related to the inflow of filamentary gas. Weisz et al. (2011), in a study of resolved stellar populations in nearby dwarf galaxies, found that their star formation histories are inconsistent with a simple closed-box model. Indeed, the SFHs measured for the isolated CSBGs show a complex behaviour, far from the typical characteristics for such a simple model, e.g., a single star-formation burst, constant sSFRs, and exponentially declining SFRs. To verify whether the gas inflow is significant in our groups of star-forming dwarf galaxies, we first tried to identify the position of both isolated and non-isolated CSBGs in the large-

scale structures of the universe (e.g. voids, sheets, filaments and knots). To do that, we used the spatial distribution of all galaxies from the Sloan Digital Sky Survey between $0 < z < 0.06$. As described in section 4.1.3, the groups appear to be in the outer regions of filaments and knots, and some isolated CSBGs can also be found in voids. To quantify the position of our galaxies relative to the large-scale structure, we used the catalogue of filaments built by Tempel et al. (2014). We verified that the groups of galaxies are all at distances ("Dist. fil."in table 1 and 4) greater than 300 kpc from their respective nearest filaments, and the luminosity ("L0.5 fil."in table 1 and 4) of these filaments does not exceed $L_{0.5} < 7 \times 10^{10}\, h^{-2} \mathrm{L}_{\odot}$ (except for group 8454 with $L_{0.5} \approx 25 \times 10^{10}\, h^{-2} \mathrm{L}_{\odot}$). In the control sample, on the other hand, the closest filaments tend to be brighter, and 7 out of the 42 isolated CSBGs are found at distances smaller than 300 kpc. Using Barnard (1945) and Fisher (1945) statistical tests, we compared the fractions of isolated and non-isolated CSBGs at distances greater than 300 kpc from their nearest filaments. Both tests indicated that there is no statistically significant difference between these distances.

## 5.3 Are interactions triggering bursts of star formation in CSBGs?

As predicted in numerical simulations (Patton et al., 2013) in which bursts of star formation are triggered by each pericentric passage of two interacting massive galaxies (which persists as the galaxies move to larger separations), we also find synchronicity in the bursts of star formation for the galaxies within the groups of our sample: figures 4.3 and 4.4 show the SFH (independently determined) of each galaxy (which have spectra available in the SDSS) of each group of the table 1. Since our sample consists of star-forming and starburst galaxies, the stellar continuum of most galaxies is dominated by massive stars, which have very few and weak absorption features, except for the hydrogen lines, which also appear in emission. For this reason, we focus on the results presented in figure 4.4, which shows the SFHs inferred by fitting the stellar continuum and a gas component, assuming a single Gaussian component to fit each emission line (i.e., without masking them, as in the case of figure 4.3). We point out, however, that the galaxy with coordinates RA/DEC: [123.6841, 36.6111] of group 18766 is classified as an AGN (according to the BPT diagram of figure 4.8). In this case, a single Gaussian component to

fit the emission lines is not enough, as it does not consider the broad emission component. Two Gaussian components would be necessary to reproduce their emission lines correctly.

To simplify the discussion about the star formation histories of the galaxies in figure 4.4, we will classify the age of each of the stellar populations formed over time as follows: between 0.001 and 0.01 Gyr as "very young"; between 0.01 and 0.1 Gyr as "young"; between 0.1 and 1 Gyr as "intermediate"; and between 1 and 14.1 Gyr as "old". First, we highlight some examples of synchronous bursts of star formation: in the group 1204, each burst of star formation of one of the member galaxies is followed by a similar event from its companion. In group 7776, in turn, we also found in three of the four galaxies intense synchronous star formation bursts only between 0.01 and 1 Gyr. When we compare with the LEGACY Survey images of figure 2.1, we verify that two galaxies of this same group (RA/DEC: [24.0604, 13.9679] and RA/DEC: [24.0632/13.9453]) have disturbed morphologies, possibly related to tidal effects. Unfortunately, we cannot accurately reproduce the dynamics of these four members throughout their cosmic history. However, the evidence of morphological perturbations and the similarities in the SFHs of these galaxies are strong indications that this group is in a more advanced dynamical state. This same hypothesis is valid for the 17182 group, with bursts of star formation from all its galaxies occurring in a small time interval. In this case, we emphasize that this group is the most compact in our sample, with $R_{\rm group} = 8.92\,{\rm kpc}$.

We also highlight the presence of an old population in practically all galaxies of figure 4.4. This is expected, as in the vast majority of cases, Blue Dwarf Galaxies (BDGs) are old galaxies that formed a significant fraction of their stars several Gyr ago but are currently experiencing a starburst of a sequence of similar events (Mamon et al., 2019). Even among the most metal-poor galaxies known in the literature (e.g. "I Zw 18"), there is a huge debate about the existence or not of an old population overshadowed by the light of younger populations (e.g. Papaderos et al., 2002; Izotov & Thuan, 2004; Aloisi et al., 2007; Contreras Ramos et al., 2011). In figure 4.4, we observe this sequence of star formations extending throughout the entire history of most galaxies. In particular, we highlight groups 1631 and 1854 that, in addition to having bursts of star formation in all four previously defined age intervals, also have homogeneous star formation rates throughout their cosmic history. Another intriguing feature in this figure is the presence

of synchronous star formation gaps between neighbour galaxies: group 1204 does not have intermediate-age populations in any of its members, while groups 7776, 12799, 15609 and 17182 do not have older populations (between 1 and 10 Gyr), which gives us clues about the dynamical age of the group and the history of galaxy-galaxy interactions.

Bekki (2008), who performed several numerical simulations on the formation of Blue Compact Dwarfs (BCDs), found that these galaxies may be the product of mergers between gas-rich dwarf galaxies with extended H I gas discs. Furthermore, the BCD characteristic of being compact is probably related to the colours of these galaxies becoming dominated by young stellar populations due to starbursts triggered by merging. Thus, isolated CSBGs can also be the product of past mergers: as described earlier, the SFHs of these galaxies are complex, which may also be linked to past interactions and mergers in their cosmic histories. In this scenario, our groups can represent an earlier stage of the isolated CSBGs. Looking at the velocity dispersions of galaxies within groups, this is a likely future scenario for most of these groups, and the resulting post-merger galaxy would be gas-rich and maintain the star-forming activity as observed in isolated CSBGs. This merger scenario of star-forming and gas-rich dwarf galaxies strengthens the idea that these systems are local analogues of interacting high-$z$ SFGs (galaxies that, when merged, result in the intermediate-mass star-forming galaxies that we find in the current Universe).

## 5.4 How do interactions influence the chemical evolution of CSBGs?

To investigate if gas-rich environments affect the chemical evolution of CSBGs, we compare the oxygen abundances of isolated and non-isolated CSBGs (Sec. 4.2.4). Figure 4.10 shows this comparison, in which the $p$-value of the KS test indicates no statistically significant difference between the oxygen abundances of both samples. This result indicates that, regardless of the efficiency of the neutral gas inflow and/or outflow and the intensity of the star formation bursts in CSBGs (which is also similar between the two samples, as shown in figure 4.9), the interactions do not play a central role in the chemical evolution of CSBGs. On the other hand, figure 4.11, shows the variation of the

oxygen abundance as a function of stellar mass between galaxies of the same group for each group. As described in section 4.2.4, we see a tendency for CSBGs to have lower oxygen abundance compared to the other members of the groups, with no significant mass variation between them. In this case, a possible explanation is that the high concentration of CSBGs makes their potential well deeper than their companions, increasing the efficiency of gas accretion, both filamentary and from neighbour galaxies. In this context, the accreted low-metallicity gas would be diluting the gas present in the interstellar medium of the CSBG, making it less metal-rich than the other group members. On the other hand, this difference between the oxygen abundances of CSBGs and their neighbours may also be linked to the high ionization potential of CSBGs (Fig. 4.12), whose indirect method of Pilyugin & Mattsson (2011) may not have the ideal calibrations for such extreme galaxies. Besides, two groups ('15609' and '17182') are far below the mass-metallicity relation fitted over the 3611 CSBGs of Trevisan et al. (in prep.), and these two groups are also among the three most compact groups in the sample. This suggests that although interactions do not play a central role in the chemical evolution of CSBGs, perhaps even more extreme environments (in this case, smaller group radii) result in more noticeable variations in the chemical abundances of their member galaxies.

In this scenario, there is a large number of published studies describing the role of interactions in different galaxy systems, i.e., pairs, groups and galaxy clusters (e.g. Noeske et al., 2001; Pearson et al., 2016, 2018; Privon et al., 2017b). Using cosmological simulations, Martin et al. (2021) investigated how mergers and fly-bys drive the mass assembly and structural evolution of dwarf galaxies in groups. The authors found that mergers and interactions typically drive moderate increases in the SFR of these galaxies (3 or 4 times at $z = 1$) for low and intermediate redshifts ($z < 3$). Moreover, the authors also found that non-merger interactions increase the SFR of these galaxies by around two times. However, given their higher frequency relative to mergers, these interactions still account for around 10 per cent of stellar mass formed in the dwarf regime. Stierwalt et al. (2015b), on the other hand, carried out an observational study of star formation and subsequent processing of the interstellar medium of 104 pairs of dwarf galaxies. They verified an SFR enhancement on these galaxies by a factor of 2.3 ($\pm$0.7) at pair separations $< 50$ kpc relative to unpaired analogues, with a decrease in this factor with increasing pair separation (as large as 100 kpc). Besides, starbursts were identified in 20% of the dwarf

pairs, compared to only $6\% - 8\%$ of the matched unpaired dwarfs. The authors also found that starbursts are more commonly triggered in the lower mass member of the pair. This result agrees with our work: the CSBG is not the most massive galaxy in 10 out of the 12 groups in our sample. Pearson et al. (2016), however, points out that in the work of Stierwalt et al. (2015b), the authors did not look into pair separation bins smaller than 50 kpc, which could bias the results. Then, investigating four pairs of dwarf galaxies with separations $< 20$ kpc, Pearson et al. (2016) found no sign of a systematic increase in SFRs compared to more separated dwarf pairs. This result agrees with what we found about the sSFRs between CSBGs within groups compared to isolated CSBGs (Fig. 4.9).

## 5.5 Caveats

Since Gemini observations cover a narrower wavelength range (4640Å−6939Å) compared to SDSS spectra (3700Å−6900Å), their stellar population ages slightly differ from each other. In the interval between 3700Å−4640Å, there are some critical features for determining the contribution of the stellar component to these galaxy spectra, among them, the 4000Å break. Consequently, the ages inferred from Gemini spectra tend to be higher than those determined from SDSS spectra, as seen in table 1: in order of stellar population age, galaxies whose spectra were obtained in observations at the Gemini Observatory occupy 7 out of the 8 first positions among all galaxies in the sample.

In the discussion about the morphological stability of CSBGs while interacting with neighbours with clear signs of morphological perturbation due to tidal effects: there is a selection bias where CSBGs were selected to meet the requirement of being "C"ompact. Thus, it is expected that we will not find morphological perturbations in the CSBGs studied in this work. Therefore, we cannot state in our work that CSBGs are more resistant to morphological perturbations caused by interactions than common SFGs. Furthermore, we are limited to the image depth of the surveys available for our dataset. As discussed in the previous sections, there is evidence of morphological perturbations even in CSBGs that would likely appear in deeper surveys. Even so, we consider the existence of CSBGs with faint morphological features in extreme environments as a very relevant topic to be discussed in this work.

# 6 SUMMARY AND CONCLUSIONS

To investigate the effect of the environment and gas-rich interactions on the formation and evolution of Compact Starburst Galaxies (CSBGs), we defined a sample of 67 group candidates using data from the Sloan Digital Sky Survey (SDSS). These groups contain a spectroscopically confirmed CSBG and at least two other star-forming dwarf galaxies. They are compact ($R_{\rm group} < 100\,{\rm kpc}$), and 7 out of the 12 groups are completely isolated, i.e., there are no massive galaxies ($M_\star > 10^{10}{\rm M}_\odot$) within $R < 10R_{\rm group}$ and $\sigma = \pm 3000\,{\rm km\,s^{-1}}$. Besides, there should be no galaxies in the red sequence within $R < R_{\rm group} + 50\,{\rm kpc}$. Among the candidates, only eight had SDSS spectra available for all group members. For this reason, observations were carried out at Gemini South and North Observatories, leading to a sample of 12 spectroscopically confirmed groups, which correspond to the sample studied in this work. We also defined a redshift-paired control sample of 42 isolated CSBGs. We calculated the radius of the groups of star-forming dwarf galaxies, the velocity dispersion of their members, the fraction of neutral hydrogen gas, their surface brightness, total mass density and their position relative to the large-scale structures of the Universe. For isolated and non-isolated CSBGs, as well as neighbour SFGs, we performed stellar population synthesis analysis to determine their stellar masses and SFHs, estimated their specific star-formation rates (sSFR), gas metallicity and ionization properties. Furthermore, we searched for morphological perturbations in the group images and analysed structural parameters such as the concentration, surface brightness and mass density of these galaxies. Below, we summarize the main results of this work:

- **Star formation rates and ionization conditions:** To investigate if CSBGs are more extreme in groups of dwarf galaxies, we compared the sSFRs and ionization parameters between isolated and non-isolated CSBGs. As shown in Figs. 4.8, 4.9, and 4.12, we find that the sSFR and ionizing conditions are very similar between these two samples. These results indicate that the ionizing conditions of CSBGs are more related to processes internal to the galaxy than to environmental effects.

- **Structural parameters:** the group environment does not affect the CSBG morphologies, as indicated by galaxy concentration and surface brightness (Figs. 4.5 and 4.6), although we found several morphological perturbations in the SFG neighbours within groups. However, this conclusion is not straightforward, given that the sample of CSGBs was selected to be compact and have similar morphologies.

- **Gas metallicity:** the oxygen abundance can indicate the origin of the CSBG ISM gas, being more metal-poor if accreted from the cosmic web. Besides, metal-poor CSGBs are more likely to be considered analogues of high-$z$ galaxies. However, most of our CSBGs have normal gas metallicities, as shown in Figs. 4.10 and 4.11. On the other hand, compared to a general sample of CSBGs, two groups of galaxies are particularly metal-poor (groups "15609"and "17182"), which is perhaps associated with the radius of these groups since they are among the most compact in the sample. Furthermore, there seems to be a trend that among the galaxies in the same group, the CSBG is the most metal-poor.

- **Effect of interactions in the mass assembly of CSBGs:** Investigating the star formation history of galaxies within groups, we found clear signs of synchronous bursts of star formation among members of some groups in our sample (Figs. 4.3 and 4.4). Furthermore, we find that all CSBGs have an old stellar population ($> 10\,\mathrm{Gyr}$).As for the isolated CSBGs, we conclude that they also have a complex SFH, which may indicate a possible previous merge event, as well as the accretion of filamentary neutral gas.

- **Groups of star-forming dwarf galaxies:** About the nature of isolated groups of star-forming dwarf galaxies, we find that 11 of the 12 groups are likely to be gravitationally bound (according to the velocity dispersions values of their member galaxies). We also identified clear signs of morphological perturbations in the galaxies of some groups in the sample, such as clumpy and irregular morphologies, tidal tails and diffuse stars in the intragroup medium. Finally, we highlight (based on Table 1): the "5073", "15609" and "17182" groups as being extremely compact ($R_{\mathrm{group}} < 20\,\mathrm{kpc}$); the "15609" and "17182" groups for their low gas metallicity in all their member galaxies; the "5073" and "7776" groups for their high gas fractions

($f_{\rm gas}$ > 0.5) and the "2671" and "15609" groups for their very high specific star formation rates (log(sSFR/yr) > −9).

## 6.1 Future work

- **Effect of interactions in the interstellar medium of CSBGs:** As described in section 1.2, recent studies (e.g. Izotov et al., 2018d) have shown that the escape of ionizing photons in CSFGs appears to be the result of a combination of factors, among them, interactions between galaxies in systems such as our isolated groups of star-forming dwarf galaxies. These interactions may increase the turbulence and inhomogeneities in the ISM gas, creating escape paths for the ionizing radiation. Seeking to investigate the effect of these interactions on the structure and kinematics of the interstellar medium of CSBGs, we submitted a proposal to the Gemini South Observatories (program "GS-2020B-Q-250") for the observation of two CSBGs using the GMOS instrument in the Integral Field Spectroscopy mode. The observation was successful, and we have already reduced the data from these observations. The following steps are to prepare ionization, extinction and velocity dispersion maps and compare them with the work of Bosch et al. (2019), who investigated these same properties for an isolated CSBG.

- **Simulations on isolated groups of dwarf galaxies:** In Freitas et al. (in prep.), work in which I collaborate, we are analyzing, among other things, the gas distribution in groups of dwarf galaxies using ILLUSTRIS TNG50 (Nelson et al., 2018) simulations. Recent results strengthen the hypothesis that these groups of dwarf galaxies are young and gas-rich systems. Furthermore, the simulations also suggest that gas is more easily stripped from galaxies due to the interactions and low gravitational potential of these dwarf galaxies. Finally, with the simulations, it will also be possible to explore the distribution of dark matter in these groups of galaxies.

- **Distribution of neutral gas in isolated groups of star-forming dwarf galaxies and the effects of interactions on the gas cycle in galaxies:** In collaboration with Dr Pedro Beaklini, we intend to carry out radio observations using the radio astronomy observatory VLA (Very Large Array) to map the distribution

of H I in these isolated groups of star-forming dwarf galaxies. This will allow us to better understand the gas cycle and the role of interactions in the stripping and re-accretion of gas to the ISM of these galaxies.

| **Group ID** | $RA_{group}$ [deg] | $DEC_{group}$ [deg] | $\bar{z}$ | $N_{gal}$ | Source | $R_{group}$ [kpc] | $R_{group}$ inertial [kpc] | $\mu_{group}$ [mag arcsec$^{-2}$] | $\sigma_{W\&T}$ [km s$^{-1}$] | $\sigma_{Y}$ [km s$^{-1}$] | log ($M_{vir}/M_{\odot}$) |
|---|---|---|---|---|---|---|---|---|---|---|---|
| **1204** | 208.6436 | -2.8526 | 0.0371 | 4 | GS2018/01 | 47.4 | 63.5 | 28.1 | 71.6 | 65.7 | 11.38 |
| **1631** | 33.2153 | -0.8970 | 0.0421 | 3 | SDSS | 45.3 | 47.4 | 27.2 | 161.5 | 141.2 | 12.07 |
| **1854** | 132.3470 | 1.4038 | 0.0342 | 3 | SDSS | 39.8 | 47.9 | 28.0 | 74.7 | 63.3 | 11.52 |
| **2671** | 194.7241 | 12.7893 | 0.1752 | 5 | GS2018/01 | 67.0 | 81.9 | 25.6 | 75.7 | 69.3 | 11.69 |
| **5073** | 224.5114 | 5.0948 | 0.0453 | 3 | GS2018/01 | 10.5 | 10.5 | 24.6 | 42.4 | 36.6 | 10.45 |
| **7776** | 24.0725 | 13.9603 | 0.0238 | 4 | GN2019/02 | 37.8 | 46.0 | 27.6 | 46.0 | 44.9 | 11.11 |
| **8454** | 240.9449 | 16.5320 | 0.0421 | 3 | SDSS | 58.4 | 66.4 | 28.0 | 560.9 | 499.3 | 13.47 |
| **12799** | 193.5524 | 39.2012 | 0.0446 | 3 | SDSS | 47.0 | 48.9 | 27.5 | 86.9 | 73.7 | 11.43 |
| **15609** | 131.3717 | 53.1513 | 0.0309 | 3 | SDSS | 15.0 | 16.5 | 25.0 | 69.1 | 60.4 | 11.05 |
| **16311** | 184.1673 | 14.2883 | 0.0235 | 4 | SDSS | 36.7 | 48.5 | 27.4 | 46.6 | 43.9 | 11.11 |
| **17182** | 46.2558 | -0.0807 | 0.0299 | 3 | SDSS | 8.7 | 8.9 | 24.9 | 64.3 | 54.5 | 10.75 |
| **18766** | 123.6889 | 36.6101 | 0.0824 | 3 | SDSS | 39.1 | 45.3 | 25.9 | 40.8 | 36.8 | 10.99 |

| **Group ID** | log ($M_{\star,\,tot}/M_{\odot}$) | log ($sSFR_{tot}$/yr) | log ($MH_{tot}/M_{\odot}$) | log ($\Sigma_{vir}$ [$M_{\odot}$ kpc$^{-2}$]) | log ($\Sigma_{\star}$ [$M_{\odot}$ kpc$^{-2}$]) | Dist. fil. [$h^{-1}$ Mpc] | L0.5 fil. [$10^{10}h^{-2}L_{\odot}$] | $Iso_{M}$ | $Iso_{D<500}$ | $Iso_{D<1000}$ |
|---|---|---|---|---|---|---|---|---|---|---|
| **1204** | 9.71 | -8.40 | - | 7.28 | 5.61 | 9.635 | 1.785 | ✓ | ✓ | |
| **1631** | 10.24 | -8.96 | - | 8.22 | 6.39 | - | - | | | |
| **1854** | 10.16 | -9.70 | 9.89 | 7.66 | 6.30 | 3.292 | 5.941 | | | |
| **2671** | 11.29 | -8.11 | - | 7.37 | 6.97 | - | - | ✓ | ✓ | |
| **5073** | 9.67 | -8.48 | 9.83 | 7.91 | 7.13 | 0.317 | 1.007 | ✓ | | |
| **7776** | 9.85 | -8.17 | 10.43 | 7.29 | 6.03 | - | - | ✓ | ✓ | ✓ |
| **8454** | 10.53 | -9.70 | - | 9.32 | 6.39 | 1.970 | 25.141 | | | |
| **12799** | 10.58 | -9.83 | - | 7.56 | 6.71 | 0.987 | 1.950 | ✓ | ✓ | ✓ |
| **15609** | 9.99 | -8.71 | - | 8.12 | 7.06 | 1.930 | 6.790 | ✓ | ✓ | |
| **16311** | 10.36 | -9.33 | 9.84 | 7.25 | 6.49 | 3.223 | 0.309 | | | |
| **17182** | 9.27 | -8.61 | - | 8.35 | 6.88 | - | - | ✓ | | |
| **18766** | 11.09 | -9.13 | - | 7.18 | 7.28 | 0.539 | 4.005 | | | |

**Table 1:** General properties of the selected groups of star-forming galaxies containing at least one CSBG. From left to right, from top to bottom: i) right ascension of the group centre; ii) declination of the group centre; iii) average redshift of member galaxies; iv) number of galaxies members (including the CSBG); v) source of the data (Gemini or SDSS observations); vi) radius of the smallest circle containing all galaxy members; vii) inertial radius (Eq. 4.1); viii) surface brightness (Eq. 4.7); ix) velocity dispersion measured following Wainer & Thissen (1976) method (Eq. 4.4); x) velocity dispersion measured following Yaryura et al. (2020) method (Eq. 4.5); xi) virial mass (Eq. 4.6); xii) total group stellar mass; xiii) total group specific star formation rate; xiv) logarithm of the total group hydrogen gas mass; xv) bi-dimensional virial mass density (Eq. 4.8; xvi) bi-dimensional stellar mass density (Eq. 4.9; xvii) distance to the filament point in units of $h^{-1}$ Mpc; xviii) the sum of luminosities of observed galaxies that are closer than $0.5\,h^{-1}$ Mpc to filament axis (in units of $10^{10}\,h^{-2}\,L_{\odot}$); xix) groups that do not have massive galaxies ($\log[M_{\star}] > 10$) within $R < 10\,R_{group}$ and $\sigma = \pm 3000\,km\,s^{-1}$; xx) groups that do not have massive galaxies closer than 500 kpc; xxi) groups that do not have massive galaxies closer than 1 000 kpc.

| **Group ID** | RA [deg] | DEC [deg] | Redshift | log ($M_\star/M_\odot$) | $m_r$ [mag] | $Radius_r$ [kpc] | $Age_L$ gmean [Gyr] | $Met_L$ gmean [$Z_\odot$] | log(sSFR/yr) | 12+log(O/H) | $O_{32}$ |
|---|---|---|---|---|---|---|---|---|---|---|---|
| **1204** | 208.6254 | -2.8366 | 0.0368 | 9.2045 | 17.6753 | 3.5898 | 0.0535 | -0.6326 | -9.5534 | 8.1014 | 0.8729 |
| **1204** | 208.634 | -2.8501 | 0.0371 | 9.4934 | 17.1389 | 4.3178 | 0.2571 | -0.5518 | -9.8025 | 8.28 | 0.5469 |
| **1631** | 33.2015 | -0.8888 | 0.0416 | 9.4447 | 17.6479 | 2.8043 | 0.2726 | -0.233 | -9.459 | 8.0809 | 1.5971 |
| **1854** | 132.3424 | 1.4013 | 0.0344 | 9.4719 | 17.5999 | 5.5211 | 0.4531 | -0.4402 | -9.828 | 8.241 | 0.74 |
| **2671** | 194.7237 | 12.7969 | 0.175 | 10.1679 | 17.9486 | 3.4313 | 0.123 | -0.5723 | -9.1355 | 8.2508 | 0.7565 |
| **5073** | 224.5142 | 5.0965 | 0.0454 | 9.5369 | 17.5252 | 2.9403 | 0.3326 | -0.5225 | -9.8653 | 8.1948 | 0.7483 |
| **7776** | 24.0979 | 13.9504 | 0.0239 | 8.7972 | 16.6237 | 5.1874 | 0.0558 | -0.4026 | -9.4289 | 8.017 | 0.7161 |
| **8454** | 240.9547 | 16.5235 | 0.0415 | 10.0516 | 16.8244 | 3.1435 | 0.2754 | -0.4125 | -9.7893 | 8.3291 | 0.2692 |
| **12799** | 193.5696 | 39.204 | 0.0446 | 9.5796 | 17.7227 | 3.9956 | 0.3931 | -0.507 | -10.0664 | 8.1382 | 0.5683 |
| **15609** | 131.365 | 53.148 | 0.0311 | 9.3158 | 17.4187 | 5.1176 | 0.0466 | -0.2877 | -8.9591 | 7.8398 | 2.4014 |
| **16311** | 184.1638 | 14.2939 | 0.0237 | 9.0551 | 17.9105 | 3.909 | 0.5592 | -0.3901 | -10.2176 | 8.1122 | 0.8559 |
| **16311** | 184.1644 | 14.2603 | 0.0234 | 8.8978 | 17.6824 | 5.1308 | 0.3268 | -0.5926 | -9.6036 | 7.9863 | 1.1079 |
| **17182** | 46.2548 | -0.0847 | 0.0299 | 8.7476 | 17.9165 | 3.8342 | 0.0846 | -0.6375 | -10.01 | 7.8104 | 0.5835 |
| **18766** | 123.6947 | 36.6035 | 0.0823 | 10.3114 | 17.3643 | 4.6435 | 0.13 | -0.5467 | -9.2407 | 8.2957 | 0.5486 |

**Table 2:** General properties of CSBGs within groups of star-forming galaxies (Table 2). From left to right: i) CSBG identification; ii) right ascension; iii) declination; iv) redshift; v) stellar mass; vi) petrosian magnitude in the SDSS $r$-band; vii) radius containing 90% of Petrosian flux in the SDSS $r$-band; viii) weighted geometric mean age of the galaxy stellar component weighted by luminosity and measured by STARLIGHT; ix) weighted geometric mean metallicity of the galaxy stellar component weighted by luminosity and measured by STARLIGHT; x) logarithm of the specific star formation rate of the galaxy; xi) oxygen abundance of the galaxy; xii) Ionization parameter defined by $I([\mathrm{O\,III}]\lambda5007\,)/(I([\mathrm{O\,II}]\lambda3727\,)+I([\mathrm{O\,II}]\lambda3729\,))$.

| **Group ID** | RA [deg] | DEC [deg] | Redshift | log ($M_\star/M_\odot$) | $m_r$ [mag] | $Radius_r$ [kpc] | $Age_L$ gmean [Gyr] | $Met_L$ gmean [$Z_\odot$] | log(sSFR/yr) | 12+log(O/H) | $O_{32}$ |
|---|---|---|---|---|---|---|---|---|---|---|---|
| **1204** | 208.6618 | -2.8686 | 0.0373 | 7.6483 | 19.4693 | 4.031 | 0.0056 | -0.3304 | -9.0302 | 8.0904 | - |
| **1204** | 208.6391 | -2.8488 | 0.0372 | 8.6275 | 16.566 | 8.7719 | 0.003 | -0.0223 | -8.5877 | 8.2747 | - |
| **1631** | 33.2231 | -0.9085 | 0.0423 | 10.0897 | 16.3715 | 12.2669 | 0.4343 | -0.3022 | -10.3621 | 8.4661 | 0.1374 |
| **1631** | 33.2291 | -0.9052 | 0.0425 | 9.334 | 17.521 | 8.5021 | 0.2864 | -0.5114 | -9.1578 | 8.0811 | 1.1325 |
| **1854** | 132.342 | 1.4226 | 0.0342 | 9.8481 | 17.2299 | 9.4015 | 0.6433 | -0.5096 | -10.4227 | 8.3423 | 0.1173 |
| **1854** | 132.3519 | 1.385 | 0.034 | 9.6538 | 17.3043 | 5.8505 | 0.6051 | -0.4226 | -10.8668 | 8.248 | 0.3736 |
| **2671** | 194.7274 | 12.7921 | 0.1752 | 11.1555 | 17.8435 | 4.9955 | 0.2287 | -0.0681 | -9.9269 | 8.5278 | - |
| **2671** | 194.7307 | 12.7934 | 0.1755 | 9.8686 | 17.7283 | 5.0819 | 0.0054 | -0.0953 | -8.1874 | 8.5837 | - |
| **2671** | 194.7254 | 12.7889 | 0.175 | 10.2107 | 18.178 | 3.4157 | 0.0164 | 0.1468 | -9.4587 | 8.5694 | - |
| **2671** | 194.718 | 12.7844 | 0.1756 | 10.1887 | 19.8579 | 2.2017 | 0.9724 | -0.4439 | -10.412 | 8.4592 | - |
| **5073** | 224.5109 | 5.0916 | 0.0454 | 8.9995 | 18.2318 | 5.6363 | 0.0051 | 0.1048 | -9.6106 | 8.1755 | - |
| **5073** | 224.5114 | 5.0981 | 0.0452 | 8.4044 | 17.9049 | 5.1957 | 0.003 | -0.0223 | -8.5307 | 8.1354 | - |
| **7776** | 24.0632 | 13.9453 | 0.0239 | 9.6148 | 16.3783 | 8.6792 | 0.2045 | -0.4199 | -10.2962 | 8.2046 | 0.3994 |
| **7776** | 24.047 | 13.9701 | 0.0236 | 9.3309 | 16.3695 | 8.5953 | 0.1216 | -0.4612 | -9.7224 | 8.0953 | 0.4582 |
| **7776** | 24.0604 | 13.9678 | 0.0239 | 8.3077 | 16.887 | 17.4959 | 0.0058 | 0.1062 | -8.2077 | 7.9728 | - |
| **8454** | 240.9672 | 16.5395 | 0.044 | 10.2146 | 16.9939 | 8.3826 | 0.8429 | -0.4388 | -10.431 | 8.4162 | 0.1504 |
| **8454** | 240.9227 | 16.5246 | 0.0407 | 9.8102 | 17.4537 | 4.3554 | 2.0102 | -0.2324 | -13.3572 | - | -0.0131 |
| **12799** | 193.5722 | 39.1993 | 0.0443 | 10.4241 | 16.9532 | 6.3047 | 1.2089 | -0.1855 | -10.6234 | 8.5236 | 0.1369 |
| **12799** | 193.5325 | 39.2031 | 0.0448 | 9.8855 | 17.7137 | 4.7152 | 0.9325 | -0.3769 | -10.4126 | 8.4255 | 0.2537 |
| **15609** | 131.3605 | 53.1544 | 0.0307 | 9.3484 | 16.9053 | 6.1514 | 0.0817 | -0.5059 | -9.4158 | 7.9389 | 1.4861 |
| **15609** | 131.3828 | 53.1481 | 0.031 | 9.7468 | 15.7965 | 11.1324 | 0.0831 | -0.4999 | -9.3119 | 7.9388 | 1.4855 |
| **16311** | 184.1765 | 14.2778 | 0.0235 | 10.2586 | 15.0459 | 8.8145 | 0.4526 | -0.4259 | -10.2741 | 8.4204 | 0.1907 |
| **16311** | 184.1703 | 14.3164 | 0.0234 | 9.4246 | 17.2302 | 8.4246 | 0.8019 | -0.515 | -9.9913 | 8.0797 | 0.4913 |
| **17182** | 46.2569 | -0.0767 | 0.0297 | 9.0627 | 17.0787 | 6.6713 | 0.0606 | -0.6363 | -10.1029 | 7.8931 | 1.3922 |
| **17182** | 46.2595 | -0.0816 | 0.0301 | 8.2271 | 17.9976 | 4.5895 | 0.0058 | -0.4256 | -8.6448 | 7.8102 | 2.3638 |
| **18766** | 123.6841 | 36.6112 | 0.0825 | 10.8821 | 17.0882 | 3.9984 | 1.4324 | -0.2881 | -10.4242 | 8.7729 | 1.3493 |
| **18766** | 123.6831 | 36.6168 | 0.0825 | 10.4076 | 17.5329 | 4.6503 | 0.2988 | -0.5755 | -9.8637 | 8.4439 | 0.2337 |

**Table 3:** General properties of the other star-forming galaxies (besides the CSBG) within groups. The column description is the same as in the Table 2.

| **CSBG ID** | RA [deg] | DEC [deg] | Redshift | log ($M_\star/M_\odot$) | $m_r$ [mag] | $Radius_r$ [kpc] | $Age_L$ gmean [Gyr] | $Met_L$ gmean [Gyr] | log(sSFR/yr) | 12+log(O/H) | $O_{32}$ | log(MH/$M_\odot$) | Dist. fil. [$h^{-1}$ Mpc] | L0.5 fil. [$10^{10}h^{-2}L_\odot$] |
|---|---|---|---|---|---|---|---|---|---|---|---|---|---|---|
| **1169** | 30.6683 | 0.5368 | 0.0432 | 9.8396 | 17.6091 | 3.5321 | 0.6339 | -0.5281 | -10.1046 | 8.2540 | 0.4252 | - | - | - |
| **1507** | 243.1050 | 13.8520 | 0.0313 | 9.6302 | 16.9658 | 5.6275 | 0.2095 | -0.5139 | -9.7634 | 8.3383 | 0.3897 | - | 1.522 | 4.142 |
| **1654** | 232.8054 | 5.5952 | 0.0388 | 9.9019 | 16.9823 | 6.1654 | 0.3525 | -0.4243 | -10.1460 | 8.2678 | 0.5285 | - | 0.076 | 0.781 |
| **1997** | 136.4275 | 48.9535 | 0.0821 | 10.6240 | 16.7857 | 4.3898 | 0.2278 | -0.3791 | -9.6643 | 8.4181 | 0.4182 | - | 0.132 | 11.543 |
| **2261** | 194.1314 | 7.3134 | 0.0431 | 10.2402 | 16.3372 | 5.3891 | 0.2628 | -0.5593 | -9.5922 | 8.0993 | 0.6546 | - | 0.151 | 14.692 |
| **3412** | 226.5801 | 24.1447 | 0.0439 | 10.5403 | 15.7657 | 5.9461 | 0.2085 | -0.4380 | -9.8382 | 8.4217 | 0.5320 | 10.18 | 3.205 | 6.276 |
| **4385** | 211.8747 | 0.9694 | 0.1769 | 10.4779 | 17.9938 | 2.5772 | 0.0715 | -0.3364 | -9.4095 | 8.3454 | 0.3616 | - | - | - |
| **4988** | 249.8112 | 46.8742 | 0.0826 | 10.2581 | 16.8496 | 5.3486 | 0.3029 | -0.5825 | -9.7584 | 8.4010 | 0.3741 | - | 7.921 | 18.508 |
| **5086** | 314.0246 | -6.6060 | 0.0312 | 8.6893 | 17.4889 | 4.1204 | 0.0279 | -0.3500 | -8.9514 | 8.0334 | 1.1584 | - | - | - |
| **5345** | 243.9248 | 12.9366 | 0.0343 | 9.9555 | 16.5991 | 5.5185 | 0.3160 | -0.5028 | -10.1262 | 8.3750 | 0.3154 | - | 1.051 | 3.991 |
| **5460** | 211.0088 | 25.7966 | 0.0323 | 10.1489 | 15.9717 | 5.2191 | 0.2580 | -0.4052 | -9.4190 | 8.2033 | 0.7802 | 9.86 | 0.071 | 0.853 |
| **6227** | 146.4282 | 36.5185 | 0.0329 | 10.1462 | 15.7365 | 5.2985 | 0.3669 | -0.5484 | -10.0396 | 8.4202 | 0.3544 | - | 5.068 | 6.633 |
| **6324** | 51.5604 | -0.2030 | 0.0301 | 9.7659 | 15.8916 | 4.4648 | 0.0685 | -0.5166 | -9.2032 | 8.2277 | 0.8399 | - | - | - |
| **6684** | 239.6770 | 17.3604 | 0.0368 | 9.4537 | 16.6320 | 5.4510 | 0.1137 | -0.6086 | -9.0116 | 7.9767 | 1.5070 | 9.98 | 1.051 | 17.119 |
| **7301** | 230.4262 | 34.4018 | 0.0320 | 9.8742 | 16.3715 | 3.2751 | 0.3483 | -0.5664 | -9.8270 | 8.4034 | 0.3111 | - | 0.033 | 4.869 |
| **7919** | 194.2836 | 3.4234 | 0.1737 | 10.8197 | 17.4749 | 3.6700 | 0.2548 | -0.6161 | -9.6231 | 8.3727 | 0.3339 | - | - | - |
| **8097** | 147.6205 | 32.6850 | 0.0349 | 9.5155 | 17.1269 | 4.6611 | 0.0765 | -0.4639 | -9.4844 | 7.8729 | 1.3877 | - | 3.876 | 7.654 |
| **8225** | 149.4435 | 12.2487 | 0.0448 | 9.5468 | 17.1822 | 4.1876 | 0.2762 | 0.0141 | -9.9075 | 8.2959 | 0.4403 | - | 5.501 | 1.687 |
| **8364** | 138.3060 | 21.8571 | 0.0467 | 9.9830 | 17.3223 | 4.8542 | 0.3118 | -0.4783 | -10.2337 | 8.3012 | 0.4849 | - | 4.989 | 3.018 |
| **9921** | 189.3502 | 23.0942 | 0.0461 | 9.9309 | 17.3588 | 4.7290 | 0.8111 | -0.6079 | -10.2397 | 8.2724 | 0.4887 | - | 0.681 | 8.604 |
| **10465** | 185.2915 | 18.6810 | 0.0451 | 10.1711 | 16.2574 | 4.1593 | 0.1978 | -0.5281 | -9.9568 | 8.3985 | 0.3081 | - | 0.912 | 4.839 |
| **10688** | 124.3427 | 39.1404 | 0.0416 | 9.7892 | 16.7758 | 4.8072 | 0.2779 | -0.4854 | -9.5118 | 8.3638 | 0.4879 | - | 1.779 | 12.090 |
| **11593** | 140.0921 | 43.6934 | 0.0400 | 9.7310 | 16.5447 | 4.5243 | 0.4052 | -0.3925 | -9.6560 | 8.4034 | 0.5950 | - | 1.081 | 9.335 |
| **12123** | 227.6159 | 15.7405 | 0.0462 | 10.3685 | 16.2850 | 4.6857 | 0.2542 | -0.5515 | -9.5935 | 8.3908 | 0.3834 | - | 3.259 | 3.989 |
| **12245** | 39.4563 | -9.4323 | 0.0446 | 10.3703 | 15.5025 | 6.1329 | 0.0957 | -0.3909 | -9.3040 | 8.3835 | 0.6357 | - | - | - |
| **12267** | 30.4011 | 0.0955 | 0.0432 | 9.8267 | 16.5603 | 4.0342 | 0.1597 | -0.6185 | -9.7472 | 8.1296 | 0.6409 | 9.94 | - | - |
| **12591** | 198.8524 | 3.7045 | 0.0471 | 9.8293 | 17.5881 | 3.4840 | 0.6041 | -0.5907 | -9.9310 | 8.3158 | 0.4845 | - | 1.607 | 17.208 |
| **12674** | 189.4535 | 12.8561 | 0.0432 | 9.5895 | 17.1634 | 4.2072 | 0.0720 | -0.4414 | -9.6929 | 7.9728 | 0.6081 | - | 3.515 | 1.526 |
| **13564** | 158.7157 | 10.0929 | 0.0460 | 9.8088 | 17.0231 | 3.8530 | 0.3675 | -0.4261 | -9.6014 | 8.3321 | 0.3367 | - | 3.604 | 2.900 |
| **14009** | 205.7484 | 45.4090 | 0.0327 | 10.0977 | 16.0866 | 4.7266 | 0.3338 | -0.5450 | -9.6760 | 8.3584 | 0.3952 | - | 3.098 | 9.562 |
| **14262** | 217.5799 | 64.4910 | 0.0353 | 9.5999 | 17.6890 | 3.5569 | 0.3433 | -0.5321 | -10.0567 | 8.3615 | 0.2440 | - | 2.393 | 1.860 |
| **15310** | 224.6101 | 27.9766 | 0.0472 | 10.1564 | 16.9538 | 4.3933 | 0.1794 | -0.4728 | -9.7896 | 8.3840 | 0.2225 | - | 1.128 | 1.189 |
| **15740** | 164.9203 | 26.4637 | 0.0468 | 9.5125 | 17.7245 | 3.1225 | 0.1492 | -0.5409 | -9.6515 | 8.0941 | 0.6709 | - | 3.671 | 1.248 |
| **16564** | 225.4013 | 16.7297 | 0.0319 | 10.4704 | 14.7692 | 4.5612 | 0.0582 | -0.2748 | -9.3651 | 8.3162 | 0.9979 | 9.88 | 1.078 | 1.668 |
| **16934** | 130.7899 | 24.0347 | 0.1784 | 10.7844 | 17.9537 | 4.6155 | 0.1727 | -0.3792 | -9.6181 | 8.2865 | 0.5851 | - | - | - |
| **17199** | 219.2872 | 3.4931 | 0.0328 | 9.4433 | 16.7425 | 5.4816 | 0.1015 | -0.4385 | -9.4083 | 8.1845 | 0.7448 | - | 2.878 | 7.764 |
| **17822** | 177.2698 | 15.6839 | 0.0339 | 9.6959 | 16.4654 | 6.4303 | 0.1817 | -0.5561 | -9.1644 | 8.1235 | 1.1044 | 9.79 | 3.630 | 1.252 |
| **18044** | 192.4731 | 42.8254 | 0.0290 | 9.7012 | 16.5188 | 5.0199 | 0.4170 | -0.4410 | -10.1479 | 8.3687 | 0.3599 | - | 5.576 | 1.942 |
| **18048** | 192.6145 | 17.1652 | 0.0442 | 9.8859 | 16.3606 | 4.7890 | 0.0905 | -0.6024 | -9.5367 | 8.1731 | 0.6525 | - | - | - |
| **18479** | 232.7129 | 11.1827 | 0.0438 | 9.3325 | 17.5988 | 4.4194 | 0.0719 | -0.6096 | -9.9608 | 7.9670 | 0.5630 | - | 0.041 | 3.944 |
| **18681** | 146.9242 | 28.2564 | 0.0459 | 9.7766 | 17.0084 | 3.7149 | 0.1729 | -0.5825 | -9.5761 | 8.2377 | 0.4910 | - | 0.066 | 8.156 |
| **18887** | 202.2223 | 0.8420 | 0.0824 | 10.0656 | 17.7182 | 4.4286 | 0.2348 | -0.3417 | -9.7265 | 8.3862 | 0.3293 | - | 2.265 | 13.484 |

**Table 4:** General properties of the redshift-paired isolated CSBGs. The column description is the same as in the Table 2, plus the last 3 columns as the: logarithm of the hydrogen gas mass of the galaxy; the distance to the closest filament point in units of $h^{-1}$ Mpc; and the sum of luminosities of observed galaxies that are closer than $0.5\,h^{-1}$ Mpc to filament axis (in units of $10^{10}\,h^{-2}\,L_\odot$), respectively.

| CSBG ID | Stellar component | | Gas component | |
|---|---|---|---|---|
| | $v_0$ [km s$^{-1}$] | vel. disp. [km s$^{-1}$] | $v_0$ [km s$^{-1}$] | vel. disp. [km s$^{-1}$] |
| **CSBGs within groups** | | | | |
| **1204** | -3.65 | 57.5 | -2.13 | 59.9 |
| **1631** | 25.6 | 111.0 | -1.37 | 62.4 |
| **1854** | 8.7 | 79.2 | -1.71 | 64.7 |
| **2671** | 6.1 | 86.3 | 2.72 | 73.6 |
| **3391** | -8.4 | 60.4 | -1.3 | 60.7 |
| **5073** | 3.5 | 42.9 | -2.2 | 65.0 |
| **7776** | -36.5 | 101.0 | -0.288 | 58.6 |
| **8454** | -10.5 | 64.3 | 0.618 | 63.3 |
| **12799** | -10.3 | 104.0 | -1.42 | 60.6 |
| **15609** | -85.0 | 8.08 | -1.1 | 53.1 |
| **16311** | -7.9 | 96.6 | 0.338 | 55.1 |
| **17182** | -21.2 | 197.0 | -1.05 | 65.4 |
| **18764** | -9.75 | 184.0 | 0.459 | 53.0 |
| **18766** | 26.5 | 139.0 | -3.09 | 94.8 |
| **Isolated CSBGs** | | | | |
| **1169** | 17.7 | 70.0 | 0.712 | 63.4 |
| **1507** | 6.0 | 69.7 | 0.598 | 70.8 |
| **1654** | 9.8 | 73.0 | -0.46 | 72.9 |
| **1997** | 2.9 | 155.0 | -3.19 | 121.0 |
| **2261** | -48.4 | 90.0 | 4.31 | 75.9 |
| **3412** | -19.2 | 130.0 | 0.34 | 97.1 |
| **4385** | -12.1 | 110.0 | -3.98 | 118.0 |
| **4988** | 9.9 | 69.3 | -0.772 | 64.5 |
| **5086** | 4.69 | 22.3 | -8.39 | 58.8 |
| **5345** | -3.3 | 49.0 | 0.00599 | 63.9 |
| **5460** | 36.7 | 81.7 | -3.98 | 72.3 |
| **6227** | -9.3 | 71.1 | -2.31 | 71.8 |
| **6324** | -2.3 | 178.0 | 0.0849 | 82.6 |
| **6684** | 3.6 | 101.0 | 1.15 | 64.5 |
| **7301** | 0.9 | 57.9 | -0.178 | 67.9 |
| **7919** | 4.0 | 164.0 | 0.144 | 65.9 |
| **8097** | 31.2 | 142.0 | -2.19 | 49.3 |
| **8225** | -46.6 | 145.0 | -4.25 | 71.9 |
| **8364** | 14.6 | 55.3 | 0.733 | 61.5 |
| **9921** | -11.1 | 58.9 | 0.0785 | 74.6 |
| **10465** | 9.0 | 59.5 | 0.0679 | 67.8 |
| **10688** | 15.2 | 91.8 | 0.595 | 69.5 |
| **11593** | 18.3 | 77.6 | -0.506 | 74.0 |
| **12123** | -31.2 | 96.8 | 3.26 | 88.3 |
| **12245** | 19.6 | 115.0 | 3.09 | 85.1 |
| **12267** | 4.3 | 109.0 | -0.654 | 61.4 |
| **12591** | -15.4 | 71.2 | 0.431 | 61.8 |
| **12674** | -34.3 | 182.0 | -0.153 | 66.5 |
| **13564** | 4.8 | 57.7 | 0.347 | 71.3 |
| **14009** | -4.2 | 61.6 | -0.842 | 74.9 |
| **14262** | -14.4 | 47.4 | -0.124 | 63.3 |
| **15310** | 4.3 | 53.2 | 0.11 | 74.4 |
| **15740** | 20.8 | 66.1 | -4.87 | 60.0 |
| **16564** | -5.42 | 137.0 | -3.69 | 87.9 |
| **16934** | 24.1 | 127.0 | -3.42 | 95.5 |
| **17199** | -23.1 | 61.4 | -0.142 | 73.4 |
| **17822** | -12.8 | 82.8 | 1.5 | 64.7 |
| **18044** | -13.9 | 62.1 | -0.816 | 70.1 |
| **18048** | -16.0 | 150.0 | -0.0238 | 64.1 |
| **18479** | -22.9 | 52.6 | 0.139 | 71.2 |
| **18681** | 7.7 | 63.6 | -1.17 | 63.5 |
| **18887** | 12.1 | 60.9 | 0.0812 | 69.4 |

**Table 5:** Radial velocity and velocity dispersion of the stellar and gas components of CSBGs within groups of star-forming dwarf galaxies and isolated CSBGs. Both parameters were measured using pPXF with a single Gaussian component fitted over the emission lines.

# A STARLIGHT & pPXF synthesis

In this appendix, we present the STARLIGHT results in modelling the stellar component of all galaxies in each group of table 1. In the upper panel of each figure, we indicate the observed spectrum in red with the resulting fit in black. Each figure also shows the coordinates of the galaxy, as well as whether the spectrum was collected on the SDSS or obtained via observations at the Gemini Observatory. In the lower panel, we show the residual of the fit.

At the bottom of the page, we also present the pPXF results in modelling the stellar+gas components of the CSBGs of each group. In the upper panel of each figure, the observed spectrum is indicated in black, while the fit is in blue. We used a single Gaussian component to fit the emission lines. In the lower panel, in addition to the residuals of the fit, we also present the radial velocity ($v$) and the velocity dispersion ($\sigma$) of the stellar and gaseous components.

# Group 1204:

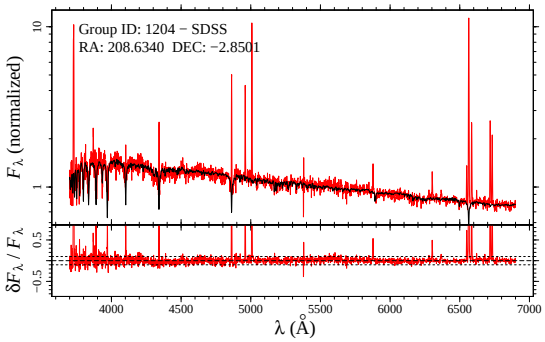
Group ID: 1204 − SDSS
RA: 208.6340 DEC: −2.8501
$F_\lambda$ (normalized)
$\delta F_\lambda / F_\lambda$
λ (Å)

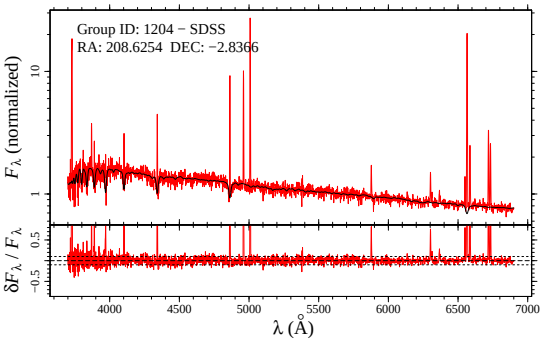
Group ID: 1204 − SDSS
RA: 208.6254 DEC: −2.8366
$F_\lambda$ (normalized)
$\delta F_\lambda / F_\lambda$
λ (Å)

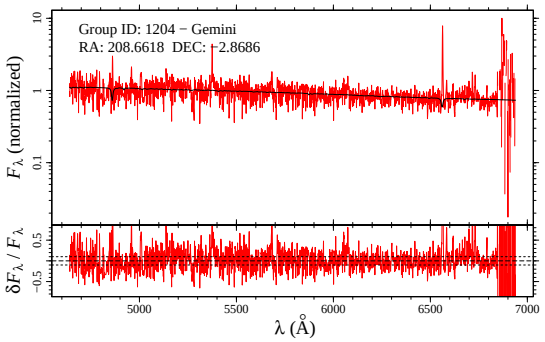
Group ID: 1204 − Gemini
RA: 208.6618 DEC: −2.8686
$F_\lambda$ (normalized)
$\delta F_\lambda / F_\lambda$
λ (Å)

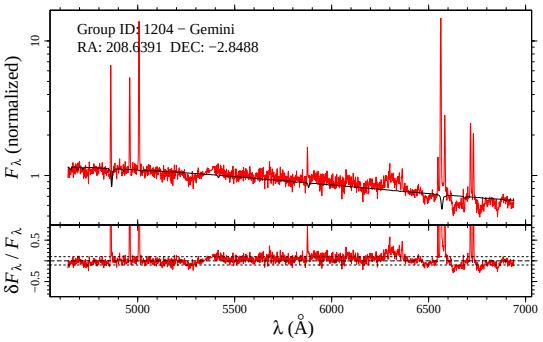
Group ID: 1204 − Gemini
RA: 208.6391 DEC: −2.8488
$F_\lambda$ (normalized)
$\delta F_\lambda / F_\lambda$
λ (Å)

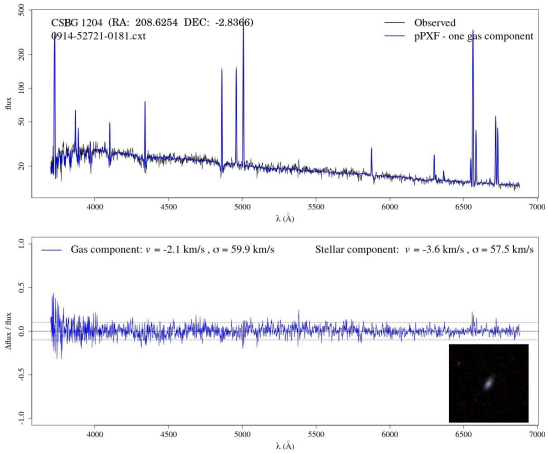
CSBG 1204 (RA: 208.6254 DEC: -2.8366)
0914-52721-0181.cxt
Observed
pPXF - one gas component
flux
λ (Å)
Gas component: v = -2.1 km/s , σ = 59.9 km/s
Stellar component: v = -3.6 km/s , σ = 57.5 km/s
Δflux / flux

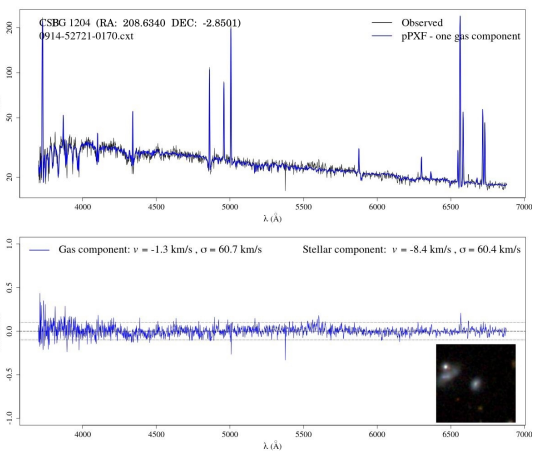
CSBG 1204 (RA: 208.6340 DEC: -2.8501)
0914-52721-0170.cxt
Observed
pPXF - one gas component
flux
λ (Å)
Gas component: v = -1.3 km/s , σ = 60.7 km/s
Stellar component: v = -8.4 km/s , σ = 60.4 km/s
Δflux / flux

# Group 1631:

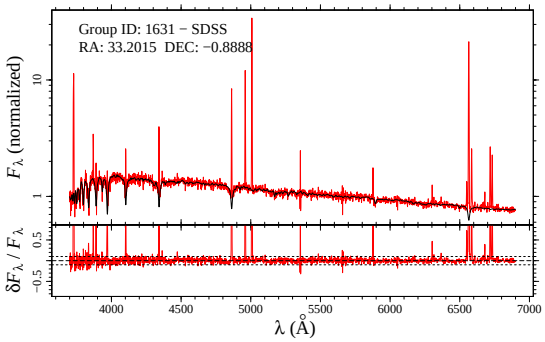
Group ID: 1631 − SDSS
RA: 33.2015 DEC: −0.8888
$F_\lambda$ (normalized)
$\delta F_\lambda / F_\lambda$
λ (Å)

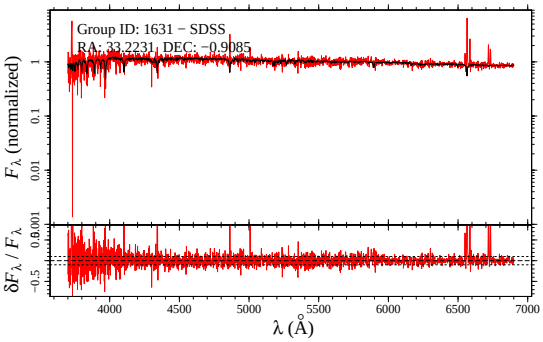
Group ID: 1631 − SDSS
RA: 33.2231 DEC: −0.9085
$F_\lambda$ (normalized)
$\delta F_\lambda / F_\lambda$
λ (Å)

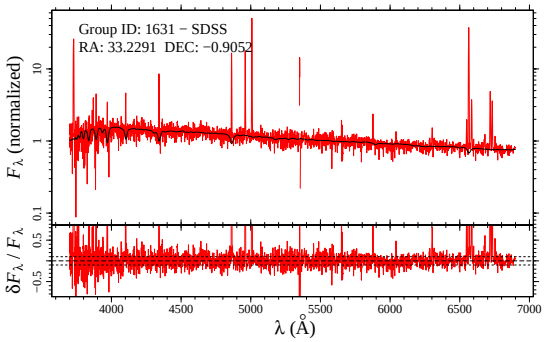
Group ID: 1631 − SDSS
RA: 33.2291 DEC: −0.9052
$F_\lambda$ (normalized)
$\delta F_\lambda / F_\lambda$
λ (Å)

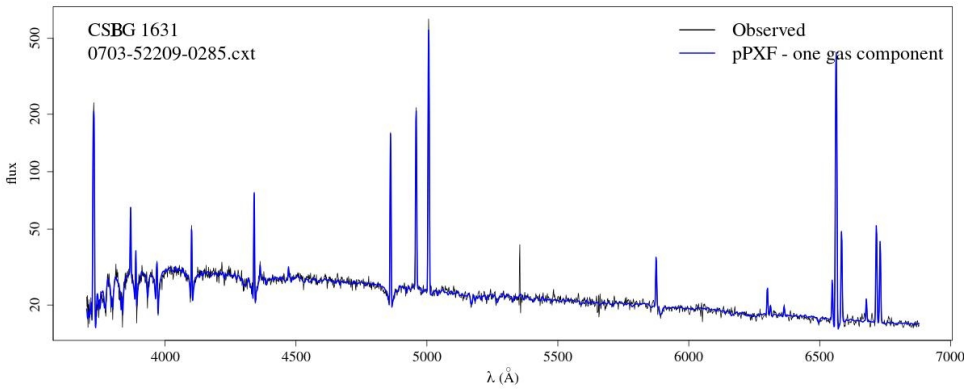
CSBG 1631
0703-52209-0285.cxt
Observed
pPXF - one gas component
flux
λ (Å)

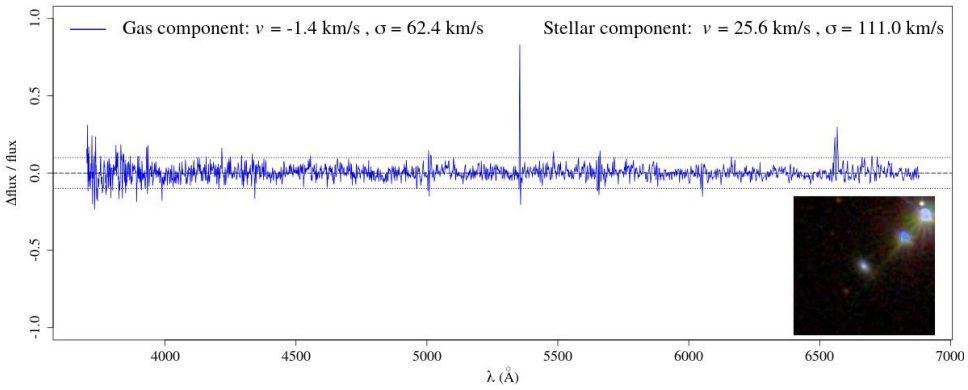
Gas component: v = -1.4 km/s , σ = 62.4 km/s
Stellar component: v = 25.6 km/s , σ = 111.0 km/s
Δflux / flux
λ (Å)

# Group 1854:

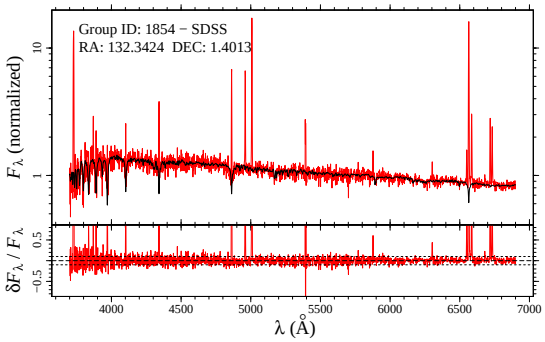
Group ID: 1854 − SDSS
RA: 132.3424 DEC: 1.4013
$F_\lambda$ (normalized)
$\delta F_\lambda / F_\lambda$
λ (Å)

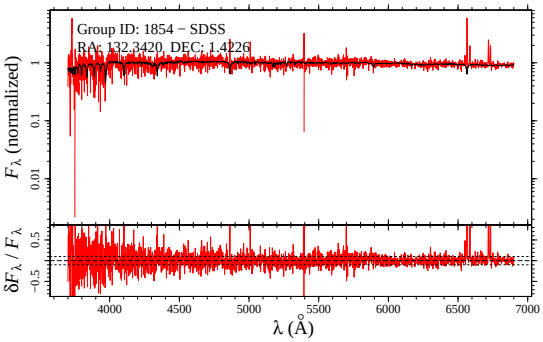
Group ID: 1854 − SDSS
RA: 132.3420 DEC: 1.4226
$F_\lambda$ (normalized)
$\delta F_\lambda / F_\lambda$
λ (Å)

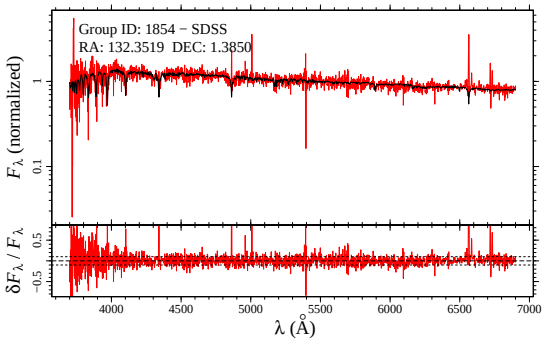
Group ID: 1854 − SDSS
RA: 132.3519 DEC: 1.3850
$F_\lambda$ (normalized)
$\delta F_\lambda / F_\lambda$
λ (Å)

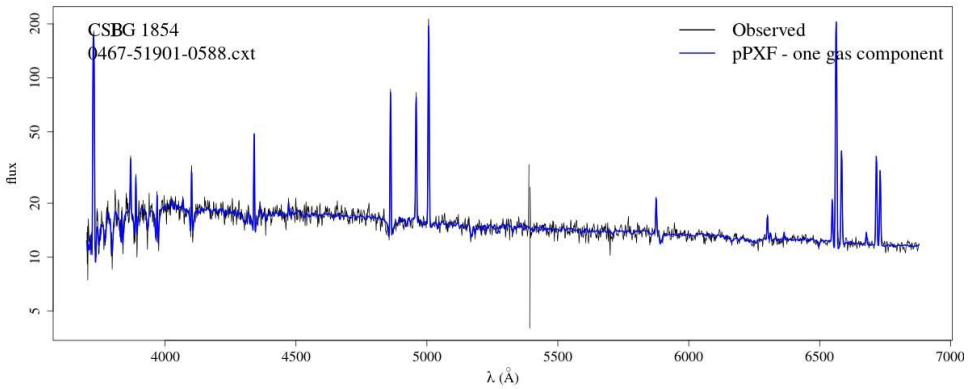
CSBG 1854
0467-51901-0588.cxt
Observed
pPXF - one gas component
flux
λ (Å)

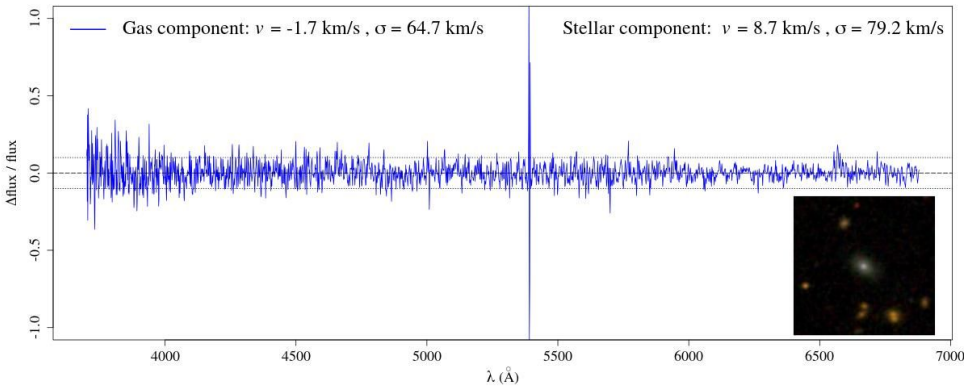
Gas component: v = -1.7 km/s , σ = 64.7 km/s
Stellar component: v = 8.7 km/s , σ = 79.2 km/s
Δflux / flux
λ (Å)

# Group 2671:

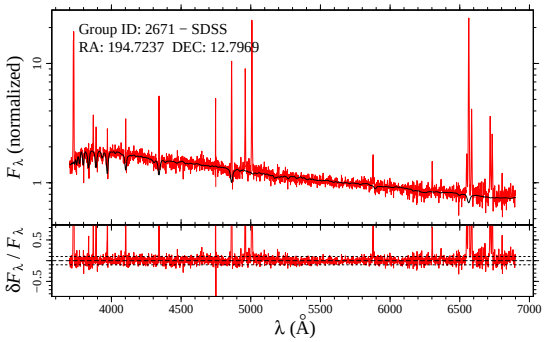
Group ID: 2671 − SDSS
RA: 194.7237 DEC: 12.7969
$F_\lambda$ (normalized)
$\delta F_\lambda / F_\lambda$
λ (Å)

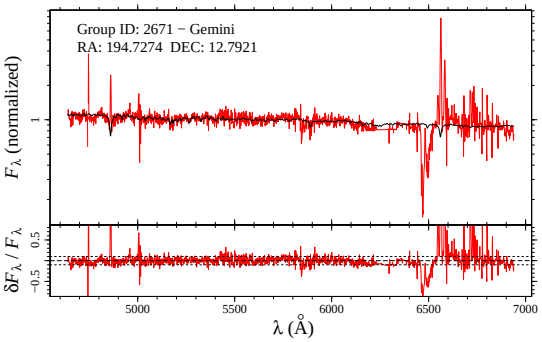
Group ID: 2671 − Gemini
RA: 194.7274 DEC: 12.7921
$F_\lambda$ (normalized)
$\delta F_\lambda / F_\lambda$
λ (Å)

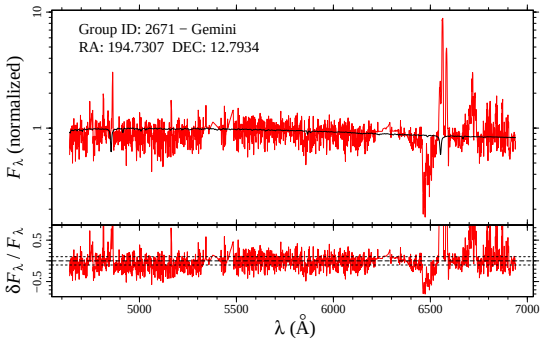
Group ID: 2671 − Gemini
RA: 194.7307 DEC: 12.7934
$F_\lambda$ (normalized)
$\delta F_\lambda / F_\lambda$
λ (Å)

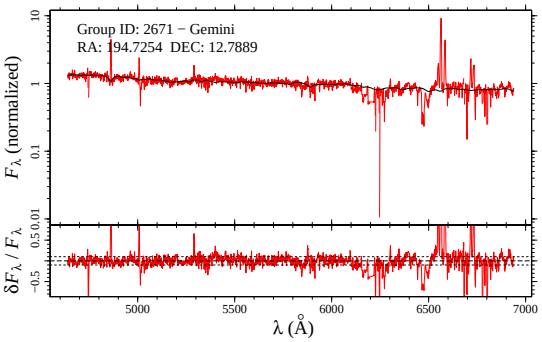
Group ID: 2671 − Gemini
RA: 194.7254 DEC: 12.7889
$F_\lambda$ (normalized)
$\delta F_\lambda / F_\lambda$
λ (Å)

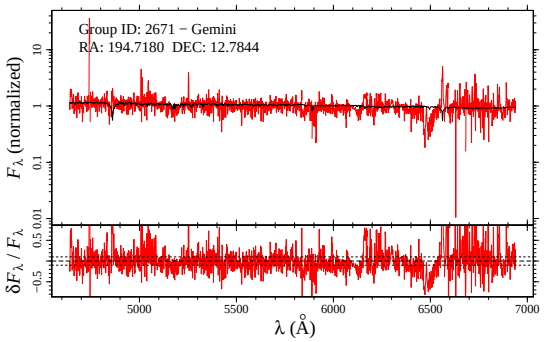
Group ID: 2671 − Gemini
RA: 194.7180 DEC: 12.7844
$F_\lambda$ (normalized)
$\delta F_\lambda / F_\lambda$
λ (Å)

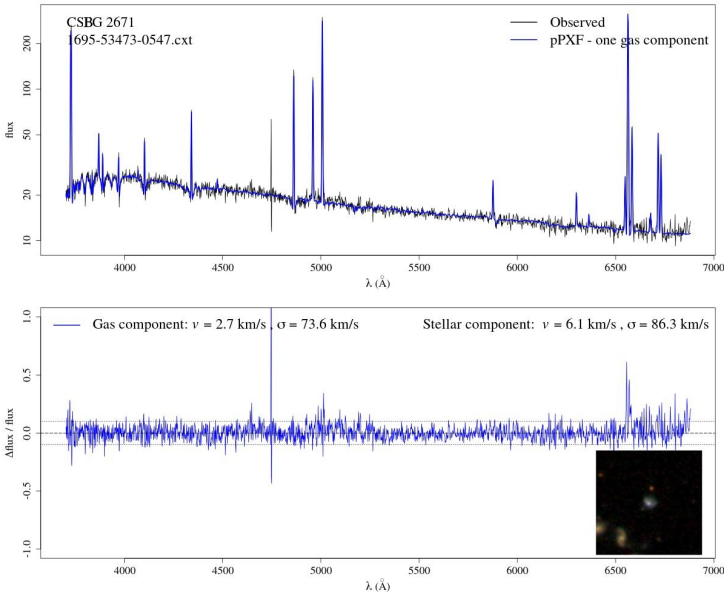
CSBG 2671
1695-53473-0547.cxt
Observed
pPXF - one gas component
flux
λ (Å)
Gas component: v = 2.7 km/s , σ = 73.6 km/s
Stellar component: v = 6.1 km/s , σ = 86.3 km/s
Δflux / flux
λ (Å)

# Group 5073:

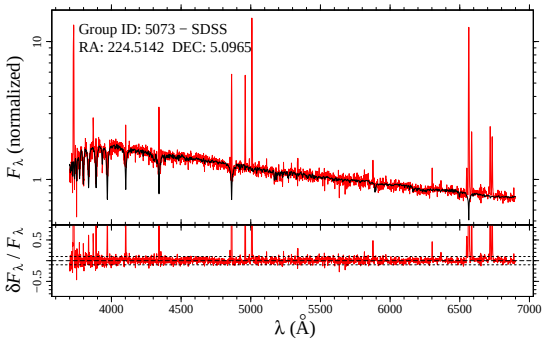
Group ID: 5073 − SDSS
RA: 224.5142 DEC: 5.0965
$F_\lambda$ (normalized)
$\delta F_\lambda / F_\lambda$
λ (Å)

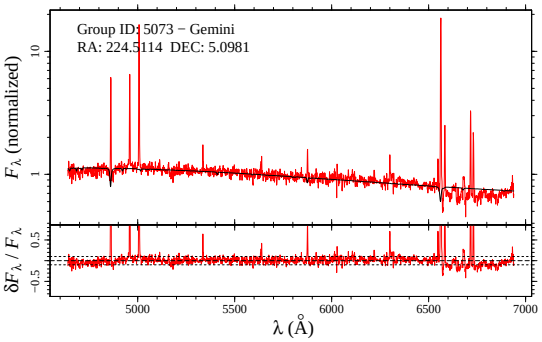
Group ID: 5073 − Gemini
RA: 224.5114 DEC: 5.0981
$F_\lambda$ (normalized)
$\delta F_\lambda / F_\lambda$
λ (Å)

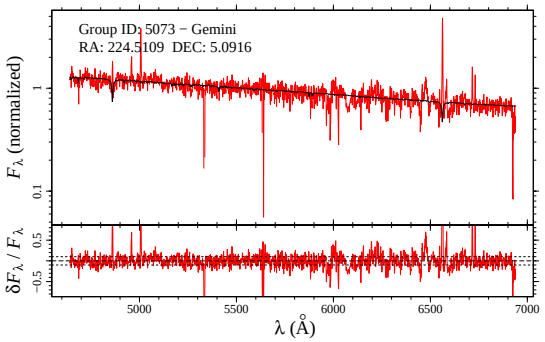
Group ID: 5073 − Gemini
RA: 224.5109 DEC: 5.0916
$F_\lambda$ (normalized)
$\delta F_\lambda / F_\lambda$
λ (Å)

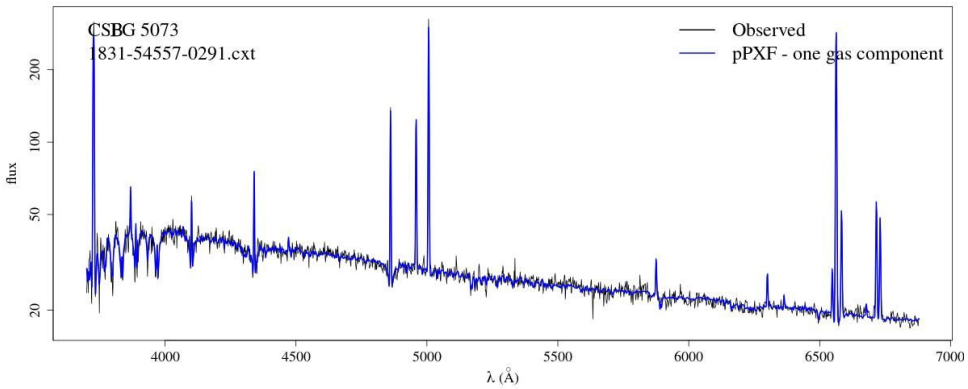
CSBG 5073
1831-54557-0291.cxt
Observed
pPXF - one gas component
flux
λ (Å)

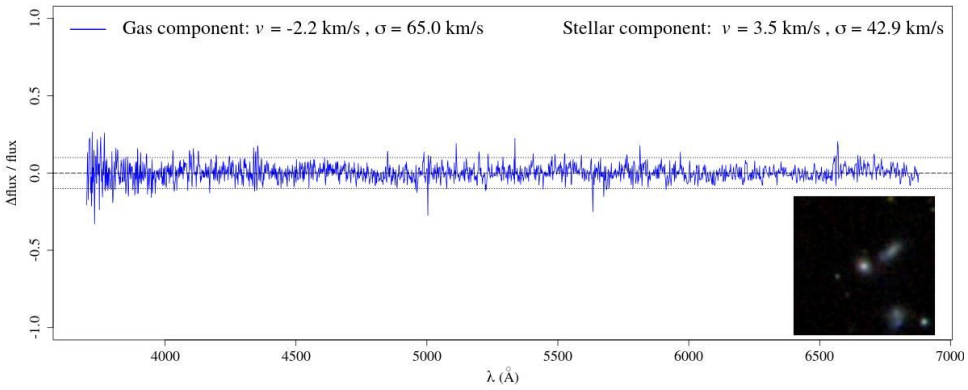
Gas component: v = -2.2 km/s , σ = 65.0 km/s
Stellar component: v = 3.5 km/s , σ = 42.9 km/s
Δflux / flux
λ (Å)

# Group 7776:

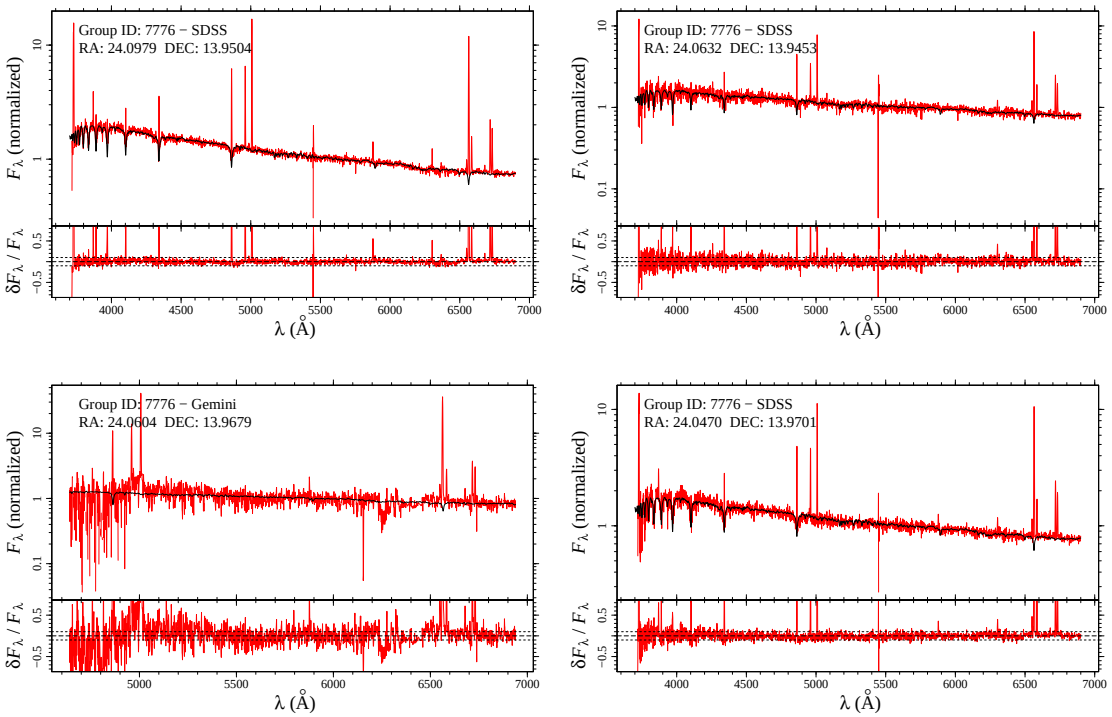
Group ID: 7776 − SDSS
RA: 24.0979 DEC: 13.9504
Group ID: 7776 − SDSS
RA: 24.0632 DEC: 13.9453
Group ID: 7776 − Gemini
RA: 24.0604 DEC: 13.9679
Group ID: 7776 − SDSS
RA: 24.0470 DEC: 13.9701
$F_\lambda$ (normalized)
$\delta F_\lambda / F_\lambda$
λ (Å)

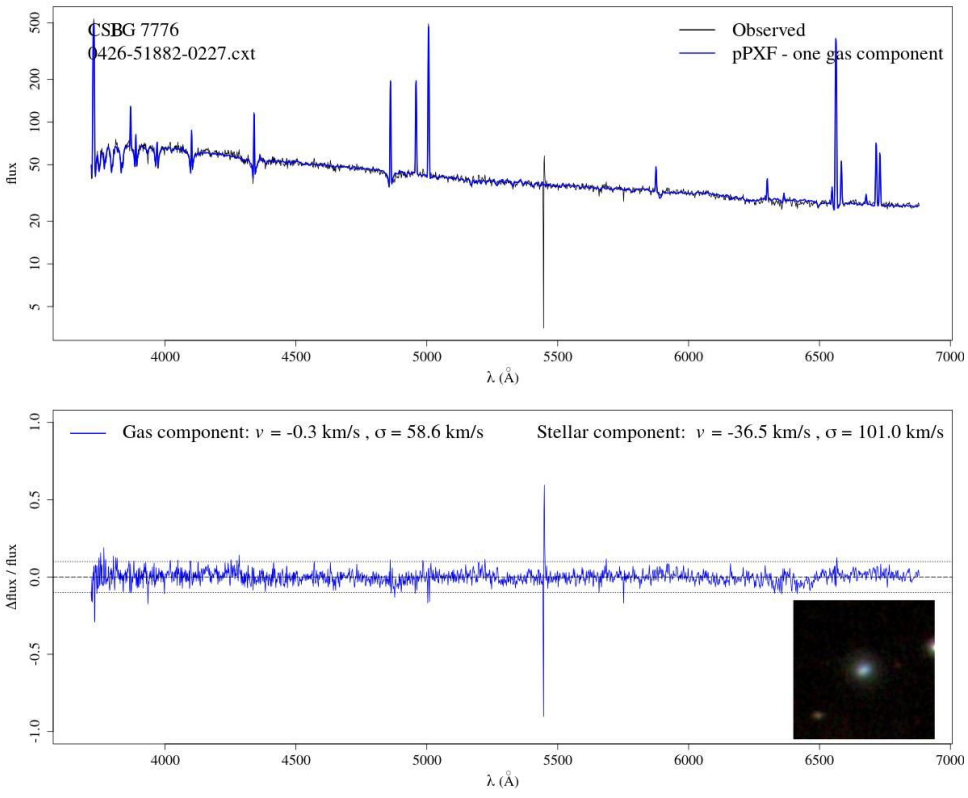
CSBG 7776
0426-51882-0227.cxt
Observed
pPXF - one gas component
flux
λ (Å)
Gas component: v = -0.3 km/s , σ = 58.6 km/s
Stellar component: v = -36.5 km/s , σ = 101.0 km/s
Δflux / flux

# Group 8454:

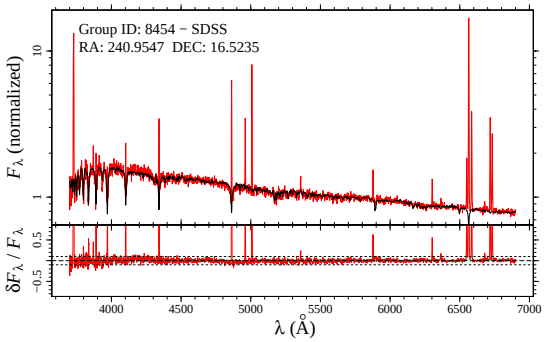
Group ID: 8454 − SDSS
RA: 240.9547 DEC: 16.5235
$F_\lambda$ (normalized)
$\delta F_\lambda / F_\lambda$
λ (Å)

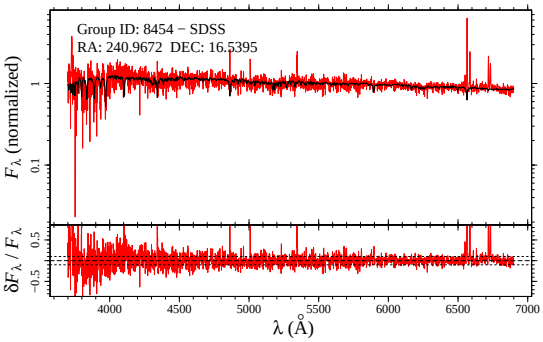
Group ID: 8454 − SDSS
RA: 240.9672 DEC: 16.5395
$F_\lambda$ (normalized)
$\delta F_\lambda / F_\lambda$
λ (Å)

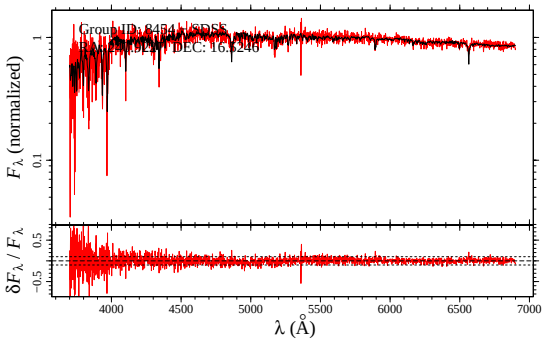
$F_\lambda$ (normalized)
$\delta F_\lambda / F_\lambda$
λ (Å)

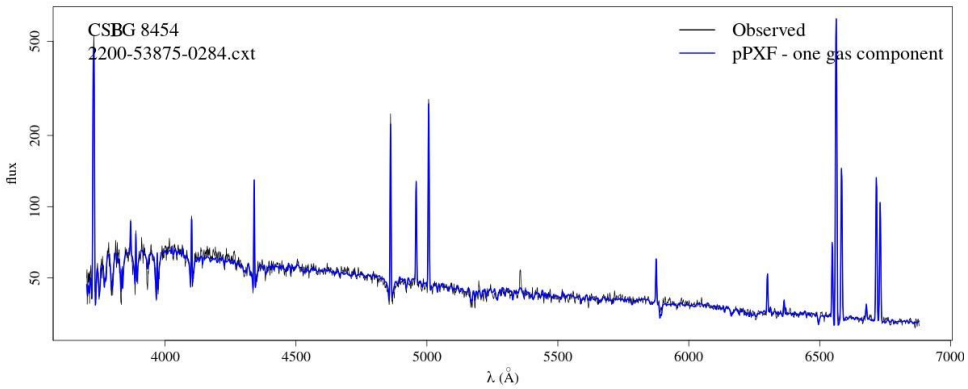
CSBG 8454
2200-53875-0284.cxt
Observed
pPXF - one gas component
flux
λ (Å)

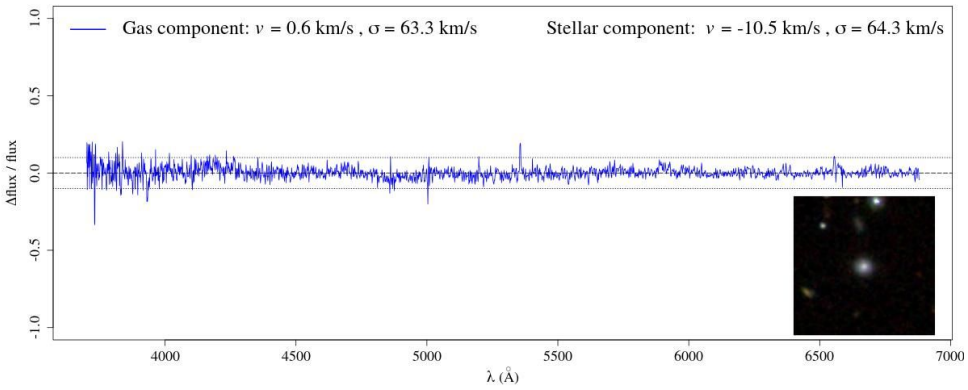
Gas component: v = 0.6 km/s , σ = 63.3 km/s
Stellar component: v = -10.5 km/s , σ = 64.3 km/s
Δflux / flux
λ (Å)

# Group 12799:

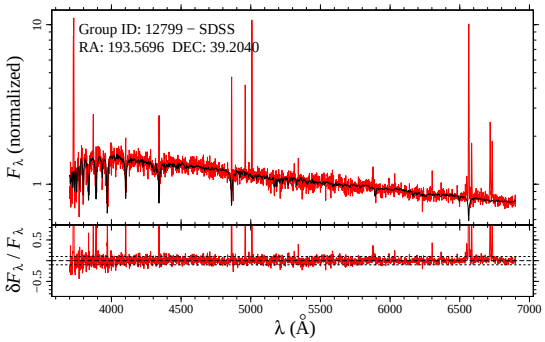
Group ID: 12799 − SDSS
RA: 193.5696 DEC: 39.2040
$F_\lambda$ (normalized)
$\delta F_\lambda / F_\lambda$
λ (Å)

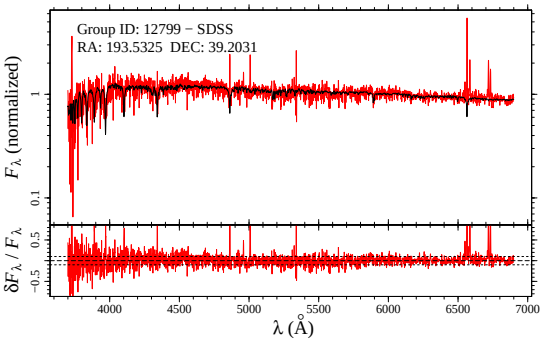
Group ID: 12799 − SDSS
RA: 193.5325 DEC: 39.2031
$F_\lambda$ (normalized)
$\delta F_\lambda / F_\lambda$
λ (Å)

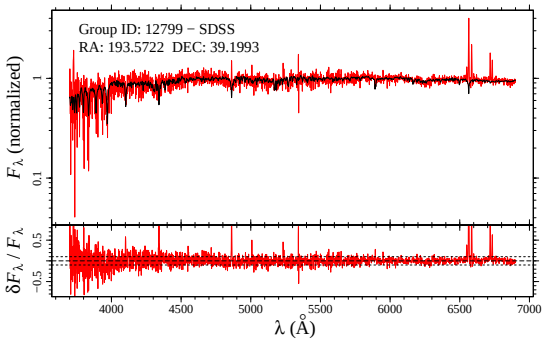
Group ID: 12799 − SDSS
RA: 193.5722 DEC: 39.1993
$F_\lambda$ (normalized)
$\delta F_\lambda / F_\lambda$
λ (Å)

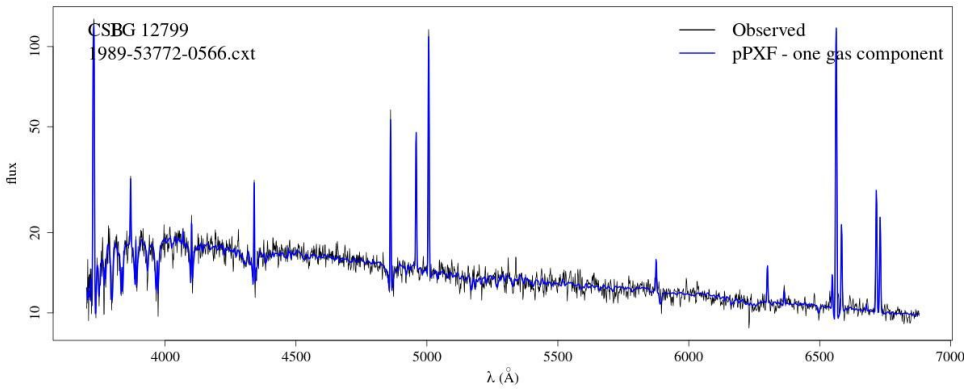
CSBG 12799
1989-53772-0566.cxt
Observed
pPXF - one gas component
flux
λ (Å)

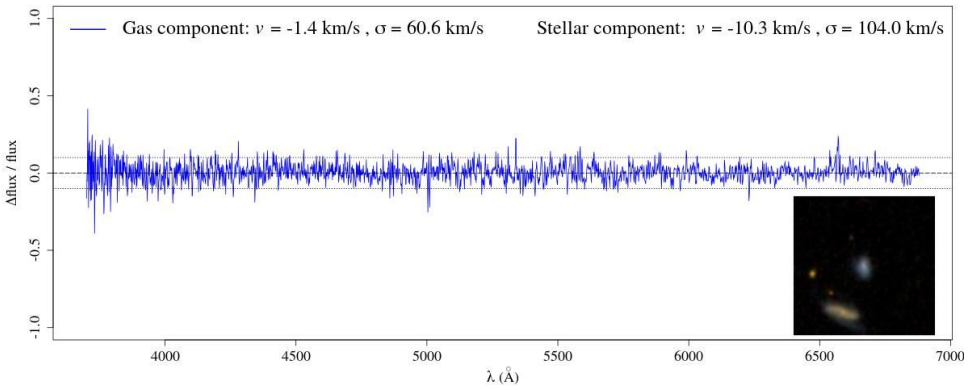
Gas component: v = -1.4 km/s , σ = 60.6 km/s
Stellar component: v = -10.3 km/s , σ = 104.0 km/s
Δflux / flux
λ (Å)

# Group 15609:

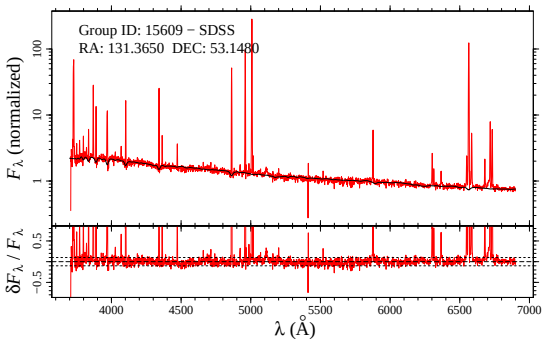
Group ID: 15609 − SDSS
RA: 131.3650 DEC: 53.1480
$F_\lambda$ (normalized)
$\delta F_\lambda / F_\lambda$
λ (Å)

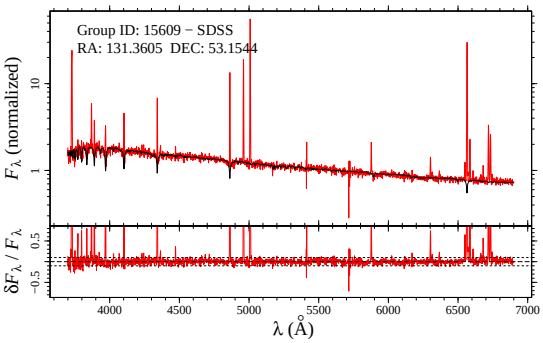
Group ID: 15609 − SDSS
RA: 131.3605 DEC: 53.1544
$F_\lambda$ (normalized)
$\delta F_\lambda / F_\lambda$
λ (Å)

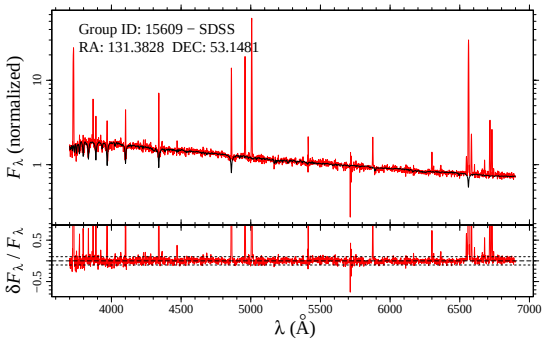
Group ID: 15609 − SDSS
RA: 131.3828 DEC: 53.1481
$F_\lambda$ (normalized)
$\delta F_\lambda / F_\lambda$
λ (Å)

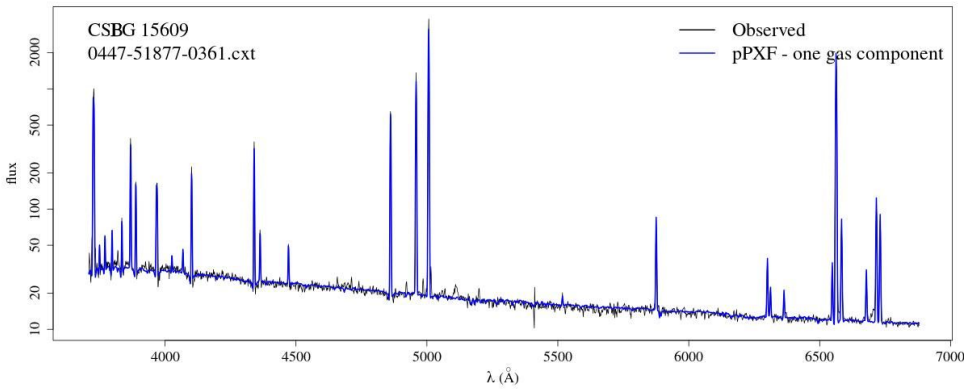
CSBG 15609
0447-51877-0361.cxt
Observed
pPXF - one gas component
flux
λ (Å)

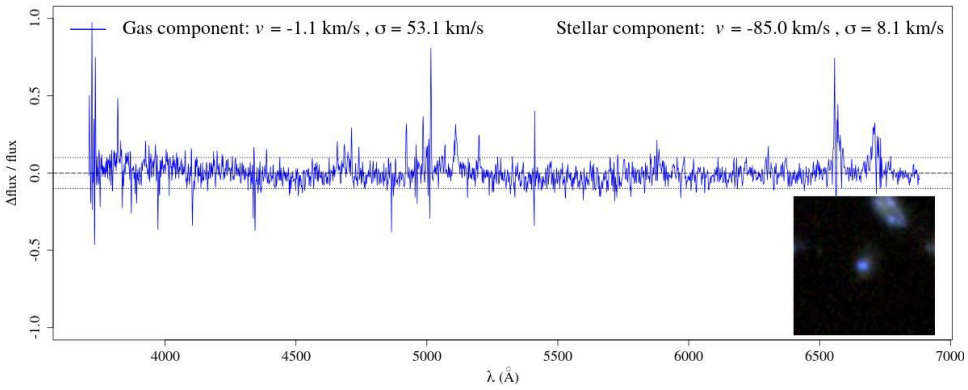
Gas component: v = -1.1 km/s , σ = 53.1 km/s
Stellar component: v = -85.0 km/s , σ = 8.1 km/s
Δflux / flux
λ (Å)

# Group 16311:

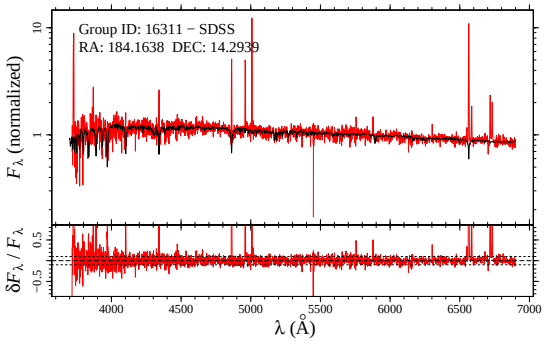
Group ID: 16311 − SDSS
RA: 184.1638 DEC: 14.2939
$F_\lambda$ (normalized)
$\delta F_\lambda / F_\lambda$
λ (Å)

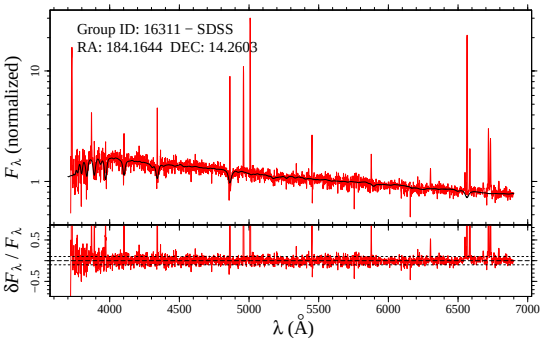
Group ID: 16311 − SDSS
RA: 184.1644 DEC: 14.2603
$F_\lambda$ (normalized)
$\delta F_\lambda / F_\lambda$
λ (Å)

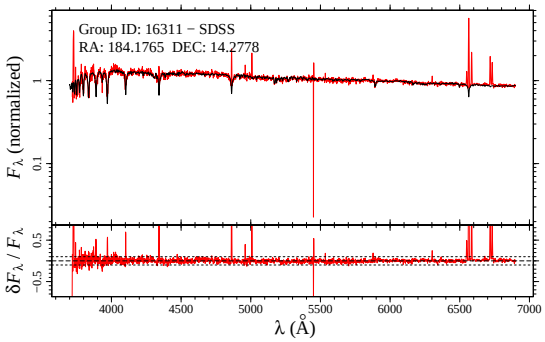
Group ID: 16311 − SDSS
RA: 184.1765 DEC: 14.2778
$F_\lambda$ (normalized)
$\delta F_\lambda / F_\lambda$
λ (Å)

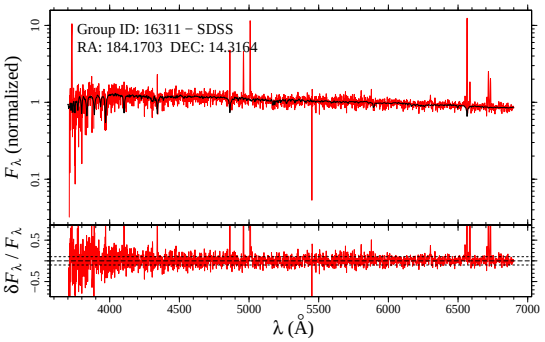
Group ID: 16311 − SDSS
RA: 184.1703 DEC: 14.3164
$F_\lambda$ (normalized)
$\delta F_\lambda / F_\lambda$
λ (Å)

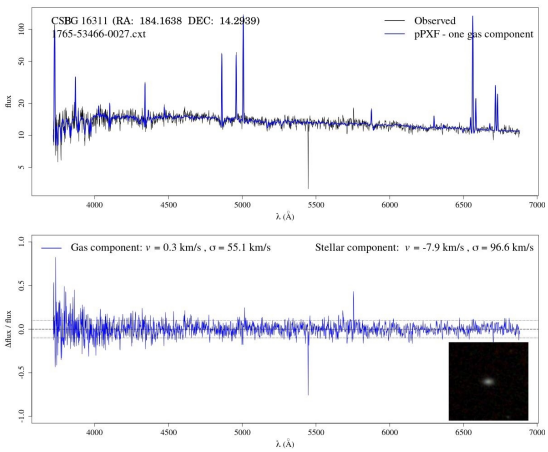
CSBG 16311 (RA: 184.1638 DEC: 14.2939)
1765-53466-0027.cxt
Observed
pPXF - one gas component
flux
λ (Å)
Gas component: v = 0.3 km/s , σ = 55.1 km/s
Stellar component: v = -7.9 km/s , σ = 96.6 km/s
Δflux / flux

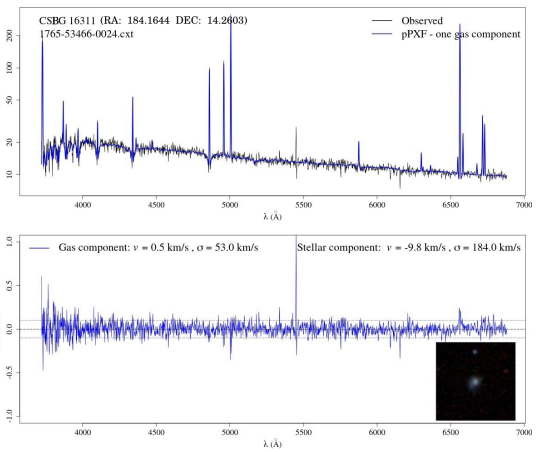
CSBG 16311 (RA: 184.1644 DEC: 14.2603)
1765-53466-0024.cxt
Observed
pPXF - one gas component
flux
λ (Å)
Gas component: v = 0.5 km/s , σ = 53.0 km/s
Stellar component: v = -9.8 km/s , σ = 184.0 km/s
Δflux / flux

# Group 17182:

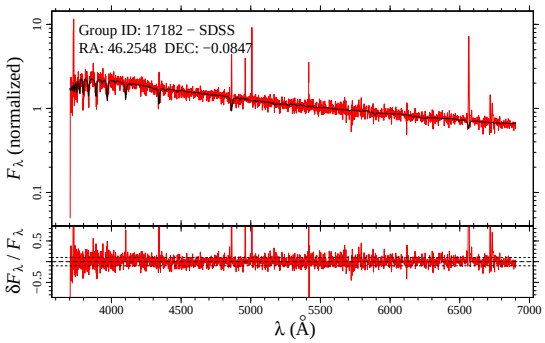
Group ID: 17182 − SDSS
RA: 46.2548 DEC: −0.0847
$F_\lambda$ (normalized)
$\delta F_\lambda / F_\lambda$
λ (Å)

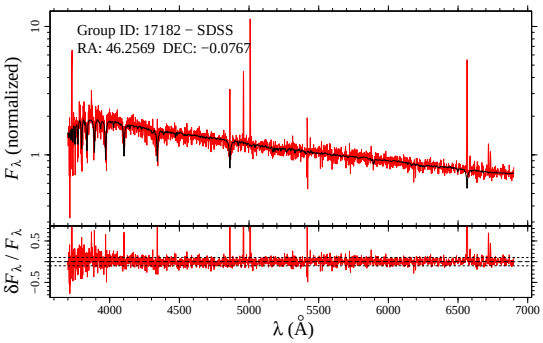
Group ID: 17182 − SDSS
RA: 46.2569 DEC: −0.0767
$F_\lambda$ (normalized)
$\delta F_\lambda / F_\lambda$
λ (Å)

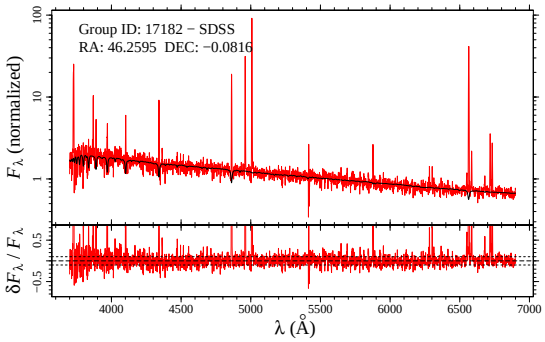
Group ID: 17182 − SDSS
RA: 46.2595 DEC: −0.0816
$F_\lambda$ (normalized)
$\delta F_\lambda / F_\lambda$
λ (Å)

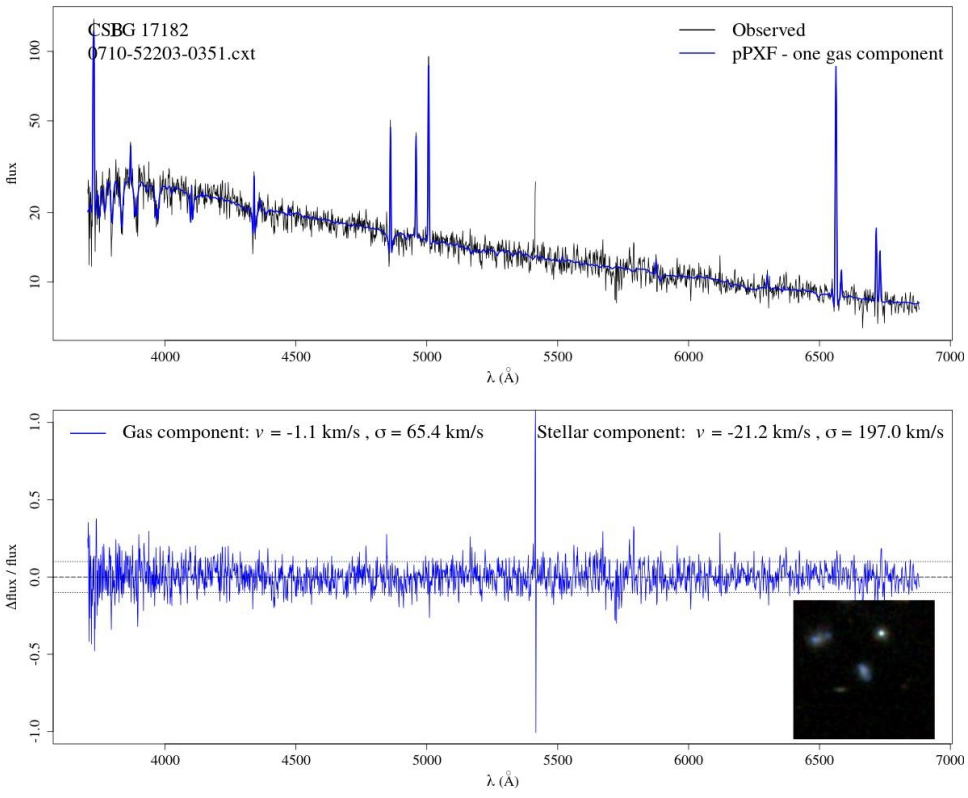
CSBG 17182
0710-52203-0351.cxt
Observed
pPXF - one gas component
flux
λ (Å)
Gas component: v = -1.1 km/s , σ = 65.4 km/s
Stellar component: v = -21.2 km/s , σ = 197.0 km/s
Δflux / flux
λ (Å)

# Group 18766:

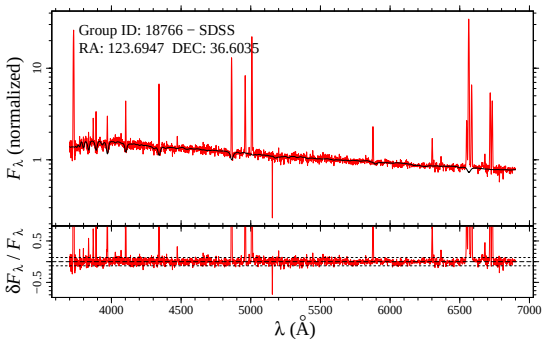
Group ID: 18766 − SDSS
RA: 123.6947 DEC: 36.6035
$F_\lambda$ (normalized)
$\delta F_\lambda / F_\lambda$
λ (Å)

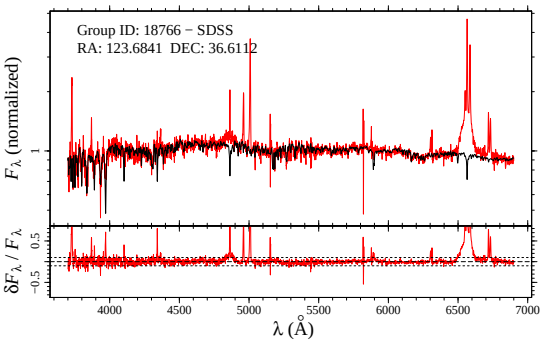
Group ID: 18766 − SDSS
RA: 123.6841 DEC: 36.6112
$F_\lambda$ (normalized)
$\delta F_\lambda / F_\lambda$
λ (Å)

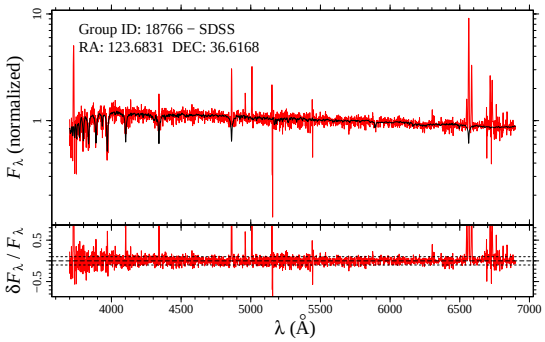
Group ID: 18766 − SDSS
RA: 123.6831 DEC: 36.6168
$F_\lambda$ (normalized)
$\delta F_\lambda / F_\lambda$
λ (Å)

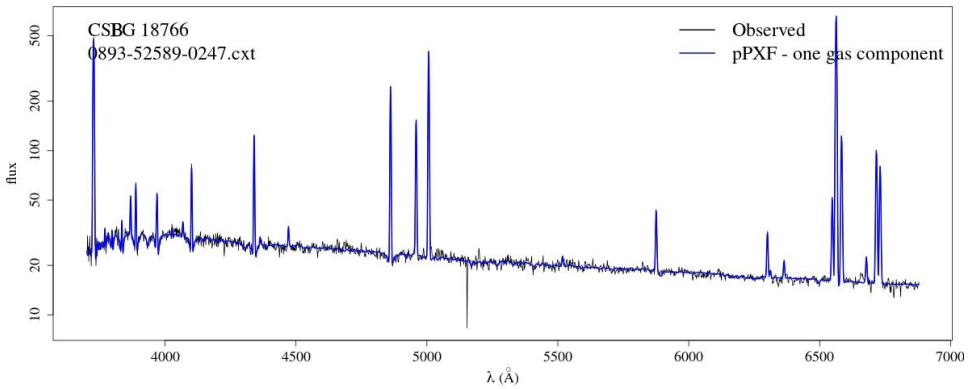
CSBG 18766
0893-52589-0247.cxt
Observed
pPXF - one gas component
flux
λ (Å)

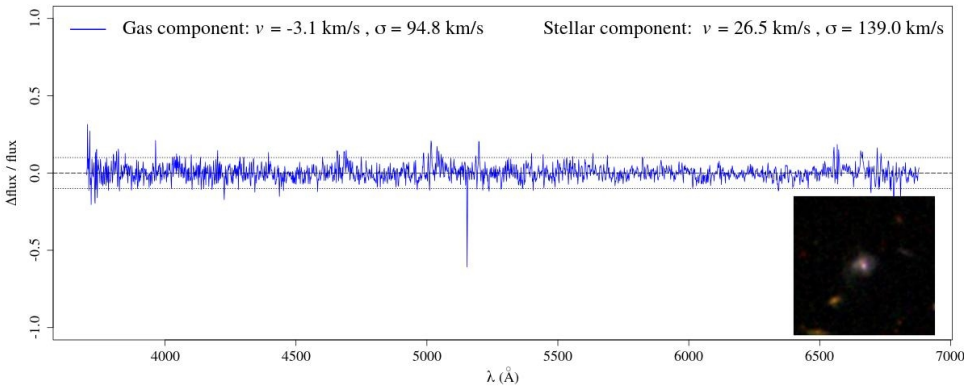
Gas component: v = -3.1 km/s , σ = 94.8 km/s
Stellar component: v = 26.5 km/s , σ = 139.0 km/s
Δflux / flux
λ (Å)

# B Press Release

## Estudo da UFRGS traz novas descobertas sobre as Galáxias Compactas que formam muitas estrelas

Pesquisadores da Universidade Federal do Rio Grande do Sul acabam de publicar um estudo que traz novas descobertas sobre as Galáxias Compactas que formam muitas estrelas (GCFEs). Essas galáxias são especialmente conhecidas por formarem muitas estrelas e por serem muito concentradas, porém os cientistas ainda não entendem muito bem as razões para isto.

A grande novidade deste estudo é que os pesquisadores encontraram algumas destas galáxias dentro de grupos de galáxias anãs. Acreditava-se que as interações entre as galáxias dentro destes grupos poderiam desencadear mudanças na estrutura das GCFEs, o que poderia ser uma possível explicação para suas propriedades peculiares.

Neste estudo, os pesquisadores selecionaram 12 grupos contendo uma GCFEs e pelo menos duas outras galáxias anãs que também formam muitas estrelas. Para isto, utilizaram dados do *Sloan Digital Sky Survey*, que é um catálogo público de galáxias, e também realizaram observações astronômicas nos supertelescópios dos Observatórios Gemini Sul e Gemini Norte. Para entender se as interações com as galáxias vizinhas estão de fato alterando as características das GCFEs, os pesquisadores também selecionaram uma amostra de GCFEs isoladas, ou seja, que não estão interagindo com nenhuma outra galáxia.

Os resultados mostraram que as peculiaridades das GCFEs estão muito mais relacionadas a processos internos às próprias galáxias do que ao ambiente externo. Ou seja, mesmo com as fortes interações, tudo indica que as GCFEs dentro dos grupos não diferem muito das GCFEs isoladas. No entanto, os pesquisadores também identificaram sinais claros de formação estelar sincronizada entre os membros de alguns grupos, o que significa que as interações estão exercendo alguma influência na evolução destas galáxias. Além disso, eles identificaram em todas as GCFEs que uma pequena fração das estrelas que nela habitam são, na verdade, bem velhas. Isto sugere que elas vêm produzindo estrelas desde que foram formadas há vários bilhões de anos.

**Palavras chave:** Galáxias anãs, Galáxias starburst, Grupos de galáxias

# References

Abdurro'uf et al., 2022, , 259, 35

Aloisi A., et al., 2007, , 667, L151

Baldwin J. A., Phillips M. M., Terlevich R., 1981, PASP, 93, 5

Barnard G. A., 1945, , 156, 177

Bekki K., 2008, Monthly Notices of the Royal Astronomical Society: Letters, 388, L10

Bishop C. M., 2006, Machine learning, 128

Blanton M. R., et al., 2005, , 129, 2562

Borthakur S., Yun M. S., Verdes-Montenegro L., 2010, The Astrophysical Journal, 710, 385

Borthakur S., Yun M. S., Verdes-Montenegro L., Heckman T. M., Zhu G., Braatz J. A., 2015, The Astrophysical Journal, 812, 78

Bosch G., et al., 2019, Monthly Notices of the Royal Astronomical Society, 489, 1787

Bradford J. D., Geha M. C., Blanton M. R., 2015, The Astrophysical Journal, 809, 146

Brinchmann J., Charlot S., White S. D. M., Tremonti C., Kauffmann G., Heckman T., Brinkmann J., 2004, MNRAS, 351, 1151

Calvi V., Stiavelli M., Bradley L., Pizzella A., Kim S., 2014, The Astrophysical Journal, 796, 102

Calzetti D., Kinney A. L., Storchi-Bergmann T., 1994, ApJ, 429, 582

Cappellari M., 2012, Astrophysics Source Code Library, pp ascl–1210

Cardamone C., et al., 2009, Monthly Notices of the Royal Astronomical Society, 399, 1191

Cardelli J. A., Clayton G. C., Mathis J. S., 1989, ApJ, 345, 245

Cattaneo, A. Mamon, G. A. Warnick, K. Knebe, A. 2011, A&A, 533, A5

Chang Y.-Y., van der Wel A., da Cunha E., Rix H.-W., 2015, , 219, 8

Chen P. S., Yang X. H., Liu J. Y., Shan H. G., 2018, , 155, 17

Cid Fernandes R., Mateus A., Sodré L., Stasińska G., Gomes J. M., 2005, MNRAS, 358, 363

Cohn J. H., et al., 2018, The Astrophysical Journal, 869, 141

Conselice C. J., 2003, The Astrophysical Journal Supplement Series, 147, 1

Contreras Ramos R., et al., 2011, , 739, 74

Crain R. A., et al., 2015, Monthly Notices of the Royal Astronomical Society, 450, 1937

Delgado R. G., Cervino M., Martins L. P., Leitherer C., Hauschildt P. H., 2005, Monthly Notices of the Royal Astronomical Society, 357, 945

Dey A., et al., 2019, , 157, 168

Douglass K. A., Vogeley M. S., Cen R., 2018, The Astrophysical Journal, 864, 144

Duffy A. R., Meyer M. J., Staveley-Smith L., Bernyk M., Croton D. J., Koribalski B. S., Gerstmann D., Westerlund S., 2012, , 426, 3385

Ellison S. L., Patton D. R., Mendel J. T., Scudder J. M., 2011, Monthly Notices of the Royal Astronomical Society, 418, 2043

Ellison S. L., Mendel J. T., Patton D. R., Scudder J. M., 2013, Monthly Notices of the Royal Astronomical Society, 435, 3627

Fernandes R. C., et al., 2014, Astronomy & Astrophysics, 561, A130

Fisher R. A., 1945, , 156, 388

Fraley C., Raftery A. E., 2002, Journal of the American Statistical Association, 97, 611

Fraley C., Raftery A. E., Murphy T. B., Scrucca L., 2012, mclust Version 4 for R: Normal Mixture Modeling for Model-Based Clustering, Classification, and Density Estimation

Geha M., Blanton M. R., Yan R., Tinker J. L., 2012, The Astrophysical Journal, 757, 85

Girardi L., Bressan A., Bertelli G., Chiosi C., 2000, A&AS, 141, 371

Guseva N. G., Izotov Y. I., Fricke K. J., Henkel C., 2017, A&A, 599, A65

Hamilton A., Tegmark M., 2004, Monthly Notices of the Royal Astronomical Society, 349, 115

Haynes M. P., et al., 2018, The Astrophysical Journal, 861, 49

Ho D. E., Imai K., King G., Stuart E. A., 2011, Journal of Statistical Software, 42, 1

Holden B., et al., 2016, The Astrophysical Journal, 820, 73

Izotov Y. I., Thuan T. X., 1998, ApJ, 497, 227

Izotov Y. I., Thuan T. X., 2004, , 616, 768

Izotov Y. I., Guseva N. G., Thuan T. X., 2011, ApJ, 728, 161

Izotov Y. I., Guseva N. G., Fricke K. J., Henkel C., 2014, A&A, 561, A33

Izotov Y., Guseva N., Fricke K., Henkel C., 2015, Monthly Notices of the Royal Astronomical Society, 451, 2251

Izotov Y., Schaerer D., Thuan T., Worseck G., Guseva N., Orlitová I., Verhamme A., 2016a, Monthly Notices of the Royal Astronomical Society, 461, 3683

Izotov Y. I., Guseva N. G., Fricke K. J., Henkel C., 2016b, , 462, 4427

Izotov Y., Orlitová I., Schaerer D., Thuan T., Verhamme A., Guseva N., Worseck G., 2016c, Nature, 529, 178

Izotov Y. I., Thuan T. X., Guseva N. G., Liss S. E., 2018a, MNRAS, 473, 1956

Izotov Y., Schaerer D., Worseck G., Guseva N., Thuan T., Verhamme A., Orlitová I., Fricke K., 2018b, Monthly Notices of the Royal Astronomical Society, 474, 4514

Izotov Y., Worseck G., Schaerer D., Guseva N., Thuan T., Verhamme A., Orlitová I., 2018c, Monthly Notices of the Royal Astronomical Society, 478, 4851

Izotov Y., Worseck G., Schaerer D., Guseva N., Thuan T., Verhamme A., Orlitová I., 2018d, Monthly Notices of the Royal Astronomical Society, 478, 4851

Izotov Y. I., Thuan T. X., Guseva N. G., 2021a, , 504, 3996

Izotov Y., Guseva N., Fricke K., Henkel C., Schaerer D., Thuan T., 2021b, Astronomy & Astrophysics, 646, A138

Janowiecki S., Salzer J. J., 2014, , 793, 109

Jaskot A. E., Oey M. S., 2013, ApJ, 766, 91

Johnson K. E., Indebetouw R., Watson C., Kobulnicky H. A., 2004, The Astronomical Journal, 128, 610

Kauffmann G., et al., 2003, MNRAS, 346, 1055

Kennicutt J. R. C., 1998, ApJ, 498, 541

Kewley L. J., Dopita M. A., Sutherland R. S., Heisler C. A., Trevena J., 2001, ApJ, 556, 121

Kewley L. J., Dopita M. A., Leitherer C., Davé R., Yuan T., Allen M., Groves B., Sutherland R., 2013, , 774, 100

Krabbe A. C., Rosa D. A., Dors O. L., Pastoriza M. G., Winge C., Hägele G. F., Cardaci M. V., Rodrigues I., 2014, MNRAS, 437, 1155

Kunth D., Östlin G., 2000, A&ARv, 10, 1

Kurtz M. J., Mink D. J., 1998, PASP, 110, 934

L'Huillier B., Combes F., Semelin B., 2012, A&A, 544, A68

Lelli F., Verheijen M., Fraternali F., 2014, , 445, 1694

Lintott C. J., et al., 2008, Monthly Notices of the Royal Astronomical Society, 389, 1179

Luber N., Pearson S., Putman M. E., Besla G., Stierwalt S., Meyers J. P., 2022, The Astronomical Journal, 163, 49

Luo W., Yang X., Zhang Y., 2014, , 789, L16

Mahalanobis P. C., 1936.

Mamon G. A., Trevisan M., Thuan T. X., Gallazzi A., Davé R., 2019, Monthly Notices of the Royal Astronomical Society, 492, 1791

Mamon G. A., Trevisan M., Thuan T. X., Gallazzi A., Davé R., 2020, MNRAS, 492, 1791

Marasco A., Crain R. A., Schaye J., Bahé Y. M., van der Hulst T., Theuns T., Bower R. G., 2016, Monthly Notices of the Royal Astronomical Society, 461, 2630

Martin G., et al., 2021, Monthly Notices of the Royal Astronomical Society, 500, 4937

Martins L. P., Delgado R. M. G., Leitherer C., Cervino M., Hauschildt P., 2005, Monthly Notices of the Royal Astronomical Society, 358, 49

Mason J. C., Handscomb D. C., 2002, Chebyshev polynomials. CRC press

McConnachie A. W., Patton D. R., Ellison S. L., Simard L., 2009, Monthly Notices of the Royal Astronomical Society, 395, 255

McQuinn K. B., et al., 2010, The Astrophysical Journal, 721, 297

Meyer M., 2009, in Panoramic Radio Astronomy: Wide-field 1-2 GHz Research on Galaxy Evolution. p. 15 (arXiv:0912.2167)

Moré J. J., 1978, in , Numerical analysis. Springer, pp 105–116

Muldrew S. I., et al., 2012, Monthly Notices of the Royal Astronomical Society, 419, 2670

Nakajima K., Ellis R. S., Robertson B. E., Tang M., Stark D. P., 2020, The Astrophysical Journal, 889, 161

Nelson D., et al., 2018, The IllustrisTNG Simulations: Public Data Release, doi:10.48550/ARXIV.1812.05609, `https://arxiv.org/abs/1812.05609`

Noeske K., Iglesias-Páramo J., Vílchez J., Papaderos P., Fricke K., 2001, Astronomy & Astrophysics, 371, 806

Papaderos P., Izotov Y. I., Thuan T. X., Noeske K. G., Fricke K. J., Guseva N. G., Green R. F., 2002, , 393, 461

Patton D. R., Torrey P., Ellison S. L., Mendel J. T., Scudder J. M., 2013, , 433, L59

Pearson S., et al., 2016, Monthly Notices of the Royal Astronomical Society, 459, 1827

Pearson S., et al., 2018, Monthly Notices of the Royal Astronomical Society, 480, 3069

Phillipps S., Davies J. I., Disney M. J., 1990, Monthly Notices of the Royal Astronomical Society, 242, 235

Pilyugin L. S., Grebel E. K., 2016, Monthly Notices of the Royal Astronomical Society, 457, 3678–3692

Pilyugin L., Mattsson L., 2011, Monthly Notices of the Royal Astronomical Society, 412, 1145

Privon G. C., et al., 2017a, ApJ, 846, 74

Privon G., et al., 2017b, The Astrophysical Journal, 846, 74

R Core Team 2015, R: A Language and Environment for Statistical Computing. R Foundation for Statistical Computing, Vienna, Austria, `https://www.R-project.org`

Riffel R., et al., 2021, Monthly Notices of the Royal Astronomical Society, 501, 4064

Rosa D. A., Dors O. L., Krabbe A. C., Hägele G. F., Cardaci M. V., Pastoriza M. G., Rodrigues I., Winge C., 2014, MNRAS, 444, 2005

Rosenbaum P. R., Rubin D. B., 1983, Biometrika, 70, 41

Roychowdhury S., et al., 2022, The Astrophysical Journal, 927, 20

Salpeter E. E., 1955, ApJ, 121, 161

Sánchez-Blázquez P., et al., 2006, MNRAS, 371, 703

Savage B. D., Mathis J. S., 1979, ARA&A, 17, 73

Schaye J., et al., 2015, Monthly Notices of the Royal Astronomical Society, 446, 521

Schlegel D. J., Finkbeiner D. P., Davis M., 1998, ApJ, 500, 525

Scudder J. M., Ellison S. L., Torrey P., Patton D. R., Mendel J. T., 2012, , 426, 549

Shapley A. E., et al., 2015, , 801, 88

Shim H., Chary R.-R., 2013, , 765, 26

Skillman E. D., Kennicutt Jr. R. C., 1993, ApJ, 411, 655

Steidel C. C., et al., 2014, , 795, 165

Stierwalt S., Besla G., Patton D., Johnson K., Kallivayalil N., Putman M., Privon G., Ross G., 2015b, The Astrophysical Journal, 805, 2

Stierwalt S., Besla G., Patton D., Johnson K., Kallivayalil N., Putman M., Privon G., Ross G., 2015a, , 805, 2

Stierwalt S., Liss S. E., Johnson K. E., Patton D. R., Privon G. C., Besla G., Kallivayalil N., Putman M., 2017, Nature Astronomy, 1, 0025

Swanson M. E., Tegmark M., Hamilton A. J., Hill J. C., 2008, Monthly Notices of the Royal Astronomical Society, 387, 1391

Tang M., Stark D. P., Chevallard J., Charlot S., 2019, Monthly Notices of the Royal Astronomical Society, 489, 2572

Tempel E., Stoica R., Martinez V. J., Liivamägi L., Castellan G., Saar E., 2014, Monthly Notices of the Royal Astronomical Society, 438, 3465

Tempel E., Tuvikene T., Kipper R., Libeskind N. I., 2017, Astronomy & Astrophysics, 602, A100

Tody D., 1986, in Crawford D. L., ed., Society of Photo-Optical Instrumentation Engineers (SPIE) Conference Series Vol. 627, Instrumentation in astronomy VI. p. 733, doi:10.1117/12.968154

Tremonti C. A., et al., 2004, ApJ, 613, 898

Trevisan M., Mamon G. A., Thuan T. X., Ferrari F., Pilyugin L. S., Ranjan A., 2021a, Monthly Notices of the Royal Astronomical Society, 502, 4815

Trevisan M., Mamon G. A., Thuan T. X., Ferrari F., Pilyugin L. S., Ranjan A., 2021b, Monthly Notices of the Royal Astronomical Society, 502, 4815

Tully R. B., et al., 2006, The Astronomical Journal, 132, 729

Tweed D. P., Mamon G. A., Thuan T. X., Menci N., Calura F., Dekel A., Cattaneo A., Silk J., 2017, MNRAS

Vazdekis A., Sánchez-Blázquez P., Falcón-Barroso J., Cenarro A. J., Beasley M. A., Cardiel N., Gorgas J., Peletier R. F., 2010, MNRAS, 404, 1639

Vazdekis A., et al., 2015, MNRAS, 449, 1177

Vazdekis A., Koleva M., Ricciardelli E., Röck B., Falcón-Barroso J., 2016, Monthly Notices of the Royal Astronomical Society, 463, 3409

Vennik J., Hopp U., Popescu C., 2000, Astronomy and Astrophysics Supplement Series, 142, 399

Wainer H., Thissen D., 1976, Psychometrika, 41, 9

Weisz D. R., et al., 2011, The Astrophysical Journal, 739, 5

Worthey G., Ottaviani D., 1997, The Astrophysical Journal Supplement Series, 111, 377

Yang H., Malhotra S., Rhoads J. E., Wang J., 2017, The Astrophysical Journal, 847, 38

Yaryura C. Y., et al., 2020, Monthly Notices of the Royal Astronomical Society, 499, 5932

de Souza R. S., et al., 2016, MNRAS, 461, 2115

van Dokkum P. G., 2001, Publications of the Astronomical Society of the Pacific, 113, 1420–1427